Lt Col Dan Brown
USAF
SAM Records
Suitland
73A-5374
19 Dec 94

Contract
Do No.

AD697425

AIR6.950109.001f

EVALUATION OF EYE HAZARDS FROM NUCLEAR DETONATIONS

I. RETINAL BURNS AND FLASHBLINDNESS

Norma D. Miller

Thomas J. White

NOVEMBER 1969

Contract F41609-68-C-0023

USAF School of Aerospace Medicine
Aerospace Medical Division (AFSC)
Brooks Air Force Base, Texas

73A-5374

USAF # 438

Lt Col Dan Brown
USAF
SAM Records
Suitland
73A-5374
19 Dec 94

EVALUATION OF EYE HAZARDS FROM NUCLEAR DETONATIONS

I. RETINAL BURNS AND FLASHBLINDNESS

Norma D. Miller

Thomas J. White

NOVEMBER 1969

Contract F41609-68-C-0023

USAF School of Aerospace Medicine
Aerospace Medical Division (AFSC)
Brooks Air Force Base, Texas

Lt Col Dan Brown
USAF
SAM Records
Suitland
73A-5374
19 Dec 94

FOREWORD

This report was prepared by the Life Sciences Division of Technology Incorporated for the USAF School of Aerospace Medicine under Contract AF41609-68-C-0023 and covers the period from 20 December 1967 to 30 June 1969. Research was performed under Project 6301, Task 630103, Work Unit 6301 03 031 and was partially funded by the Defense Atomic Support Agency under Program Element 6.16.46.01.D, Project 5710, Subtask 03.138. Mr. Everett O. Richey, Oculothermal Section, Ophthalmology Branch, USAF School of Aerospace Medicine was the Contract Monitor and Mrs. Norma D. Miller was the principal investigator.

Grateful acknowledgement is hereby made of the assistance of the following personnel of the School of Aerospace Medicine: Mr. Everett O. Richey, Col. Thomas J. Tredici, and Lt. Col. Albert V. Alder of the Oculothermal Section, and Capt. Philip S. Coogan, M/Sgt. Jesse Vasys, and S/Sgt. Fred Morris of the Cytology-Pathology Branch. Acknowledgement is also made of the helpful assistance of Dr. Ralph G. Allen, Jr., General Manager of the Life Sciences Division, throughout the entire period of the research effort.

A portion of the work described in this report covers the study of chorioretinal burns in rabbits and small primates and of flashblindness in humans. This research is a continuation of earlier work carried

Lt Col Dan Brown
USAF
SAM Records
Suitland
73A-5374
19 Dec 94

out by the Life Sciences Division of Technology Incorporated.

The primary efforts and results obtained during the contract period are documented in detail in the series of five reports listed below:

PART I

A Study of Chorioretinal Burns Produced in Rabbits and Primates by a Ruby Laser.

PART II

Retinal Burn Thresholds in Primates.

PART III

Modification of the Zeiss Photocoagulator to Produce Simulated Nuclear Detonations.

PART IV

Flashblindness Recovery Times for Human Subjects.

PART V

Model for Prediction of Retinal Temperatures.

Research performed as reported was conducted according to the Principles of Laboratory Animal Care as promulgated by the National Society for Medical Research.

Lt Col Dan Brown
USAF
SAM Records
Suitland
73A-5374
19 Dec 94

Publication of this report does not constitute Air Force
of the report's findings or conclusions. It is published only for
exchange and stimulation of ideas.

Lt Col Dan Brown
USAF
SAM Records
Suitland
73A-5274
19 Dec 94

TABLE OF CONTENTS

	Page
I. A STUDY OF CHORIORETINAL BURNS PRODUCED IN RABBITS AND PRIMATES BY A RUBY LASER	1
1. INTRODUCTION	1
2. APPARATUS	2
2.1 Semi-Q- and Q-Switching of the Laser	6
3. CALIBRATION	9
3.1 Cross Calibration of the Monitoring Photodiode	11
3.1.1 Long Pulse Mode	11
3.1.2 Q-Switched and Semi-Q-Switched Mode	16
3.2 Beam Divergence Calibration	16
3.3 Dependence of Pulsewidth on Flashlamp Energy	17
4. EXPERIMENTAL PROCEDURE AND RESULTS	20
4.1 Long Pulse Rabbit and Primate Extrafoveal Thresholds	22
4.2 Primate Thresholds for Q-Switched and Semi-Q-Switched Exposures	24
5. CONCLUSIONS	25
6. REFERENCES	29
II. RETINAL BURN THRESHOLDS IN PRIMATES	30
1. INTRODUCTION	30
2. EXPERIMENTAL PROCEDURE	32

CONTENTS (continued) Page

3. EXPERIMENTAL RESULTS 34

3.1 Time of Development of a Visible Lesion 34

3.2 Extramacular Burn Thresholds 38

3.3 Foveal Burn Thresholds 40

4. DISCUSSION OF EXPERIMENTAL DATA 40

4.1 Beam Distribution for Zeiss Photocoagulator 45

5. APPEARANCE OF THE BURN LESION AT VARIOUS TIMES FOLLOWING THE EXPOSURES 48

5.1 Histopathology of Retinal Burns 53

5.1.1 Acute Retinal Burns 53

5.1.2 Healed Retinal Burns 57

5.1.3 Abbreviations Used in Labeling the Illustrations 60

6. REFERENCES 62

III. MODIFICATION OF THE ZEISS PHOTOCOAGULATOR TO PRODUCE SIMULATED NUCLEAR DETONATIONS 63

1. INTRODUCTION 63

2. SIMULATION GUIDELINES 63

3. APPARATUS 66

3.1 Optical System 66

3.2 The First Pulse Irradiance Profile 69

3.3 The Second Pulse Irradiance Profile 70

Lt Col Dan Brown
USAF
SAM Records
Suitland

CONTENTS (continued) Page

3.4 The Variation in Retinal Image Size 71

4. SUMMARY 72

5. REFERENCES 74

IV. FLASHBLINDNESS RECOVERY TIMES FOR HUMAN SUBJECTS 75

1. INTRODUCTION 75

2. APPARATUS 76

3. CALIBRATION 80

3.1 Measurement of the Steradiancy of the Flash Tube 80

3.2 Direct Measurement of Irradiance at Cornea 89

3.3 Calibration of Flash Duration 90

3.4 Calibration of Recovery Target Luminances 92

4. EXPERIMENTAL RESULTS 93

4.1 Effect of Flash Field Size on Recovery Times Using Sloan-Snellen Letters 93

4.2 Recovery Times Using a Grating Test Object and Various Flash Field Sizes 96

4.3 Recovery Times Using a Photograph of a Primary Flight Instrument 99

5. CONCLUSIONS 102

6. REFERENCES 104

LtCol Dan Brown
USAF
SAM Records
Suitland
AF-5271

LIST OF FIGURES

No.		Page
1.	Laser Optical System	3
2.	Block diagram of calibration system	4
3.	Photodiode circuit	5
4.	Q-Switch system	7
5.	Electronic diagram of Korad calorimeter	10
6.	Calibration equipment and arrangement	12
7.	Schematic of beam geometry	18
8.	Iris setting versus beam divergence	19
9.	The time course of development of visible lesions in primate eyes following exposures to various irradiance levels	36
10.	Comparison of foveal and extramacular thresholds for the 0.25 mm image diameter	42
11.	Comparison of rabbit and primate burn thresholds for 0.26 and 0.25 mm image diameters respectively	44
12.	Relative intensity distribution across source image	47
13.	Section through a minimal burn lesion caused by exposure to white light. The lesion was produced one year before the animal was sacrificed.	50
14.	This illustrates a fresh retinal burn, 24 hours post exposure (3° cone, 100 msec, 9.6 cal/cm^2-sec)	54
15.	This illustrates a healed retinal burn 2 months post exposure (3° cone, 100 msec, 8.3 cal/cm^2-sec)	58
16.	This is a higher magnification of the healed burn of Figure 15.	58

Lt Col Dan Brown
USAF
SAM Records
Suitland
F: A-5270

FIGURES (continued) Page

17. This illustrates a small, healed retinal burn 2 months post exposure (3° cone, 100 msec, 6.1 cal/cm^2-sec) 61

18. This is a higher magnification of the small healed burn illustrated in Figure 17. 61

19. Normalized radiant emittance for a 1 MT nuclear detonation 65

20. Block diagram of simulator system 67

21. Optical diagram of simulator system 68

22. Oscilloscope traces showing the retinal irradiance profile (upper picture) and image diameter profile (lower picture) produced by the 1 MT simulation 73

23. Schematic diagram of the optical system of the flashblindness apparatus 77

24. Modified flashblindness apparatus designed to accomodate a variable luminance field 79

25. Calculated and measured values of tungsten steradiancy at various filament temperatures 82

26. Relationship between correlated color temperature and filament temperature 84

27. Tungsten ribbon filament luminance as a function of color temperature 85

28. Spectral steradiance of the xenon flash lamp filtered through KG-3 and 2B filters 88

29. The waveform of the flash exposure 91

30. Mean recovery times for five subject using Sloan-Snellen letters following flashes of 2.3×10^7 td · sec for three flash field sizes. 95

Lt Col Dan Brown
USAF
SAM Records
Suitland

FIGURES (continued) Page

31. The effect of varying the flash field diameter on recovery times for three targets 100

32. The effect of flash energy on recovery times for a primary flight instrument target 103

33. Finite difference grid 109

34. Chorioretinal heat source 115

35. Example of temperature rise calculation for Dominic test data 117

Lt Col Dan Brown
USAF
SAM Records
Suitland
FOB-5271

LIST OF TABLES

No.		Page
I.	Rabbit and primate retinal burn thresholds, using long pulse laser exposure.	23
II.	Primate retinal burn thresholds: Q-switched and semi-Q-switched exposures.	26
III.	Comparison of laser long pulse and Zeiss photocoagulator (white light) retinal burn thresholds.	27
IV.	Exposure irradiance in terms of the percent of the 5 minute threshold resulting in the 5 hour threshold for 10 monkeys.	37
V.	Five hour extramacular burn thresholds for Macacca Mulatta. The values are the retinal irradiance in cal/cm^2-sec.	39
VI.	Mean retinal irradiance H_r^{th} (cal/cm^2-sec) for production of "interocular foveal threshold" burns in rhesus monkeys.	41
VII.	Mean recovery times in seconds for 5 subjects using 19' Sloan-Snellen letters following 2.3×10^7 td · sec flashes of varying angular subtense.	94
VIII.	Mean recovery times in seconds for 5 subjects for a grating test object for a 2° and 4° flash field size.	97
IX.	Mean recovery in seconds for a grating test object for various flash field sizes.	98
X.	Mean recovery times of 3 subjects for a photograph of an artificial horizon following 8° flashes of various energy levels.	101
XI.	List of coefficients.	112
XII.	Matrix reduction algorithm.	113

Lt Col Dan Brown
USAF
SAM Records
Suitland

I. A STUDY OF CHORIORETINAL BURNS PRODUCED IN RABBITS AND PRIMATES BY A RUBY LASER

by

Kenneth R. Kay and Margaret G. Smith

1. INTRODUCTION

In a long series of experiments, retinal burn thresholds were determined for rabbits and primates using a modified Zeiss photocoagulator[1-3]. The minimum exposure duration resulting in a lesion was 165μ sec for the rabbit study and 2 msec for the primate study. In order to extend the range of exposure durations to shorter times, a Maser Optics Model 868 Ruby Laser was used. The laser is capable of a nominal output of 100 joules in a half-inch diameter beam. The laser was incorporated into an optical system providing independent control of the retinal exposure and the diameter of the retinal area exposed[2].

The laser provided a sufficiently high energy level to produce retinal lesions for exposures from 30 nanoseconds to 1.45 milliseconds. Rabbits and primates were used for the determination of retinal burn thresholds for long pulse ruby laser exposures. Q-switched and semi-Q-switched laser exposures were used to determine burn thresholds in primates. Image diameters of 1.07 and 0.52 mm were used

Lt Col Dan Brown
USAF
SAM Records
Suitland
92-5211

for the rabbits and 1.20, 0.59 and 0.29 mm for the primates. The development of burns of similar appearance was observed in both species.

2. APPARATUS

The optical system for the control of the laser beam is shown schematically in Figure 1. The diameter of the irradiated area is controlled by the iris diaphragm at the focal point of lens #3. The retinal irradiance is controlled by moving the biconcave lens (#1) along the optical axis. Each exposure was monitored by a photodiode and beam splitter assembly.

Prior to each experimental session, the monitoring photodiode was cross-calibrated against the primary calibration standard described in Section 3. The block diagram of the monitoring and cross-calibration system is shown in Figure 2. The portion of the beam reflected from the beam splitter irradiates a reflector coated with magnesium oxide paint, and the diffusely reflected light is sampled by the photodiode. This technique insures that the level of irradiance on the photodiode is such that the output of the photodiode is linear. The photodiode circuit shown in Figure 3 integrates the photodiode current and the resulting signal is displayed on a CRT and recorded on Polaroid film by an oscilloscope camera.

Lt Col Dan Brown
USAF
SAM Records
Suitland
92A-5211

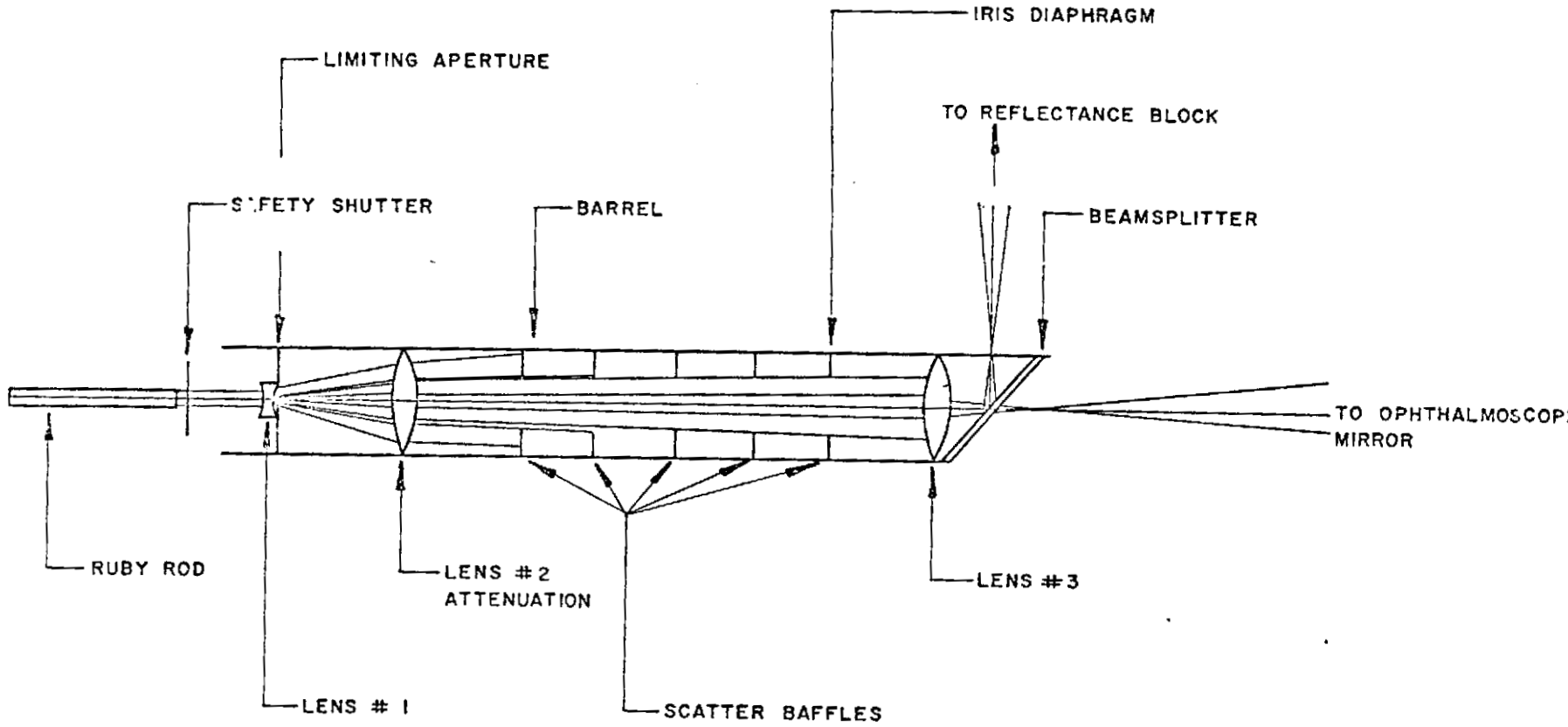

Figure 1. Laser Optical System

Lt Col Dan Brown
USAF
SAM Records
Suitland
[illegible]

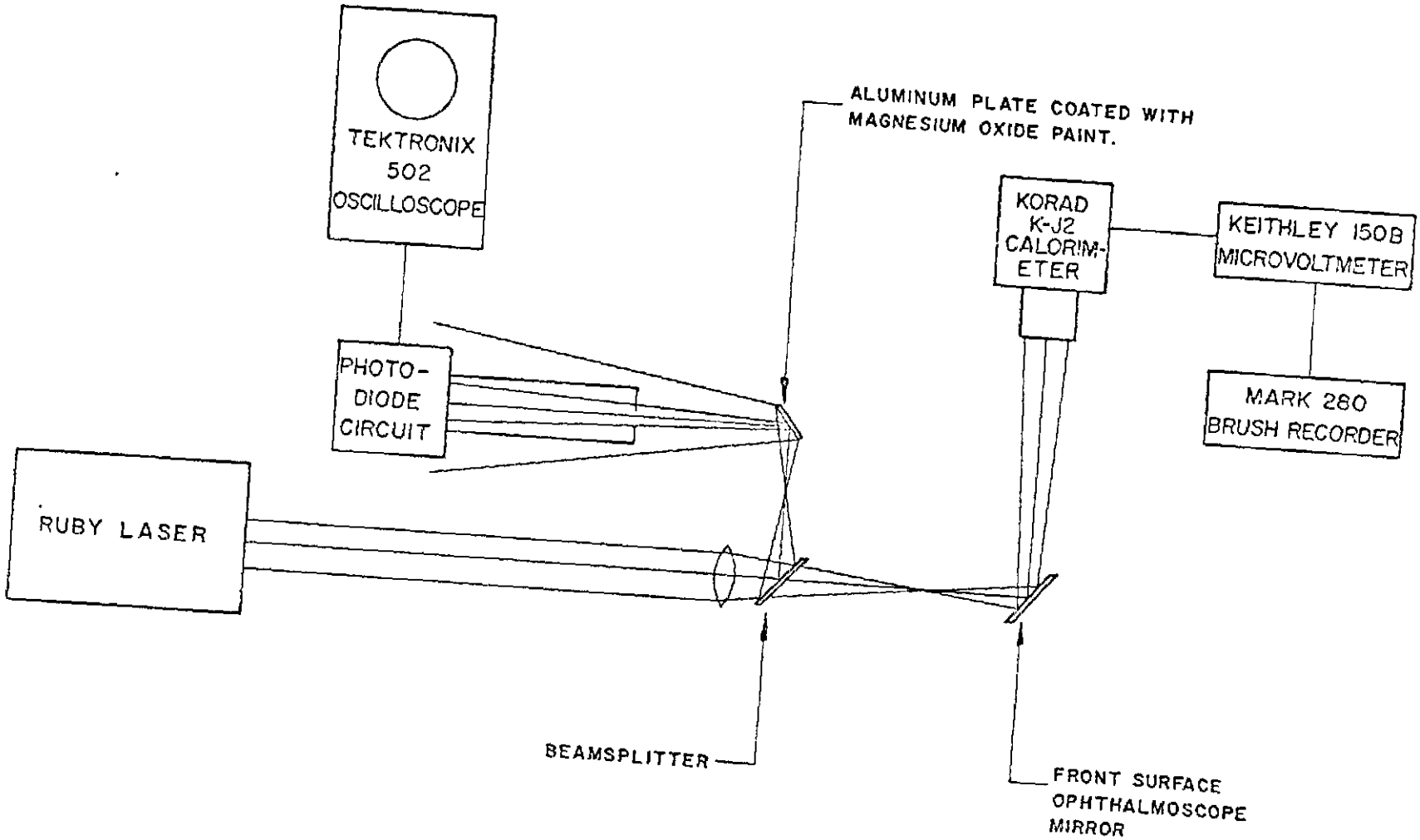

Figure 2. Block diagram of calibration system

Lt Col Dan Brown
USAF
SAM Records
Suitland

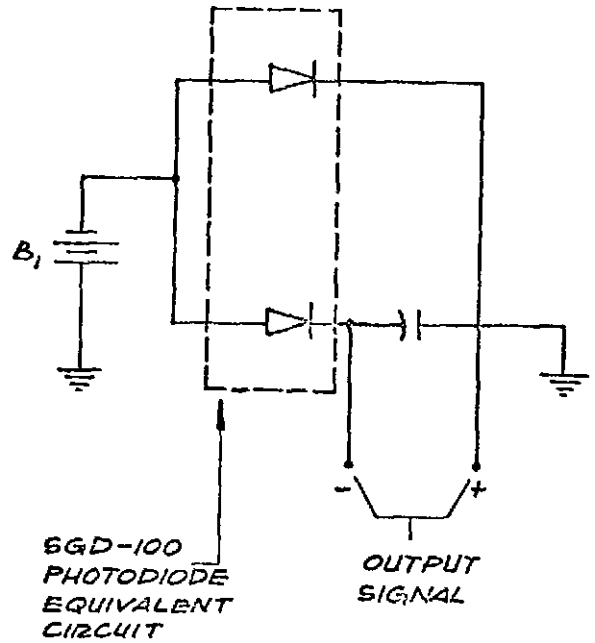

Figure 3. Photodiode circuit

LtCol Dan Brown
USAF
SAM Records
Suitland
AFA-5771

2.1 Semi-Q and Q-Switching of the Laser

The operation of a laser in the Q-switched mode is aptly described by analogy with an amplifier with a positive feed back loop. "Oscillation starts when the gain is sufficient to overcome the losses. If the feed back loop is interrupted by a shutter, oscillation will be prevented and the quantity of energy stored in the laser material will increase until equilibrium is reached between pumping and fluorescent loss. Once the shutter is opened, the feed back loop is opened and the Q of the resonator goes from a very low value to a very high one, and a portion of the stored energy is released in one giant pulse."[2]

It was decided to use a passive bleachable filter to obtain Q-switch and semi-Q-switch laser emissions in this program. In these devices, the fluorescence emitted by the laser rod bleaches the passive filter installed between an anti-reflection coated end of the crystal and a 100% reflection back mirror when the light intensity reaches a threshold value depending upon the absorption of the bleachable filter. These materials reversibly bleach out, allowing a series of pulses to be obtained with a very short period, of the order of 100μsec between pulses. The Q-switch system used in this program is shown schematically in Figure 4. A Korad standard grade ruby rod was used for the laser material. A Korad dye cell with a 100% reflecting dielectric coating on its rear

Lt Col Dan Brown
USAF
SAM Records
Suitland
92A-5270

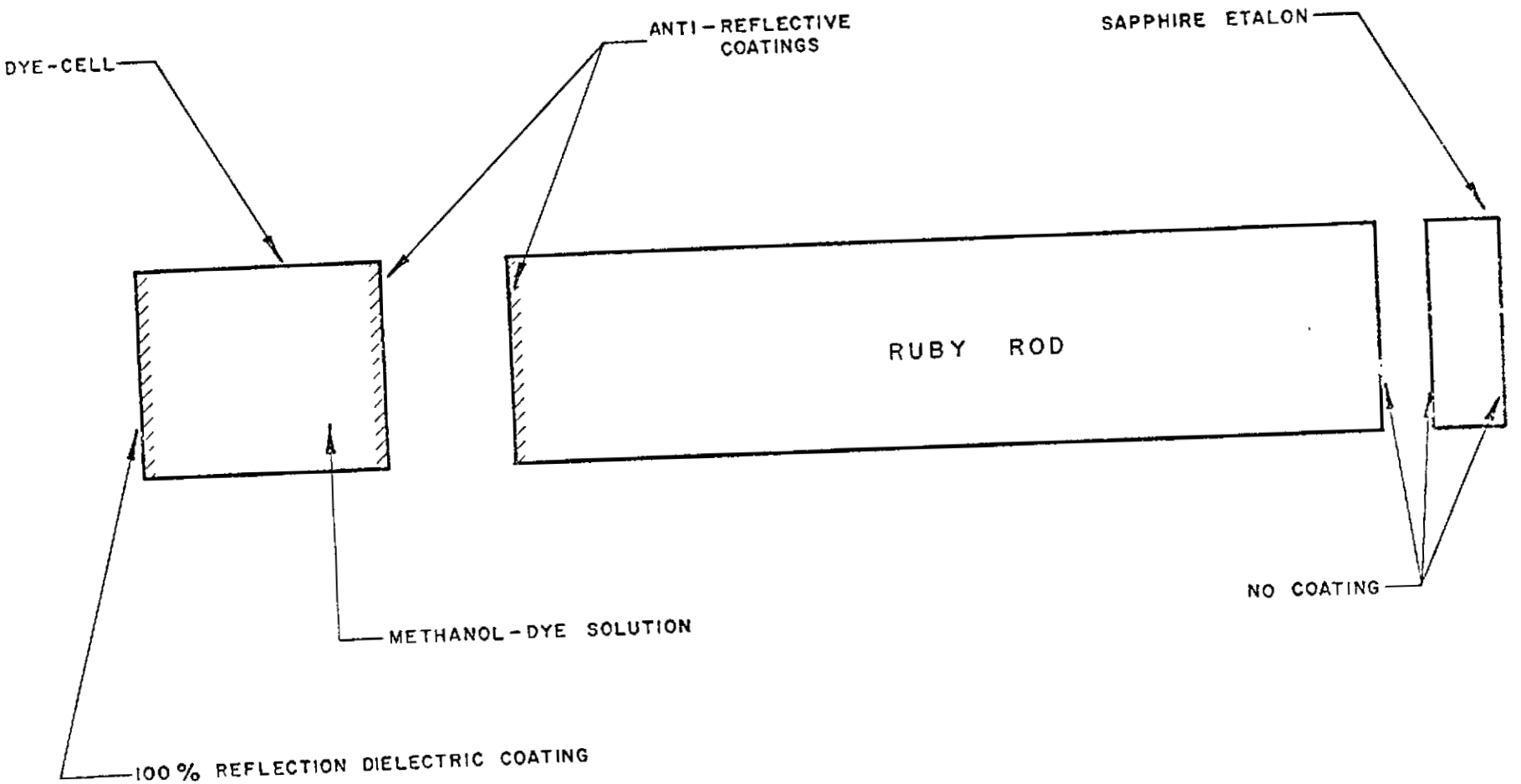

Figure 4. Q-switch System.

Lt Col Dan Brown
USAF
SAM Records
Suitland
70-A-5270

surface and a sapphire etalon were used for the resonator cavity. Experiments were performed using different dye solutions to determine the stability and reproducibility of pulses. The final solution chosen was cryptocyanine mixed with methanol. The transmission of the solution relative to pure methanol was determined to be 50% at 6943 Å. With this particular methanol dye solution, it was found that Q-switching and semi-Q-switching could be attained simply by lowering or raising the flash lamp energy levels, respectively.

The Q-switch pulses were detected with a SGD-100 photodiode with a 91 ohm load resistor. The signal from the photodiode circuit was passed into a Tektronix 555 oscilloscope through a 50 ohm terminator. The waveform appearing on the CRT was photographed with an oscilloscope camera. Unfortunately, even using Polaroid 10,000 ASA film, a photograph suitable for reproduction could not be obtained due to the high sweep speed of the CRT beam. Nevertheless, the pulse width and amplitude could be determined quite readily from the original photographs. The pulse width of the Q-switch pulse at the 50% power points was determined to be 30 nanoseconds.

As stated earlier, semi-Q-switching can be obtained simply by raising the pumping energy relative to that needed for Q-switching. By raising the pumping energy above the Q-switching threshold level, the

Lt Col Dan Brown
USAF
SAM Records
Suitland

dye solution is forced to behave as a free running on-off switch. The system will continue to emit pulses as long as a sufficiently high level of pumping energy is available to the ruby rod so that equilibrium may be reached between pumping and the loss due to lasing action. Typically, it was found that each pulse in the semi-Q-switched train was 30 nanoseconds at the 50% power points, and the pulses were separated by 30 to 150 microseconds. The number of pulses in the wave train could be varied from 2 to 50 individual pulses. The amplitudes of the individual pulses were unequal and varied over a range of 6:1 for a given wave train.

3. CALIBRATION

A Korad K-J2 liquid calorimeter was used as the primary standard for calibrating the ruby laser. The manufacturer stated that the calorimeter response has an accuracy of ± 3% and is traceable to a National Bureau of Standards calibrated detector. The calorimeter contains a fluid absorption cell which converts the incident radiation into heat and a thermopile which responds to the consequent temperature rise with a voltage signal (see Figure 5). The output of the calorimeter was continuously recorded with a Brush Mark 280 strip chart recorder coupled to the output of a Keithley 150B microvoltmeter. The recorder was calibrated against the voltage ranges on the microvoltmeter. Thus, an accurate value of the peak calorimeter response was obtained. The

Lt Col Dan Brown
USAF
SAM Records
Suitland
72A-5270

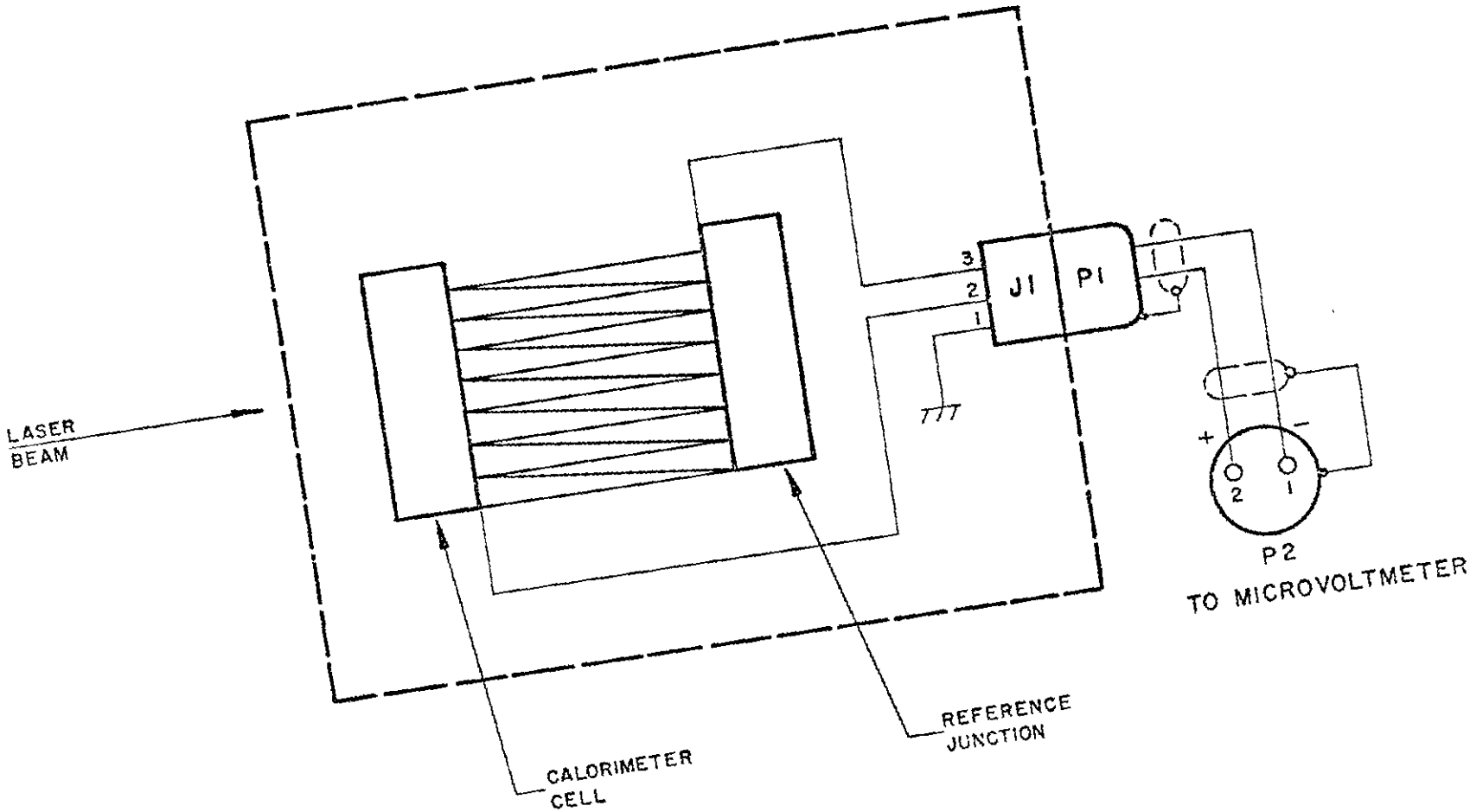

Figure 5. Electronic Diagram of Korad Calorimeter

arrangement of the calibration equipment is shown in Figure 6.

The calorimeter system was cross calibrated against a Barnes thermopile using the Zeiss photocoagulator as a light source. The thermopile calibration is also traceable to a NBS standard detector. The comparison between the two standard detectors showed a 5% difference.

The value of the laser energy, U_B, is obtained by multiplying the peak recorder reading, V_p, by the specific response, R, of the calorimeter. Hence,

$$U_B = R \cdot V_p, \tag{1}$$

where

U_B is beam energy in joules,

V_p is peak voltage in microvolts, and

R is specific response in joules/microvolt = 0.055 j/μv.

3.1 Cross Calibration of the Monitoring Photodiode

3.1.1 Long Pulse Mode

The monitoring photodiode was cross calibrated against the calorimeter by means of the system shown in the block diagram of Figure 2. With this arrangement, the photodiode response is related to the beam irradiance at the entrance port of the calorimeter by:

$$H(t) = C_1 V_D H(t) + C_2 \tag{2}$$

Lt Col Dan Brown
USAF
SAM Records
Suitland
[illegible]

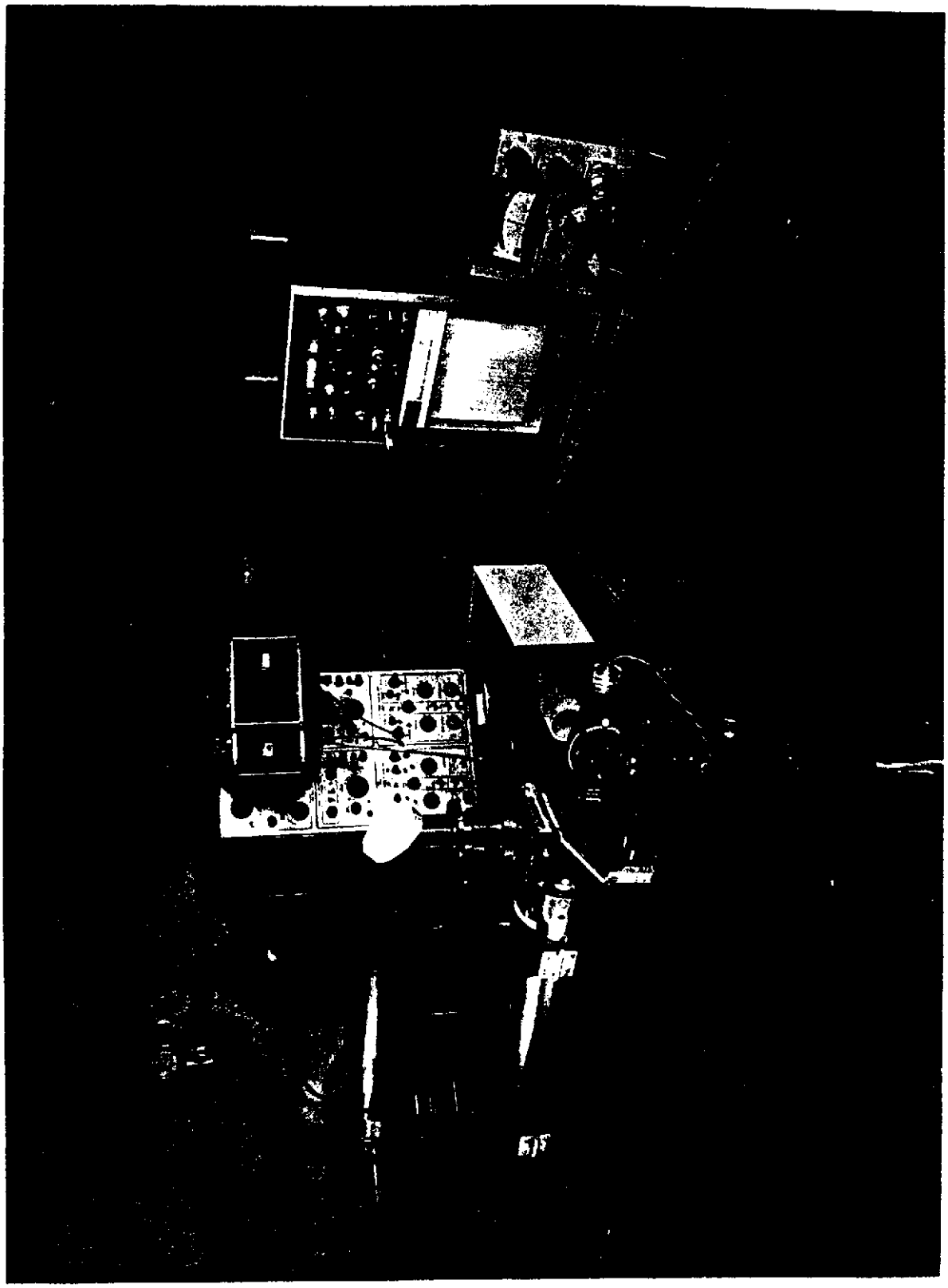

Figure 6. Calibration equipment and arrangement.

Lt Col Dan Brown
USAF
SAM Records
Suitland
FOA-5770

where

$H(t)$ = time varying beam irradiance (joules/cm^2-sec),

$V_D(H, t)$ = instantaneous photodiode response to beam irradiance (mv),

C_1, C_2 = proportionality constants, and

t = time.

The relationship between the photodiode response and the CRT trace recorded on film is given by:

$$V_i = C_3 \int_0^T V_D(H, t)dt \tag{3}$$

where

V_i = trace peak on film (volt · sec), and

C_3 = proportionality constant.

Substituting $V_D(H, t)$ from equation (2) into equation (3) yields:

$$V_i = \frac{C_3}{C_1} \int_0^T [H(t) - C_2]\, dt \tag{4}$$

$$V_i = \frac{C_3}{C_1} \int_0^T H(t)dt - \frac{C_2 C_3}{C_1} \int_0^T dt \tag{5}$$

$$V_i = \frac{C_3}{C_1} \int_0^T H(t)\, dt - \frac{C_2 C_3}{C_1}\, T, \tag{6}$$

where

T = pulsewidth in seconds.

From the definition of radiant exposure, (Q):

Lt Col Dan Brown
USAF
SAM Records
Suitland
FOA-5270

$$Q = \int_0^T H(t)\, dt\,. \tag{7}$$

Substituting (7) into (6) gives:

$$V_i = \frac{C_3}{C_1} Q - \frac{C_2 C_3}{C_1} T. \tag{8}$$

Rearranging equation (8) for Q gives:

$$Q = \frac{C_1}{C_3} V_i + C_2 T. \tag{9}$$

The total beam energy is defined by

$$U_B = Q \cdot A_B \tag{10}$$

where

A_B = area of the beam entering the calorimeter.

Substituting equation (9) into equation (10) for Q produces:

$$U_B = [\frac{C_1}{C_3} V_i + C_2 T]\, A_B. \tag{11}$$

By equating the right sides of equation (11) and (1):

$$R \cdot V_p = [\frac{C_1}{C_3} V_i + C_2 T]\, A_B \tag{12}$$

or

$$V_p = [\frac{C_1}{C_3} V_i + C_2 T] \frac{A_B}{R}. \tag{13}$$

If a constant beam area and a fixed pulsewidth are assumed, then equation (13) becomes:

$$V_p = C_4 V_i + C_5 \tag{14}$$

Lt Col Dan Brown
USAF
SAM Records
Suitland
[illegible]

where

$$C_4 = \frac{A_B C_1}{R C_3} \qquad \text{and} \qquad C_5 = \frac{A_B C_2 T}{R} .$$

Thus, a linear relationship exists between the integrated photodiode response and the peak voltage from the calorimeter. Substituting equation (14) into equation (1) yields:

$$U_B = R\,[C_4 V_i + C_5]. \tag{15}$$

Assuming that the whole beam enters the animal's eye during an exposure, the retinal incident energy, U_R, is determined by:

$$U_R = U_B \times T_e, \tag{16}$$

where

T_e = transmission of the animal's eye.

Substituting equation (15) into equation (16) gives:

$$U_R = T_e\, R\,[C_4 V_i + C_5]. \tag{17}$$

Equation (17) is the basic equation used to determine the incident, retinal energy. The constants C_4 and C_5 were experimentally determined prior to each experimental session, and C_5 was found to be = 0. .For a given experiment, both the beam divergence and pulsewidth were held constant.

Once the retinal energy (U_R) has been determined, a straightforward calculation yields the corresponding retinal irradiance (H_R). The average retinal irradiance for an exposure is given by:

$$\overline{H_R} = \frac{U_R C}{A_R T} . \tag{18}$$

LtCol Dan Brown
USAF
SAM Records
Suitland
AQA-5271

where

U_R = incident retinal energy (mj) determined from (16),

T = total exposure duration (sec) determined from pulsewidth,

C = conversion constant, $\frac{1.0 \text{ cal} \times 10^{-3}}{4.186 \text{ mj}}$, and

A_R = retinal area exposed. Defined by

$$A_R = \pi f^2 (\tan \theta/2)^2, \tag{19}$$

where

f = 1.0 cm for rabbit, 1.35 cm for primate, and

θ = beam divergence (degrees).

3.1.2 Q-Switched and Semi-Q-Switched Mode

The total energy in either mode was determined by cross-calibrating a photodiode against the Korad calorimeter system. In these two modes, semi-Q and Q-switched, the sum of the peak photodiode response(s) was found to be proportional to the total energy measured by the calorimeter. Once the proportionality constant was determined, the incident retinal energy of each exposure could be ascertained.

3.2 Beam Divergence Calibration

In order to calculate the average irradiance, the beam divergence θ, must be known. The beam divergence is changed in the laser system by varying the size of an adjustable iris diaphragm which was calibrated in terms of the beam divergence angle.

Lt Col Dan Brown
USAF
SAM Records
Suitland
70-A-5711

Calibration was accomplished using an oscilloscope camera with the lens removed. This camera was positioned to intercept the beam so that photographs of the beam could be made at various iris settings. Measurements of the beam diameter, d, were made from the photographs. Using the geometry and designations of Figure 7, the beam divergence θ was calculated. A graph of the beam divergence, θ, versus the iris setting was made and a least squares fit of the data yielded the equation

$$\theta = 2.97\,P + 0.39^{\circ}, \tag{20}$$

where P = a unitless number indicating iris position. The results are shown in Figure 8.

3.3 Dependance of Pulsewidth on Flashlamp Energy

The pulsewidth is dependent upon the energy delivered by the flashlamps and absorbed by the ruby rod. Flashlamp energy levels are dependent upon the charge voltage of the capacitor bank according to the equation:

$$E = 1/2\ CV^2$$

where

E = stored energy (joules)

C = total capacitance (farads)

and

V = charge voltage (volts).

Lt Col Dan Brown
USAF
SAM Records
Suitland

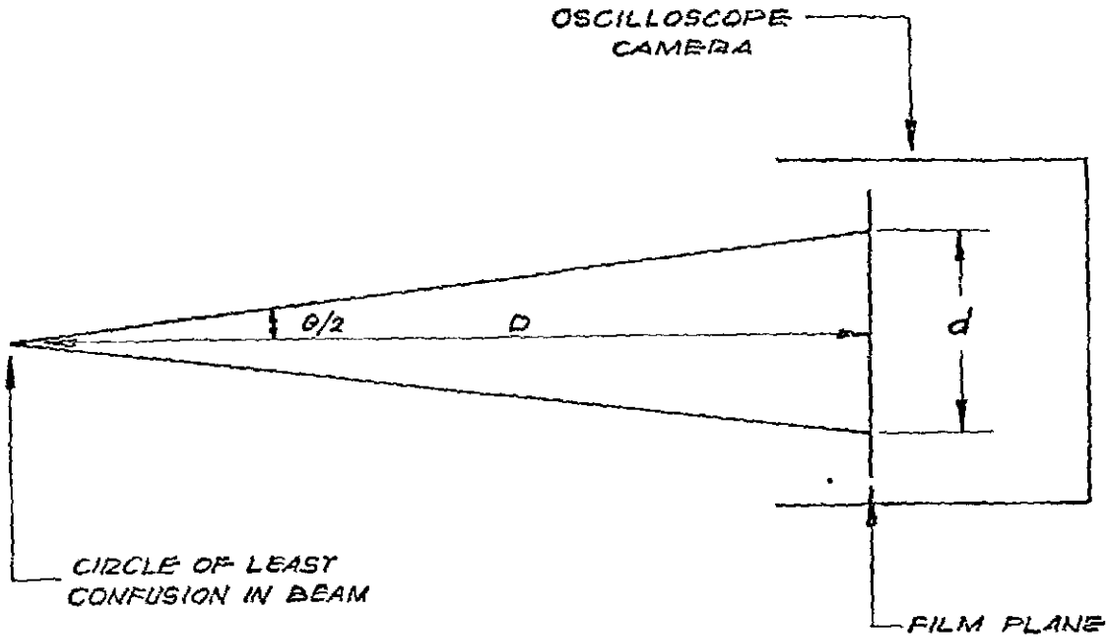

Figure 7. Schematic of beam geometry

Lt Col Dan Brow
USAF
SAM Records
Suitland
70-A-5270

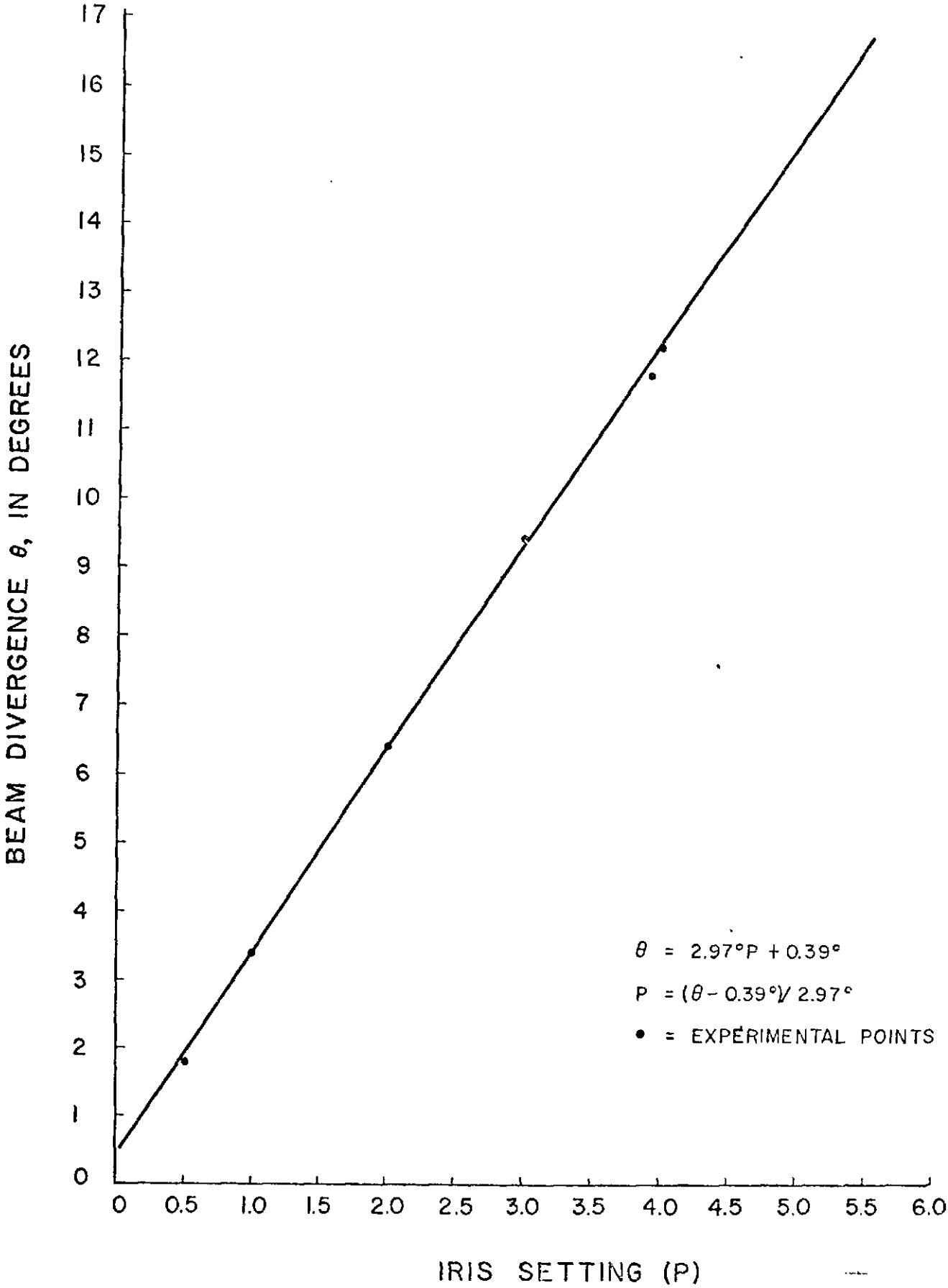

Figure 8. Iris setting versus beam divergence.

Lt Col Dan Brown
USAF
SAM Records
Suitland

The capacitor bank is composed of a total of six, 375μf, oil filled capacitors in parallel. For long pulse calibration and threshold determination, all six capacitors were available. Therefore, C = 2250 x 10^{-6} farads, and the flashlamp energy equation becomes

$$E = 1.125\,V^2 \times 10^{-3} \text{ joules.}$$

Flashlamp energies between 2700 joules and 4960 joules were delivered to the ruby rod. The corresponding pulse width range was between 0.46 msec and 1.45 msec.

For the Q-switched and semi-Q-switched modes, one capacitor was removed. Therefore, C equals 1875 x 10^{-6} farads, and the flashlamp energy equation becomes:

$$E = 0.9375\,V^2 \times 10^{-3} \text{ joules.}$$

The semi-Q-switched flashlamp energy, E, equaled 3380 joules. For the Q-switched mode, the flashlamp energy equaled 2630 joules. A single Q-switched laser pulse, and each of the pulses in the semi-Q-switched pulse train, were approximately 30 nanoseconds long at the 50% power points.

4. EXPERIMENTAL PROCEDURE AND RESULTS

Five-minute thresholds were determined by successive irradiation of the fundus with pulses decreasing in 5% to 10% energy steps until the "no-burn" stage was reached. The threshold levels reported represent the ave

Lt Col Dan Brown
USAF
SAM Records
Suitland
92A-5211

of the minimal energy value (mj) required for the production of a burn and the next lower exposure in the sequence which did not produce a burn. A period of at least 5 minutes elapsed between successive exposures.

Laser exposures with successively decreasing energy produced a series of lesions each of which was less severe and required more time for development than the preceding one. However, the maximum exposure producing no burn within 5 minutes almost always produced a burn within about an hour. Manifestations of supra threshold exposures in both rabbit and primate fundi were similar. An immediate burn, well above threshold, appeared to be a homogeneous white circular spot the same size or slightly larger than the irradiated area. As the energy levels decreased, the burns developed as collections of irregular darkened areas, each having a definite white center. With further energy decrements these darkened areas became smaller and fewer, requiring more time for development. The relative size of the white center of each dark area became progressively smaller. The "no-burn" was reached when the only evidence of exposure after five minutes of observation was one or two small areas of darkening. No white or grey-white was observed in the no-burn area of exposure.

It was observed in the primate white light study with the Zeiss photocoagulator that if a burn developed within 5 minutes, it developed immediately.

Lt Col Dan Brown
USAF
SAM Records
Suitland

Gradual development within the five minutes was seldom observed. This did not hold true in the laser investigation.

4.1 Long Pulse Rabbit and Primate Extrafoveal Thresholds

Ophthalmoscopic observation permitted the baseline selection of rabbits having uniform choroidal pigment and clear media. Rabbits weighing less than 2.3 kg, were not used since there was some indication from past observations that young rabbits have significantly lower retinal thresholds than adult rabbits. About one hour prior to exposure the animal's eyes were dilated with 1% atropine sulfate ophthalmic solution, and about half an hour before the experiment, the animal was anesthetized with 75-150 mg sodium Nembutal. Care was taken throughout the experiment to avoid corneal dehydration by frequent lavage with normal saline or simulated tears.

Twenty rabbit eyes were exposed to normal mode laser pulses (1.3 msec). Beam divergences of 6.1° and 3.0°, corresponding to image diameters of 1.07 and 0.52 mm, were investigated. Table I summarizes the threshold data for rabbits exposed to normal mode ruby laser pulses. The standard deviation is given in parenthesis after each threshold value. Tables A-I and A-II in Appendix A list the individual data.

Approximately 8-pound Macacca mulattas were used for the

Lt Col Dan Brown
USAF
SAM Records
Suitland

Table I. Rabbit and primate retinal burn thresholds, using long pulse laser exposures.

Image diameter (mm)	Number of Eyes	Exposure duration (msec)	Average thresholds	
			$\overline{Q_R}$ (cal/cm^2)	$\overline{H_r}$ (cal/cm^2-sec)
		[Rabbit]		
1.07	10	1.3	0.27 (± 0.05)	210 (± 38)
0.52	10	1.3	0.41 (± 0.12)	312 (± 95)
		[Primate]		
1.20	6	1.2	0.07 (± 0.01)	55 (± 6.9)
0.59	5	0.98	0.06 (±0.001)	64 (± 0.94)
0.29	6	1.4	0.17 (± 0.03)	122 (± 20)

LtCol Dan Brown
USAF
SAM Records
Suitland
[illegible]

primate study. Ophthalmoscopic examination provided a means of screening the animals and any exhibiting defective corneas, or opacities in the ocular media were not used. Preliminary sedation with an intramuscular injection of approximately 4 mg of Sernylan was followed by irridal dilitation with 1% atropine sulfate ophthalmic solution. A 17-gauge intraveneous catheter was introduced into a posterior superficial leg vein, and after the attainment of maximal mydriasis, the primate was anesthetized with 50 mg sodium Nembutal via the intracath. Deep anesthesia was maintained by the administration of additional small amounts of Nembutal as needed. Corneal dehydration was prevented using the same technique as that used with rabbits.

Seventeen primate eyes were exposed with beam divergences of 5.09°, 2.50° and 1.23°, corresponding to image diameters of 1.20, 0.59 and 0.29 mm. Table I also summarizes the threshold data for primates exposed to the normal ruby laser pulses (0.98 to 1.4 msec). The standard deviation is given in parenthesis after each threshold value. Tables A-III through A-V in Appendix A list the individual data.

4.2 Primate Thresholds for Q-Switched and Semi-Q-Switched Exposures

During exposure to the Q-switched and semi-Q-switched laser pulses, the primate eyes were dilated with Mydriacyl, 1%. Mydriacyl is not as long acting as atropine, but seems to decrease the severity of corneal dehydration.

Lt Col Dan Brown
USAF
SAM Records
Suitland

Thresholds for the Q-switched pulses were determined for 3 eyes, at a beam divergence of 5.08°. Thresholds for the semi-Q-switched pulses were determined in 4 eyes at 5.08° and 3 eyes at 2.50°. The semi-Q-switched pulses used the threshold determinations consisted of 4 to 8 individual pulses. The results of the experiment are summarized in Table II. The individual data are listed in Tables A-VI through A-VIII in Appendix A.

5. CONCLUSIONS

The comparison of Zeiss photocoagulator (white light) and laser thresholds for rabbits and for primates is summarized in Table III in terms of average retinal exposure, $\overline{Q_R}$. The white light data for rabbits are taken from the Final Report for Contract AF 41(609)-3099.[2] The white light data for primates are taken from Part II of this report. In performing the calculations of the retinal exposures, transmittance values of 0.59 for the primate eye and 0.89 for the rabbit eye were used. This value for the primate eye was obtained using the measurements of the direct spectral transmission made by Boettner[6] and the distribution of the xenon source. The rabbit eye transmission value was obtained from measurements made by Geeraets, et al.[7] of the total light transmitted by the rabbit eye. This value was used throughout the Zeiss photocoagulator study of rabbit thresholds.[2]

Lt Col Dan Brown
USAF
SAM Records
Suitland

Table II. Primate retinal burn thresholds: Q-switched and semi-Q-switched exposures.

Image Diameter (mm)	Eyes per Point	Number of Pulses	Average Threshold Q_R(cal/cm^2)
1.20	3	1 †	0.02
1.20	4	4-6	0.07
0.59	3	5-8	0.12

† Q-switched exposure

Lt Col Dan Brown
USAF
SAM Records
Suitland
[illegible]

Table III. Comparison of laser long pulse and Zeiss photocoagulator (white light) burn thresholds.

LASER			ZEISS		
Image diameter (mm)	Average duration (msec)	Average $\overline{Q}_R$ (cal/cm^2)	Image diameter (mm)	Average duration (msec)	Average $\overline{Q}_R$ (cal/cm^2)
		[Rabbit]			
1.07	1.3	0.27 (±0.05)	1.07	1.0	0.21 (±0.03)
0.52	1.3	0.41 (±0.12)	0.52	1.0	0.23 (±0.05)
		[Primate]			
1.20	1.2	0.07 (±0.01)	0.72	2.0	0.10 (±0.003)
0.59	0.98	0.06 (±0.001)	0.35	2.0	0.07 (±0.003)
0.29	1.4	0.17 (±0.03)	0.25	2.0	0.17 (±0.01)

Lt Col Dan Brown
USAF
SAM Records
Suitland

Inspection of Table III indicates that the thresholds for laser and white light exposures do not appear to be different for the two sources for either species.

Comparison of the results shown in Table II with those of Table III indicates that the average threshold retinal exposure, $\overline{Q_R}$, for the semi-Q-switched, and normally pulsed laser are in reasonable agreement for the 1.20 mm image diameter for primates. The data for the 0.59 mm image diameter are more divergent with a Q_R of 0.062 cal/cm^2 for the long pulse and 0.12 cal/cm^2 for the Q-switched case.

The Q-switched primate data showed more than a factor of 3 lower threshold exposure than the semi-Q-switched case for the 1.20 mm image diameter. This result could be indicative of a thermal-mechanical damage process as opposed to a thermal damage in the semi-Q-switched and long pulse laser exposures. However, the problems inherent in calibration of exposures as short as 30 nanoseconds must be considered in making any direct comparisons. Every effort was made to reduce the time constants of the recording circuits to insure valid measurements of the pulse energies, but the possibility remains that the low threshold found for the Q-switched case may be the result of inaccurate calibration.

Lt Col Dan Brown
USAF
SAM Records
Suitland

6. REFERENCES

1. Alexander, T.A., R.G. Allen, R.L. Bessey, et al., "Research on Ocular Effects Produced by Thermal Radiation," Final Report on Contract AF 41(609)-2906 for USAF School of Aerospace Medicine, 1966.

2. Allen, R.G., W.R. Bruce, K.R. Kay, et al., "Research on Ocular Effects Produced by Thermal Radiation," Final Report on Contract AF 41(609)-3099 for USAF School of Aerospace Medicine, 1967.

3. Miller, N.D., W.R. Bruce and M.G. Smith, "Retinal Burn Thresholds in Primates," Interim Report on Contract AF 41(609)-68-C-0023 for USAF School of Aerospace Medicine, 1968.

4. Laser Technology and Applications, Marshall, S.L., Editor, Semi-Conductor Products and Solid State Technology, Cowan Publishing Corporation, McGraw-Hill Book Company, New York, N.Y., 1968, p. 59.

5. Farrer, D.M., E.S. Graham, W.T. Ham, Jr., et al., "The Effect of Threshold Macular Lesions and Sub-Threshold Macular Exposures on Visual Acuity in the Rhesus Monkey," Submitted for publication in the Journal of American Industrial Hygiene Association, 1969.

6. Boettner, E.A., "Spectral Transmission of the Eye," Final Report on Contract AF 41(609)-2966 for USAF School of Aerospace Medicine, 1967.

7. Geeraets, W.J. and E.R. Berry, " Ocular Spectral Characteristics as Related to Hazards from Lasers and Other Light Sources," Am. J. Ophthal., 66, 15-20, 1968.

Lt Col Dan Brown
USAF
SAM Records
Suitland

II. RETINAL BURN THRESHOLDS IN PRIMATES

by

Norma D. Miller, William R. Bruce and Margaret G. Smith

1. INTRODUCTION

A large amount of data on retinal burn thresholds in rabbits has been previously reported. Under Contract AF 41(609)-3099 with the USAF School of Aerospace Medicine, the Life Sciences Division of Technology Incorporated performed a long series of experiments in which 615 thresholds were determined for sixty-six combinations of exposure durations and image diameters.[1] The rabbit data, however, do not allow valid extrapolation for human threshold predictions due to the species differences in anatomical structure, and in the quality of the optical image at the retina. The present study, using primates, was undertaken to replicate some of the threshold conditions investigated in the rabbit study in order to compare the thresholds for the two species. The primates used were approximately 8-10 pound Macacca mulatta. The entire visual structure of this species is morphologically closer to that of the human than is the rabbit. Man shares with the species investigated certain characteristic retinal structures such as: (1) retinal blood vessels anterior to the receptor layer, (2) both rod and cone receptors with

Lt Col Dan Brown
USAF
SAM Records
Suitland

a well-defined foveal area, and a larger macular area. These characteristics are not present in the rabbit. The focal length of the monkey eye is about 35% longer than the rabbit eye, but only 80% as long as the average human eye; however, the optical structure of the monkey's image forming media is scaled proportionally so that the entire image quality is close to that of the human.

Throughout the rabbit retinal burn threshold investigation, a 5 minute criterion was used. The eye was irradiated and if a visible lesion appeared within 5 minutes, the next exposure was reduced by a few percent until a point was reached where no lesion appeared within 5 minutes. The threshold irradiance recorded was the average of the exposures producing a visible lesion and the next lower producing no visible lesion in 5 minutes. This criterion was abandoned in the case of the monkey because it was found that if a lesion was to appear in 5 minutes, it appeared almost instantaneously after the exposure. It was also observed that the 5 minute no-burn exposures became very noticeable lesions within a few hours following the irradiation, and that the 5 minute no-burn exposure left very noticeable scars in animals returned for reuse. An experiment was performed in which decreasing levels of irradiation were observed over long periods of time. The observations were made hourly up to 5 hours and again at 24 hours. It was found that if a lesion did not develop within 5 hours, it rarely appeared at a later

Lt Col Dan Brown
USAF
SAM Records
Suitland
[illegible]

time. As a result of this, a 5 hour criterion was adopted for the primate threshold burn study.

In the current investigation, two different types of thresholds were determined for the monkey eyes, the extramacular thresholds and the foveal thresholds. Exposure durations from 2 msec to 1 sec were used for both types of thresholds. The image diameters ranged from 0.12 mm to 1.46 mm in diameter, assuming a focal length of 1.35 cm^2.

2. EXPERIMENTAL PROCEDURE

The animals were screened by careful ophthalmoscopic examination. Animals with defects or opacities in any portion of the media, including the cornea, were not used. Animals requiring more than ± 1 diopter ophthalmoscopic correction were not used. A 1% atropine sulfate ophthalmic ointment was introduced into the conjunctival sac on the evening preceding the threshold determinations. This produced maximally stable iris dilation with less corneal trauma than administration of either atropine, Cyclogel or neosynepherine drops prior to irradiation. The dehydration of the cornea was carefully avoided. The animal's eyes were kept closed except during actual aiming, irradiation and observation. Since under deep anesthesia, tearing is usually suppressed, the eyes were frequently flooded with "monkey tears" prepared to simulate the lachrymal secretion

Lt Col Dan Brown
USAF
SAM Records
Suitland

of the primate.

The primates were initially sedated with approximately 4.0 mg of Sernylan I.M. A 17-gauge intraveneous catheter was introduced into the posterior superficial vein in the leg. Approximately 1 cc of 50 mg/cc Nembutal was administered by way of the intracatheter. Irradiations were begun 45 minutes after administration of the Nembutal. The waiting period was carefully controlled after pilot studies indicated that the effect of initial anesthesia in many animals was to produce a falsely high 5 minute threshold. Later work indicated that it seemed to have no observable effect on the 5 hour thresholds which were adopted as the criterion; however, the 45 minute delay before starting exposures was continued. Additional Nembutal was administered in small increments as needed to maintain deep anesthesia. A total of 3 to 5 cc's were required per animal per day.

The flash source used in the primate study was identical to that used in the rabbit study, and has been previously described in detail.[3] The source was a Meyer-Schwickeraph photocoagulator, which had been modified for controlled pulsed operation. Aircraft batteries provided the power for the Zeiss coagulator for the pulse durations of 2 msec through 1 sec used in this investigation. The source was calibrated by an Eppley thermopile calibrated by the National Bureau of Standards.

Lt Col Dan Brown
USAF
SAM Records
Suitland

The thermopile was used to determine the total irradiance output of the Zeiss coagulator. The thermopile and an EG&G SD-100 photodiode were used simultaneously to record the irradiance output of the coagulator for a 10 sec pulse. Once the 10 sec baseline was established, the output of the photodiode was recorded for pulse widths less than 10 sec and cross calibrated against the thermopile.

Before each experimental session, a fundus photograph of the animal's eye was made on Polaroid film using a Zeiss fundus camera. This provided a photographic map of the animal's fundus as an aid in locating the various exposures for subsequent observation of the development of the burn lesion. For the actual exposures, the animal was placed in a restraining chair, and aligned in front of the Zeiss beam director where the eye could be examined using a modified Keeler ophthalmoscope. Initially, an estimate was made of an appropriate irradiance to produce a 5 minute burn based on the data from the rabbit study, and pilot studies on the monkeys. If an immediate lesion was formed, additional exposures were made reducing the irradiance by 5 to 10% increments and hourly observations of the fundus were made to determine the 5 hour threshold.

3. EXPERIMENTAL RESULTS

3.1 Time of Development of a Visible Lesion

Lt Col Dan Brown
USAF
SAM Records
Suitland

Early in the primate threshold burn studies, an effort was made to follow the course of development of burns to determine the lowest level of retinal exposure that would eventually develop into a visible lesion. Observations were made hourly for 5 hours and again at 24 hours in many cases. The irradiances were reduced by increments of about 5% from the 5 minutes burn thresholds to 60 or 70% of that threshold. The graphs in Figure 9 show the results of hourly observations following the exposures. The abscissae are the elapsed time in hours after exposure, and the ordinates are the percentage of the exposures showing as a visible lesion at each of the observation times. The encircled numbers indicate the number of exposures at the various irradiance levels.

The graph on the left indicates that the 5 minute burn criterion is a false criterion in terms of predicting the appearance of a visible lesion, inasmuch as 100% of the five minute no-burn exposures had converted into visible lesions in 4 hours. It is even more startling that 11.5% of exposures at a level 60-69% of the 5 minute threshold developed into visible lesions in 5 hours.

Ten animals were examined 24 hours after irradiation and in no instance was a lesion found that had not developed 5 hours after exposure. The data for the ten animals are listed in Table IV. The

Lt Col Dan Brown
USAF
SAM Records
Suitland

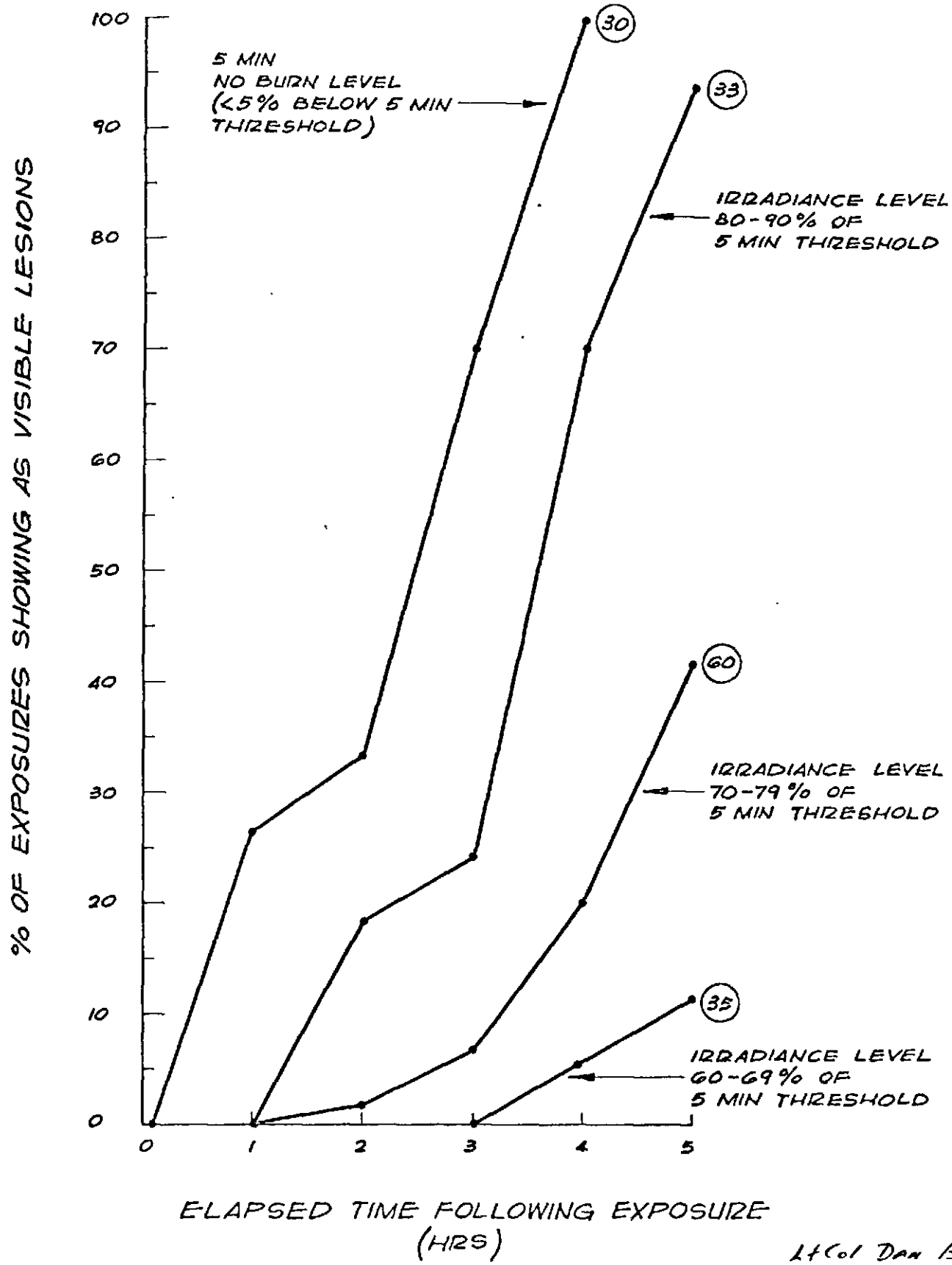

Figure 9. The time course of development of visible lesions in p following exposures to various irradiance levels.

Lt Col Dan Brown
USAF
SAM Records
Suitland

Table IV. Exposure irradiance in terms of the percent of the 5 minute threshold resulting in the 5 hour threshold for 10 monkeys. All eyes were examined 24 hours later and in no case did the 5 hour no burn exposure result in a visible lesion the next day.

Animal		5 hour visible lesion	5 hour no visible lesion	% difference
08E	R	67	63	4
	L	67	63	4
32D	R	74	63	8
	L	74	66	8
34D	R	76	71	5
	L	76	71	5
78D	R	82	78	4
	L	82	78	4
44D	R	80	75	5
	L	74	67	7
46D	R	78	74	4
	L	80	75	5
72D	R	80	75	5
	L	78	74	4
82D	R	81	74	7
	L	81	74	7
90V	R	77	73	4
	L	81	77	4
7P1	R	77	73	4
	L	89	84	[illegible]
MEAN		78	73	

Lt Col Dan Brown
USAF
SAM Records
Suitland
[illegible]

irradiance level for the 5 hour burn and 5 hour no-burn condition is given in terms of the percentage of the 5 minute burn threshold. The last column shows the percentage difference between the two exposures resulting in visible lesion and no visible lesion in 5 hours. The reduction in energy to 75% of the 5 minute threshold is a significant reduction in terms of predicting visible damage from radiation. The 5 hour burn criterion was used in the threshold determinations for the primate study. It is felt that it is a meaningful criterion in the sense that if no lesion develops in 5 hours, there is a very low probability that one will develop at a later period.

3.2 Extramacular Burn Thresholds

Thresholds were determined for 24 different combinations of exposure time and image diameter with a minimum of 12 eyes per threshold determination. The image diameters were 1.46, 0.72, 0.35, 0.25 and 0.12 mm, on the monkey retina. The exposure times were 2, 10, 40, 100 and 1000 msec, except for the 1.46 mm diameter image where the 2 msec exposure time did not produce a burn with the available energy. The results are summarized in Table V, showing the retinal irradiance for each of the threshold conditions in cal/cm^2-sec at the retina. The numbers in the small box at the right give the number of eyes used in the threshold determinations and the numbers in the larger box on the left give the standard deviations. A transmission

Lt Col Dan Brown
USAF
SAM Records
Suitland

Table V. Five hour extramacular burn thresholds for Macacca Mulatta. The values are the retinal irradiance in cal/cm^2-sec.

Image diameter mm	Exposure time (msec)									
	2		10		40		100		1000	
1.46			28		11		5.7		1.8	
			1.3	12	0.34	12	0.30	12	0.18	12
0.72	47		34		10		7.8		3.5	
	1.3	12	5.0	14	0.68	12	0.87	20	0.48	12
0.35	33		23		12		9.2		4.3	
	1.2	12	1.7	12	0.71	12	0.63	12	0.44	12
0.25	83		42		20		14		6.7	
	1.9	12	1.3	12	0.79	12	0.81	12	0.46	12
0.12	79		49		33		31		18	
	1.3	12	2.5	12	0.99	12	1.1	12	0.72	12

NOTE: The numbers in the small boxes give the number of monkey eyes used in obtaining the average retinal irradiance listed.

The numbers in the medium size boxes give the standard deviation (σ).

Lt Col Dan Brown
USAF
SAM Records
Suitland

factor of 0.59 was used for the ocular media in calculating these values.

3.3 Foveal Burn Thresholds

The area of the fovea is so small that a new technique had to be developed to define a burn threshold. In the first pair of eyes irradiated, one eye was exposed well above the estimated 5 hour threshold and one eye exposed well below the estimate. In the next pair of animals, an attempt was made to narrow this range based on the observations made on the first animals. The average data are for all three sets of points, or all three animals. The threshold so determined is actually an interocular threshold, that is, the threshold value is the average irradiance for the condition of one eye showing a burn lesion whereas the other eye exposed to a level some 10% to 20% below showing no burn lesion. The interocular thresholds are recorded in Table VI for the various combinations of image size and exposure durations used. A total of 57 animals were used to establish the interocular thresholds for 5 image diameters and 4 exposure durations.

4. DISCUSSION OF EXPERIMENTAL DATA

The primate extramacular threshold data for the 0.25 mm image diameter is shown in the upper curve of Figure 10; and the lower curve shows the foveal interocular burn thresholds for the same image size.

Lt Col Dan Brown
USAF
SAM Records
Suitland
92-5711

Table VI. Mean retinal irradiance H_r^{th} (cal/cm^2-sec) for production of "interocular foveal threshold" burns in rhesus monkeys. The numbers in brackets refer to the number of animals included in the mean.

Image diameter (mm)	Average Foveal interocular thresholds			
	Pulsewidth in msec			
	2 msec	10	100	1000
6.2° (1.46 mm)		20 (3)	5 (3)	1.3 (3)
3.07° (0.72 mm)	.35 (3)	26 (3)	5.7 (3)	2.4 (3)
1.47° (0.35 mm)	24 (3)	17 (3)	7.5 (3)	4.2 (3)
1.05° (0.25 mm)	65 (3)	32 (3)	10 (3)	5.3 (3)
0.52° (0.12 mm)	62 (3)	34 (3)	24 (3)	13 (3)

Lt Col Dan Brown
USAF
SAM Records
Suitland

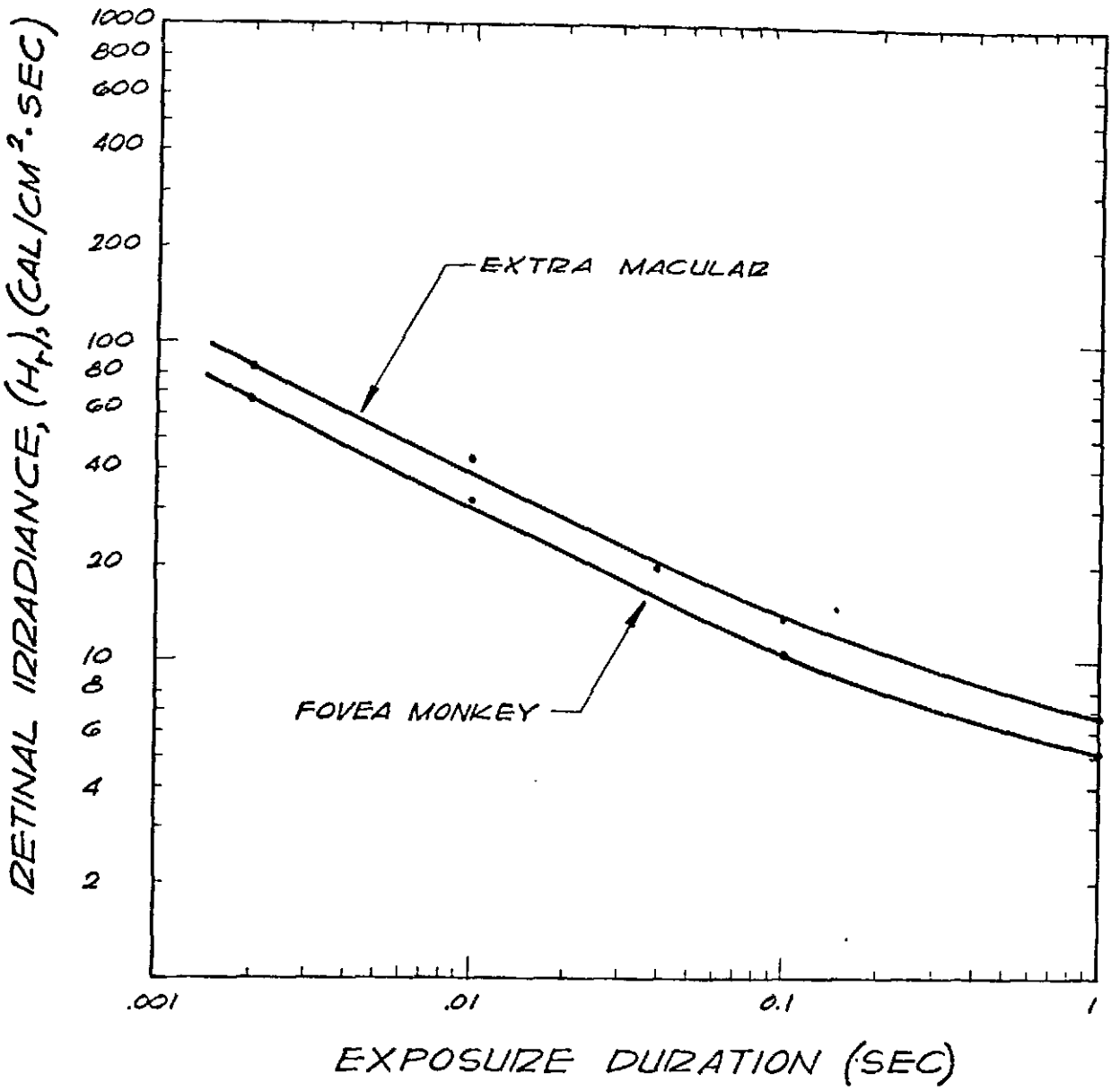

Figure 10. Comparison of foveal and extramacular thresholds for the 0.25 mm image diameter.

Lt Col Dan Brown
USAF
SAM Records
Suitland

The significant point in the comparison of the two curves is the consistent drop in threshold for the fovea as opposed to the extramacular portion of the primate eye. For all conditions of exposure duration and image size tested, the foveal threshold irradiance averaged 0.76 of the extramacular threshold level with a standard deviation of 0.044.

The primate extramacular burn thresholds are shown in Figure 11 for the 0.25 mm image diameter for comparison with the rabbit burn thresholds for 0.26 mm image. The rabbit data are taken from the Final Report for Air Force Contract AF41(609)-3099 of July 1967. The conditions as reported for the two species are not directly comparable so the data plotted in Figure 11 have been adjusted to provide a more valid comparison. The 5 minute burn criterion was used throughout the rabbit study and the 5 hour criterion was used in the primate study. The results listed in Table IV indicate that the 5 hour threshold irradiance is approximately 75% of the 5 minute threshold level for the primates. This value has been used to adjust the values in Table V to refer to a 5 minute criterion, similar to that used for the rabbit thresholds.

The average transmission for the rabbit eye was assumed to be 0.89 in performing the calculations of retinal irradiance throughout the rabbit study. The transmittance value was based on work by Geeraets, et al.,[4] who measured the total transmission of the eye. Later work by

Lt Col Dan Brown
USAF
SAM Records
Suitland
72A-5911

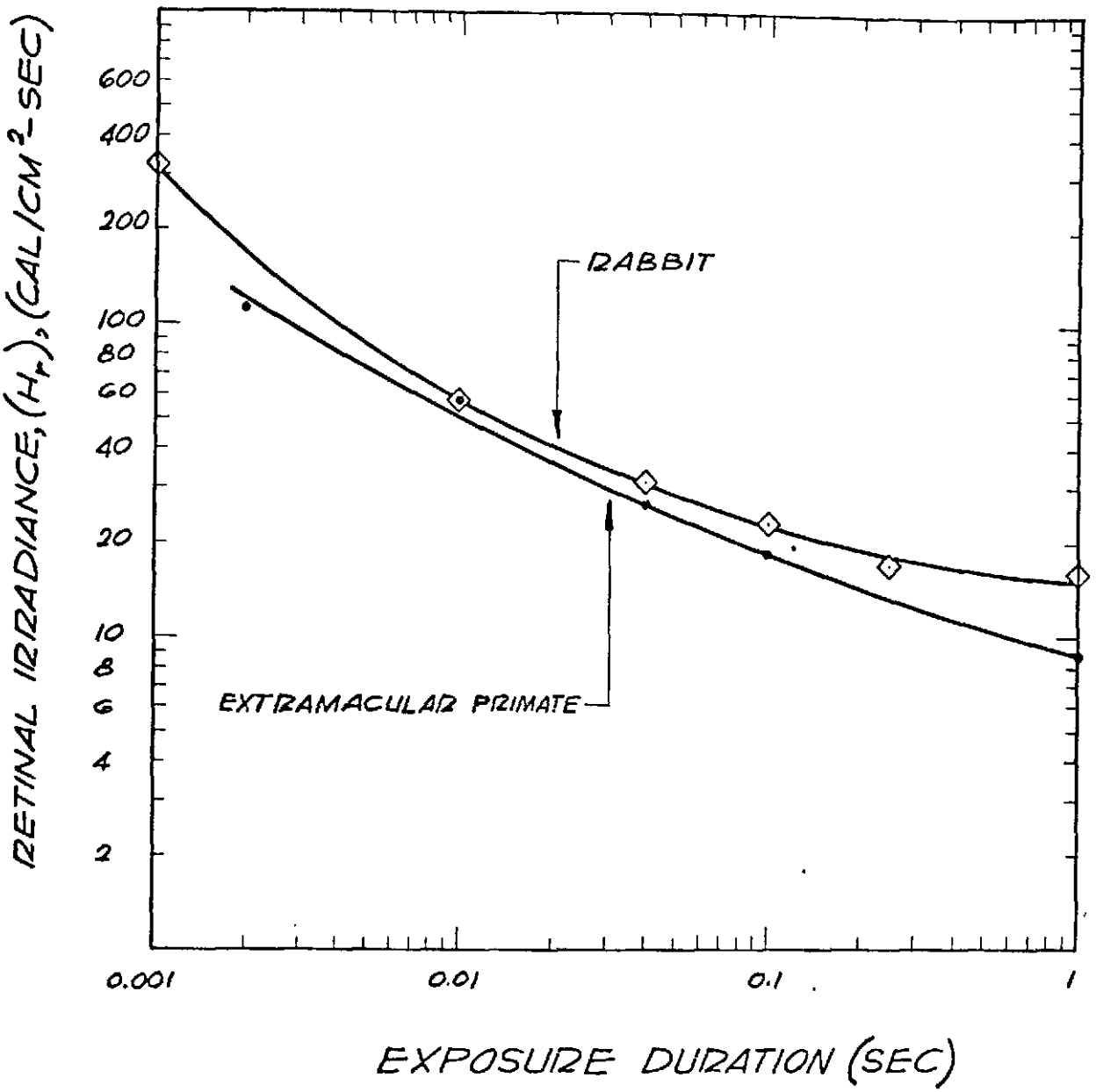

Figure 11. Comparison of rabbit and primate burn thresholds for 0.26 and 0.25 mm image diameters respectively. The primate data have been recalculated to represent the 5 minute burn criterion.

Lt Col Dan Brown
USAF
SAM Records
Suitland

Boettner[5] provided spectral transmission values for the direct image. On the basis of his work, an average transmittance of 0.59 for the xenon source of the Zeiss was adopted for the primate study. The rabbit data plotted in Figure 11 refers to a transmittance of 0.89 because this is the value used in all previous rabbit studies.

4.1 Beam Distribution for Zeiss Photocoagulator

A surprising inversion is apparent in the threshold data listed in Table V. The calculations of the retinal irradiance are based on the assumption of uniform beam distribution across the irradiated area. In fact, the entire calibration procedure is also based on the same assumption. Photographs of the beam for various exposing conditions were made with a 135 mm lens on a 35 mm camera to determine the degree of uniformity of the beam. The image on the film was a faithful reproduction of the intensity distribution at the plane of the field size cone and similar to that formed on the retina by the eye. The major differences in the two cases are: (1) the film image was more than 10 times larger than the retinal image due to the long focal length of the camera lens, and (2) the camera lens focuses all wavelengths in nearly the same plane, whereas there is strong longitudinal chromatic aberration in the eye.

The pictures were exposed through a series of neutral density

Lt Col Dan Brown
USAF
SAM Records
Suitland

filters, each photographic exposure was reduced by an increment of 0.1 density from the previous exposure. The roll of film was developed under controlled conditions to insure uniform development. The film was then contact-printed onto high contrast Kodalith film under carefully controlled exposure and development conditions to produce iso-density contour pictures. The extent of the area within the iso-density contours was measured and the relative intensity level calculated from the exposure data. The resulting beam distributions are shown in Figure 12 for the 3° cone size for steady state and pulsed operation. The relative intensities shown on the figure have been found by normalizing to the same average total irradiance.

The marked lack of uniformity in the pulsed condition as compared with the steady state condition provides possible explanation for the apparent inconsistencies in the threshold data. The calibration of the monitoring photodiode is performed by comparing its response for the steady state beam against a calibrated thermopile placed at the center of the beam. The monitoring photodiode receives light scattered within the lens mount tube and hence measures the average beam irradiance. The beam distributions shown in Figure 12 show that the central portion of the 3° beam has nearly the same central intensity for the same average value (as read by the monitoring photodiode) for

Lt Col Dan Brown
USAF
SAM Records
Suitland
92A-5274

3° CONE - STEADY STATE

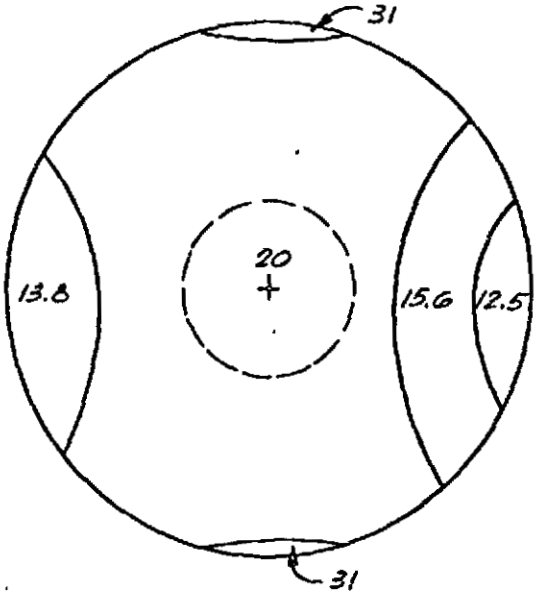

3° CONE - 4 MSEC

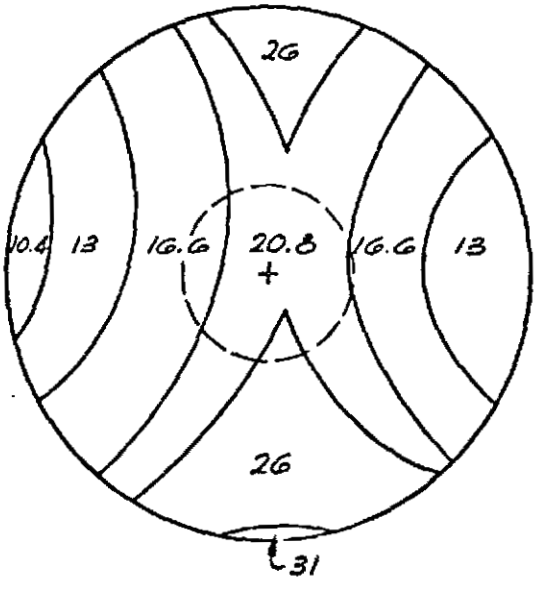

Figure 12. Relative intensity distribution across source image.

Lt Col Dan Brown
USAF
SAM Records
Suitland

both the pulsed and steady state conditions. However, the distribution is much more uniform for the steady state than for the pulsed condition.

Inspection of the data in Table V shows that the threshold irradiances for the long pulses increases as the image diameters decrease. A nearly uniform beam distribution insures that the cross calibration of the photodiode with the thermopile will provide accurate values of the irradiance for each cone size. A non-uniform distribution such as is obtained in the short pulses, will cause the photodiode calibration to vary as different portions of the beam are sampled with the various cone sizes. The dotted circles in Figure 12 show the portion of the beams that were sampled for calibration and for actual exposures for the 1° (0.25 mm) image diameter. The beam distribution is dependent upon the distance between the electrodes of the xenon arc for any pulse duration. In making the animal exposures, the electrodes are positioned to provide the most uniform steady state beam for 6°, and are repositioned for beam uniformity for the 3° cone when images smaller than 6° are used.

5. APPEARANCE OF THE BURN LESIONS AT VARIOUS TIMES FOLLOWING THE EXPOSURES

A few monkeys that had received extramacular 5 minute burn exposures were kept for a period of a year providing information on the

Lt Col Dan Brown
USAF
SAM Records
Suitland
70A-5271

appearance of the burned area over a long period of time. Some of the animals were sacrificed at the end of one year and histological sections of the irradiated area of the eye were prepared. Figure 13 shows a photomicrograph of such a section. The burn and no-burn areas of irradiation were viewed with an ophthalmoscope and photographed with a Polaroid camera. The same areas were localized in the formalin fixed excised eye with the aid of a dissecting microscope. Tissue blocks were cut to include the irradiated areas. Routine 8 micron parafin sections were cut and stained with hematoxylin and esosin.† Dr. Philip S. Coogan of the School of Aerospace Medicine examined the sections and described the pathology of the retinal lesions observed. The irradiated area that had developed into a lesion in 5 minutes showed the same pathological changes as an area that had received 10% lower irradiance and had not produced a visible lesion in 5 minutes. Figure 13 shows the typical appearance of the retinal defect. The primary histological characteristic of the lesion is the total absence of the outer segments and their nuclei; the outer nuclear layer. In the sections through the largest diameter of the lesion, the inner limiting membrane exhibits a central disruption that is an artifact. The extent of the lesion in the outer plexiform layer is difficult to assess and no definite changes are

†We wish to express our appreciation to M/Sgt. Vasys for the extremely skillful performance of the tissue processing.

Lt Col Dan Brown
USAF
SAM Records
Suitland
92A-5271

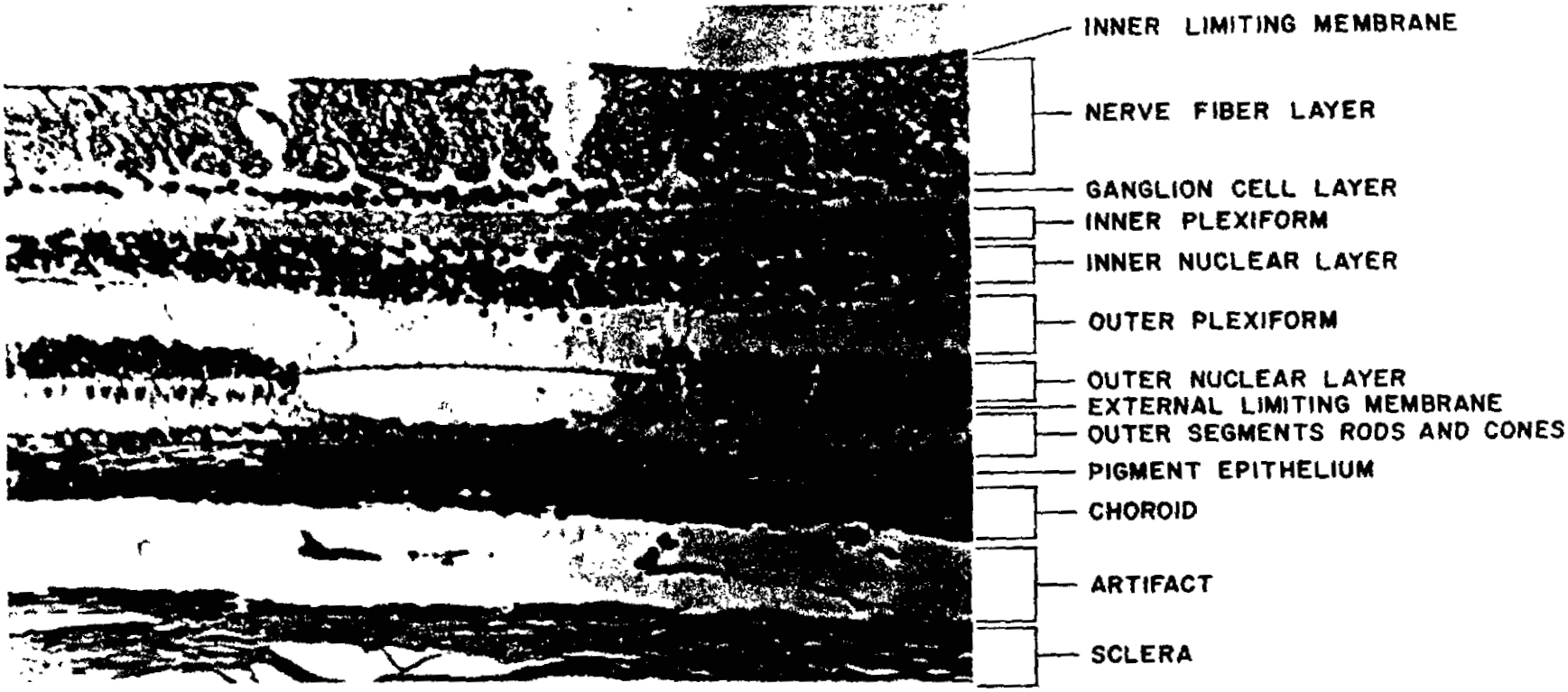

Figure 13. Section through a minimal burn lesion caused by exposure to white light. The lesion was produced one year before the animal was sacrificed.

Lt Col Don Brown
USAF
SAM Records
Suitland
[illegible]

observed in the inner nuclear and superior layers of the retina. The second histological characteristic of the lesion occurs in the retinal pigment epithelium. A portion of the pigment epithelium immediately beneath the retinal defect contains a marked increase in the number of pigment granules. On either side of this hyperpigmented region is an area of hypopigmentation. Ophthalmoscopically the lesions are observed as concentric light and dark rings, but as yet, the variations in pigment density in the pigment epithelium cannot be correlated with funduscopic observations. Although in the hyperpigmented areas the pigment granules appear abnormally large and spherical, the cells of pigment epithelium do not appear to be damaged.

On ophthalmoscopic examination immediately after exposure, the 5 minute burn appears bleached and mottled in the irradiated area. Five minutes later, according to the definition of the 5 minute burn, a white area appears and the area of white is sharply defined and rarely larger than the area irradiated. The white area often seems to develop from a central coalescing of small spots of bleaching or mottling. At the end of 5 hours, the entire irradiated area is white and the lesion appears to grow larger than the irradiated area; however, the edge is more diffuse than at the 5 minute period. A faint halo is seen surrounding the lesion. Twenty-four hours later, a ring formation has developed

Lt Col Dan Brown
USAF
SAM Records
Suitland

in the form of faint concentric rings. The white area turns to a dull gray, and there is still a faint halo present surrounded by a well-defined outer dark ring. At the end of two months, the outer ring is well-defined, the white area has become very dull gray, the halo usually has disappeared, and often, three or four rings are seen concentrically placed within the irradiated area. At the end of one year, there is a definite set of concentric light and dark rings with a well-defined center, and the total area involved seems to be larger even than at two months.

The appearance of the 5 hour burn is entirely different from the 5 minute burn. There is no change immediately, in fact, the fundus photographs are required as a map in order to find the irradiated area. There is still no visible change at the end of 5 minutes. At the end of 5 hours, however, a white center appears and is always much smaller than the irradiated area, but is very well-defined. There seems to be a small faint halo around the lesion but the total area of the lesion and the halo is less than the irradiated area. At the end of 24 hours, the white lesion is dull gray in color, and is surrounded by a darker ring. The faint halo is still usually seen. At the end of 2 months, there are no longer any well-defined rings. The center white area becomes a reddish-brown color. No animals have been examined as long as a year after a 5 hour burn.

Lt Col Don Brown
USAF
SAM Records
Suitland

5.1 Histopathology of Retinal Burns

Through the generous cooperation of Dr. Philip S. Coogan of the School of Aerospace Medicine, histological sections of irradiated retinal areas were prepared. Dr. Coogan examined the sections and described the pathology of the retinal lesions observed. His report is reproduced in the following Sections 5.1.1 and 5.1.2. This histological study was made possible by improvisations in tissue preparation and sectioning procedures. Staff Sargeant Fred Morris, SMBC, was in large part, responsible for these improvisations. Mr. Orville V. Anderson, SMSP, took the photographs.

5.1.1 Acute Retinal Burns

The retinal burns are sharply circumscribed bands of necrosis and/or edema involving the receptor cells, pigment epithelium and underlying choroid (Figure 14). Protein rich edema fluid mixed with fibrin is present within the band of necrosis and, at times, extends beyond, especially along the planes of the outer plexiform layer and the junction of the outer segments with the pigment epithelium. The nuclei of the rods and cones in the outer nuclear layer are pyknotic and fragmented. The external limiting membrane is not detected in the band of necrosis. The inner segments of the rods and cones are enlarged, foamy, irregular in outline and pale staining. The outer segments

Lt Col Dan Brown
USAF
SAM Records
Suitland

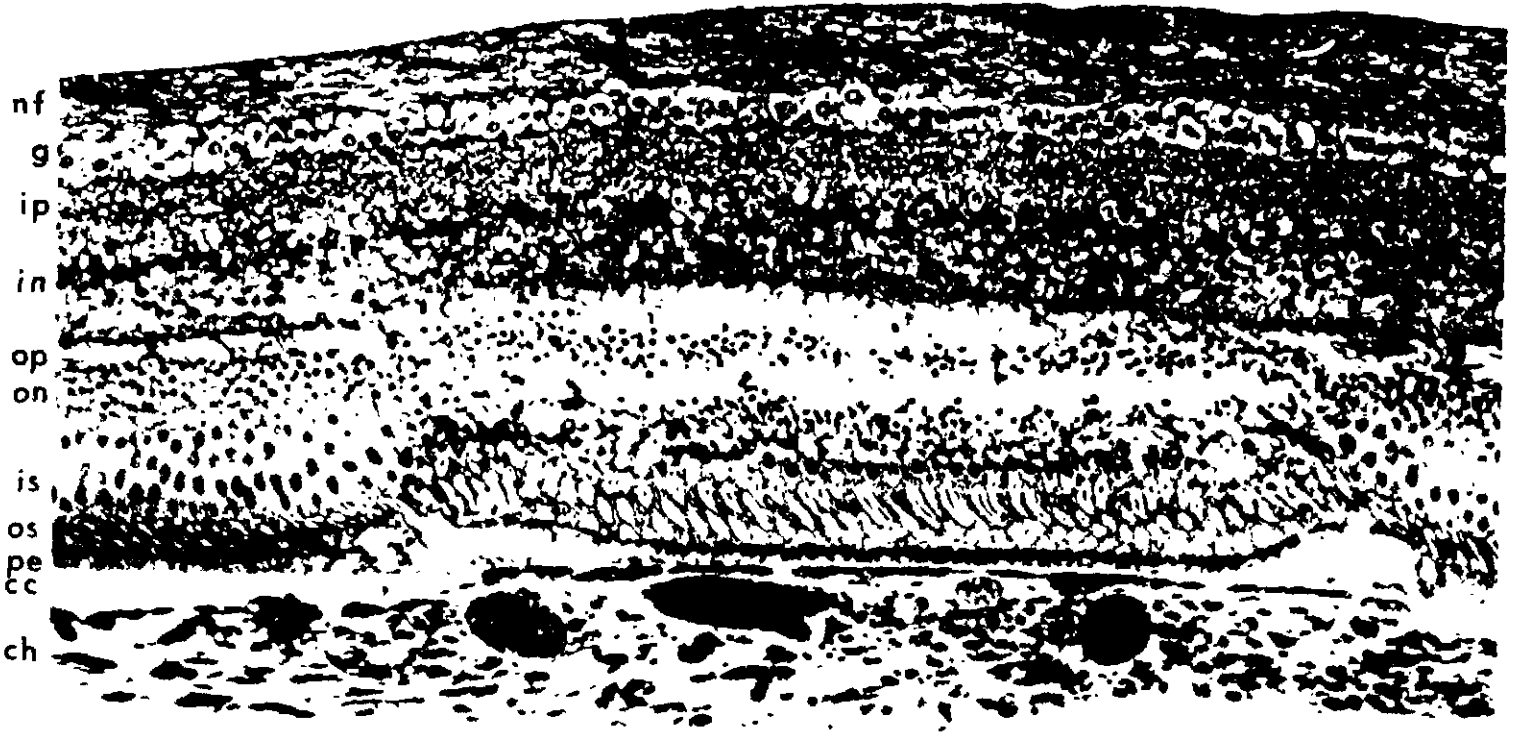

Figure 14. This illustrates a fresh retinal burn, 24 hours post exposure (3°cone, 100 msec, 9.6 cal/cm^2/sec). The receptor cells, pigment epithelium and choroid are necrotic and edematous. The receptor nuclei (on) are pyknotic and fragmented. The pigment epithelium (pe) in the center of the burn is coagulated and adheres to Bruch's membrane. At the burn margins, the pigment epithelium fragments and is displaced forward by edema. Edema fluid also dissects laterally about the axons of the outer plexiform layer (op). The choriocapillaris (cc) is occluded within the burn and the underlying choroid (ch) is inflammed.

Lt Col Don Brown
USAF
Stan Records
Switzland

are more separated from one another than normal by edema fluid. The outer segments are thickened and the lamellae clumped, creating the appearance of a stack of discs. The coagulated pigment epithelium cells are shrunken, having clumped dark cytoplasm and small, homogeneous, pale nuclei. In the more central portions of the coagulated pigment epithelium, the cells remain intact and attached to Bruch's membrane. At the lateral margins, the pigment epithelial cells fragment and are displaced forward by edema fluid. This fluid often disrupts the junction between apparently normal outer segments and pigment epithelial cells at the margin of the burn. In the center of the burn, the spindle shaped pigment granules appear normal and are not displaced, but as the pigment epithelium fragments at the burn margins, they lose their palisaded orientation and are randomly scattered in the necrotic debris. Bruch's membrane remains intact. The choriocapillaris beneath the necrotic pigment epithelium is occluded by both swollen endothelial cells and thrombus. Often the thromboses extend into large veins. The choroid beneath the burn is edematous. In the outer plexiform layer, axons of the necrotic rods and cones undergo degeneration. This degeneration is evidenced by interstitial edema, swelling, vesiculation and hyperchromasia of axons, rod terminal knobs and cone foot processes. Since the axons often course oblique to the axis of the rods and cones for a considerable distance, the necrosis and edema extend beyond the

Lt Col Dan Brown
USAF
SAM Records
Suitland

the area of thermal coagulation. This should be clearly understood, or one could misinterpret the area of thermal coagulation and the most sensitive portion of the receptor-epithelial cell complex. No necrosis or edema is noted in the inner portion of the outer plexiform layer comprised of the processes of the horizontal cells and fibers of Muller. The inner nuclear layer and all layers inner to it appear normal.

Measurements at the maximum diameter of the 3^{o}(720μ) burns produced by 9.6 cal/cm^2-sec, 100 msec exposures, are as follows: necrosis of the outer nuclear layer, 600μ; edema, 650μ; occlusion of choriocapillaris, 560μ.

Measurements at the maximum diameter of the 3° burns produced by exposures of 8.3 cal/cm^2-sec for 100 msec, are as follows: necrosis of the outer nuclear layer, 4 μ; edema, 450μ; occlusion of the choriocapillaris, 340μ.

A few sections of one 3° burn was examined which resulted from an exposure of 6.1 cal/cm^2-sec for 100 msec. Material was insufficient to determine if the sections examined were from the maximum diameter of the burn. The necrosis of the outer nuclear layer measured 170μ and the edema 380μ. No occlusion of the choriocapillaris was noted. The average threshold irradiance for a 3°, 100 msec exposure is 7.8 cal/cm^2-sec based on the appearance of a visible lesion in 5 hours.

Lt Col Dan Brown
USAF
SAM Records
Suitland

The histological examination shows that there is a similar pathology, though smaller in area, for exposurss to irradiance levels only 80% of the threshold level.

5.1.2 Healed Retinal Burns

Two months after exposure, a primate was sacrificed and histological sections of the irradiated areas were prepared. Three old 3° burns were examined. The burns resulted from 100 msec exposures of 9.6, 8.3 and 6.1 cal/cm^2-sec. Figure 15 shows the section through the 8.3 cal/cm^2-sec exposure. The burn consists of a central defect of receptor cells and a larger area of retinal epithelial depigmentation. No damage can be demonstrated in the outer portion of the outer plexiform layer. In general, the receptor defect is truncate, with its wider base at the junction of the outer segments and the pigment epithelium, and its narrower base at the junction of the inner and outer portions of the outer plexiform layer. The retinal defect at the top measured approximately 2/3 of the base at the center of the healed burn. However, in larger "marker" burns, scarring extends into the inner nuclear layer. The receptor defect between the outer limiting membrane and the inner portion of the outer nuclear layer is filled with acellular, fibrillar scar which appears glial in origin (Figure 16). The defect between the outer limiting membrane and the pigment epithelium contains Muller's fibers

Lt Col Dan Brown
USAF
SAM Records
Suitland

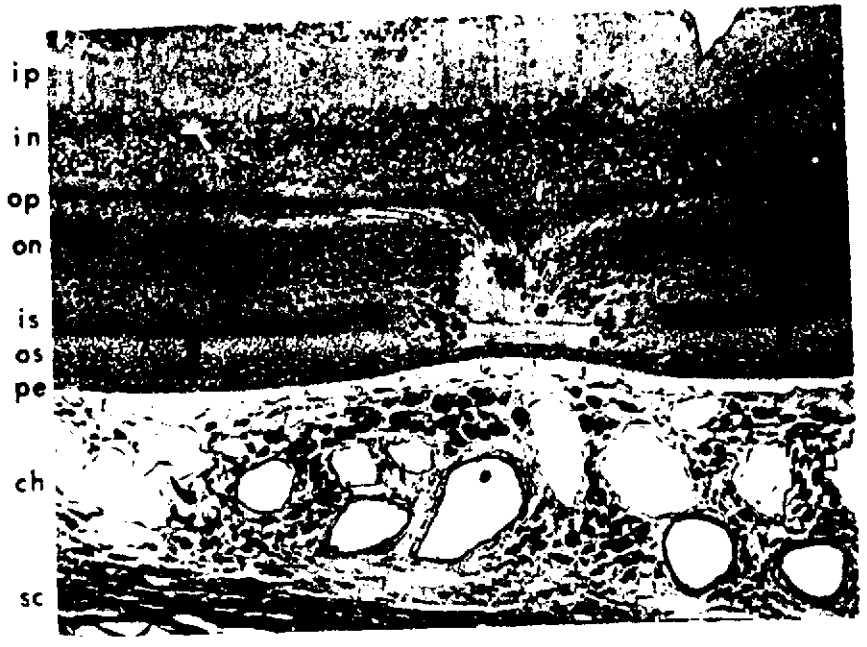

Figure 15. This illustrates a healed retinal burn 2 months post exposure (3° cone, 100 msec, 8.3 cal/cm^2/sec). The healed burn consists of a central defect of receptor cells and a much larger area of depigmentation (between the arrows) of the pigment epithelium (pe). Within the receptor defect there are many macrophages containing retinal epithelial pigment.

Figure 16. This is a higher magnification of the healed burn of Figure 15. The receptor defect on the vitrial side of the outer limiting membrane (olm) is filled with glial fibers. The pigment epithelium (pe) has lost its fusiform pigment granules from its microvilli. Large spherical pigment granules are present in the apical cytoplasm. Pigment laden macrophages are evident. The choriocapillaris (cc) is again patent. At the margin of the receptor defect cone nuclei are present outside the outer limiting membrane (olm) and the inner segments of these cones are enlarged and distorted.

1Lt Col Dan Brown
USAF
SAM Records
Suitland

projecting from the outer limiting membrane and microvilli from the pigment epithelium. These two types of processes intertwine in some areas. No change was noted in the Muller cell nuclei. Scattered within the receptor defect are macrophages filled with fusiform pigment granules. This is the pigment from the microvilli of the pigment epithelium and is well preserved in the macrophages which suggests that it is resistant to digestion by these cells. There are also pigment laden macrophages around retinal vessels inner to the receptor defect. Presumably, these cells phagocytized the pigment while within the burn and migrated to surround the retinal vessels. The pigment epithelium beneath the receptor defect has nuclei which are normal in size, appearance and location. There is a substantial loss of spindle pigment from the microvilli. In the apical cytoplasm are a few large spherical pigment granules. The lipofuschin pigment is substantially reduced. A few cells are noted to have large amounts of pigment clumped in the basal portions of their cytoplasm. Bruch's membrane beneath the receptor defect has only a minimal increase in collagen fibers. The choriocapillaris is unremarkable as is the deeper portion of choroid. The receptors continguous to the receptor defect are depleted and those present are abnormal. Because of the decreased population, the interstitium between the outer segments is conspicuous. Their nuclei are outside of the outer limiting membrane and their outer segments are hypertrophied and often appear

Lt Col Dan Brown
USAF
SAM Records
Suitland

fused to contiguous receptors. Their outer segments are widened and composed of central vacuoles separated from one another by dark staining discs.

Measurements could not be made at the greatest diameter of the lesion produced by the 9.6 cal/cm^2-sec, 100 msec exposure. The measurements at approximately the greatest diameter of a step-section sampling of the lesion produced by a 8.3 cal/cm^2-sec, 100 msec exposure, are as follows: receptor cell defect at the level of the outer limiting membrane is 230μ, depigmented retinal epithelium, 650μ.

The lesion produced by 6.1 cal/cm^2-sec, 100 msec exposure, is different from the two lesions produced by higher dose exposures in that it has no receptor cell defect per se (Figures 17 and 18). There is a depletion of receptor cells in the center of the exposed area, but no cavity is formed. The receptor cells in this area have changes identical to those seen at the margins of the lesions produced by higher dose exposures. The greatest diameter of the depigmented epithelium is 150μ.

5.1.3 Abbreviations used in labeling the illustrations:

nerve fiber layer	nf	inner segment	is
ganglion	g	outer segment	os

(continued)

Lt Col Dan Brown
USAF
SAM Records
Suitland

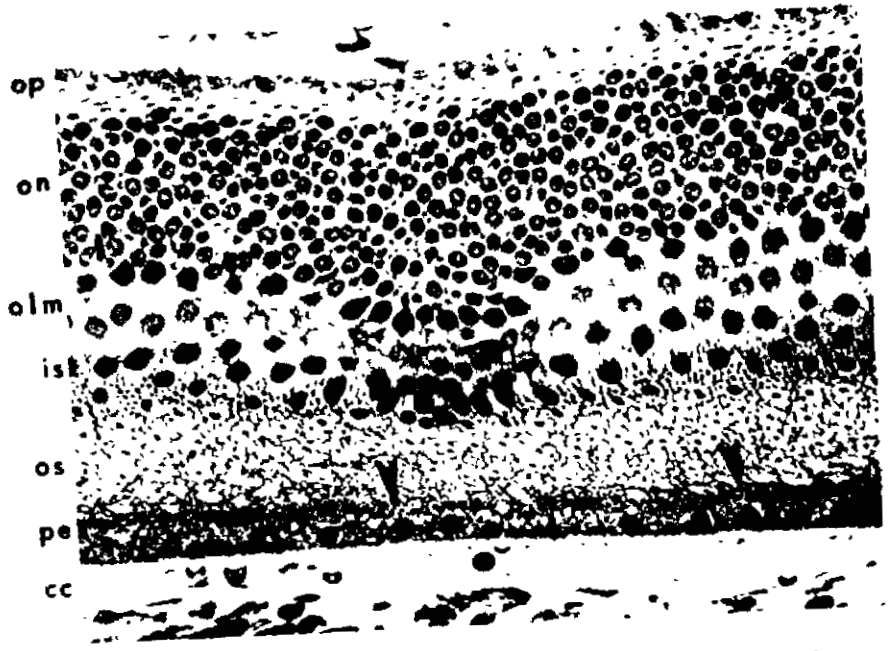

Figure 17. This illustrates a small, healed retinal burn 2 months post exposure (3°cone, 100 msec, 6.1 cal/cm^2/sec). Note there is no receptor cell defect but only a focal depletion of receptor cells. This is most apparent in the outer nuclear layer (on). The remaining receptor cells at times have their nuclei displaced outside of the outer limting membrane (olm) and their inner segments (is) enlarged and distorted. A segment of depigmentation (between arrows) of the pigment epithelium (pe) is demonstrated.

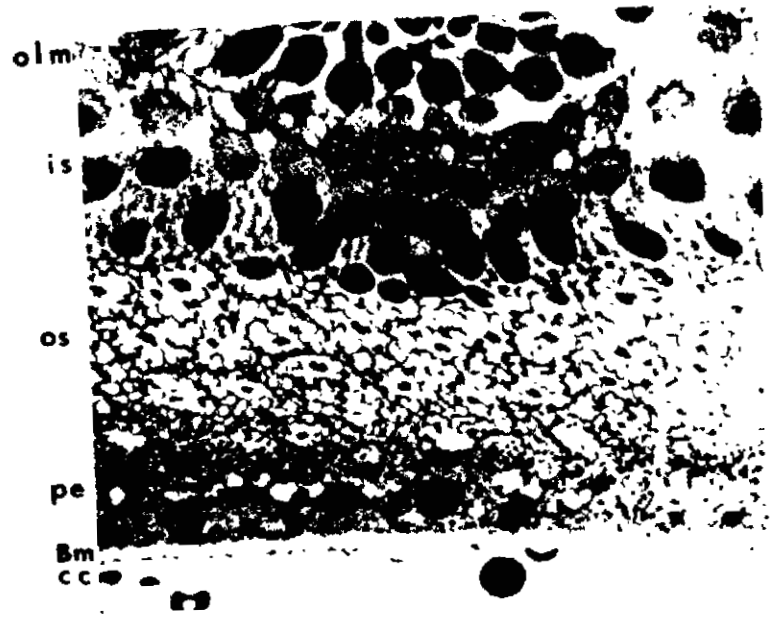

Figure 18. This is a higher magnification of the small healed burn illustrated in Figure 17. The displacement of receptor cell nuclei outside of the outer limiting membrane (olm) and the enlargement and distortion their inner segments (is) are clearly demonstrated. Uniform, fusiform pigmentation of the microvilli is lost. Clumps of pigment are present deep within two pigment epithelial cells. Bruch's membrane (Bm) appears normal as does the choriocapillaris (cc).

Lt Col Dan Brown
USAF
SAM Records
Suitland

inner plexiform layer	ip	pigment epithelium	pe
inner nuclear layer	in	Bruch's membrane	Bm
outer plexiform layer	op	choriocapillaris	cc
outer nuclear layer	on	choroid	ch
outer limiting membrane	olm	sclera	sc

6. REFERENCES

1. Allen, R.G., W.R. Bruce, K.R. Kay, et al., "Research on Ocular Effects Produced by Thermal Radiation," Final Report on Contract AF 41(609)-3099 for USAF School of Aerospace Medicine, 1967.

2. Farrer, D.M., E.S. Graham, W.T. Ham, Jr., et al., "The Effect of Threshold Macular Lesions and Sub-Threshold Macular Exposures on Visual Acuity in the Rhesus Monkey," Submitted for publication in the Journal of American Industrial Hygiene Association, 1969.

3. Alexander, T.A., R.G. Allen, R.L. Bessey, et al., "Research on Ocular Effects Produced by Thermal Radiation," Final Report on Contract AF 41(609)-2906 for USAF School of Aerospace Medicine, 1966.

4. Geeraets, W.J. and E.R. Berry, "Ocular Spectral Characteristics as Related to Hazards from Lasers and Other Light Sources," Am. J. Ophthal., 66, 15-20, 1968.

5. Boettner, E.A., "Spectral Transmission of the Eye," Final Report on Contract AF 41(609)-2966 for USAF School of Aerospace Medicine, 1967.

Lt Col Dan Brown
USAF
SAM Records
Suitland

III. MODIFICATION OF THE ZEISS PHOTOCOAGULATOR TO PRODUCE SIMULATED NUCLEAR DETONATIONS

by

Norma D. Miller, Kenneth R. Kay, and

Charles E. Bryson, III

1. INTRODUCTION

Almost all retinal burn threshold determinations have been made with square pulses of light. Since the maximum retinal temperature is a function of the exposure history and not of the total O_r, it is desirable to investigate the burn threshold for simulated nuclear detonations. A light source system has been constructed to produce a double pulse of light which closely simulates the retinal irradiance time course, and image sizes experienced with nuclear detonations. Two sources are optically coupled for the simulation and profiles comparable to detonations in the range from 10 Kt to 1 Mt can be realized.

2. SIMULATION GUIDELINES

When it becomes desirable or necessary to simulate a phenomenon of the physical world in the laboratory, a few points of guidance should always be considered:

A. Determine the basic questions or problems associated with the phenomenon that warranted the attention.

LtCol Dan Brown
USAF
SAM Records
Suitland

B. Determine as many properties as possible of the real world phenomenon.

C. Then decide from a need to know basis which of the physical properties is the most important in relation to the questions or problems that warranted the attention to the phenomenon.

D. Once the decision in C. has been made, it should then be decided which of the relative properties can be realistically and feasibly simulated - not necessarily duplicated - in the laboratory and provide answers for the questions asked about the phenomenon.

These guidelines were applied to the problem of providing a nuclear detonation simulator that could be used for the determination of retinal burn thresholds. The properties of time dependent source radiant emittance profiles, (see Figure 19) and fireball diameters emerged as the basis for the experimental guidelines. These experimental guidelines would be manifested in simulation by time dependent irradiance profiles and retinal image diameters. Once retinal burn data and irradiance and image histories are determined in the laboratory, predictions can be made with the temperature model concerning the effects of exposure to the real world phenomena of nuclear detonations.

Lt Col Don Brown
USAF
SAM Records
Suitland

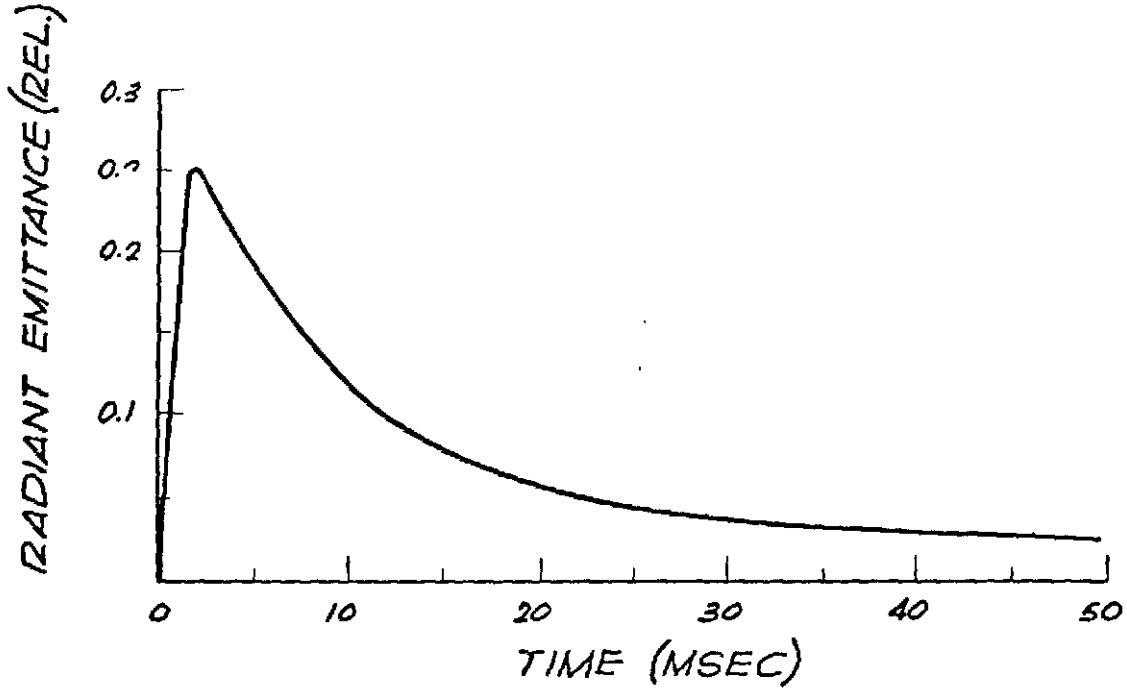

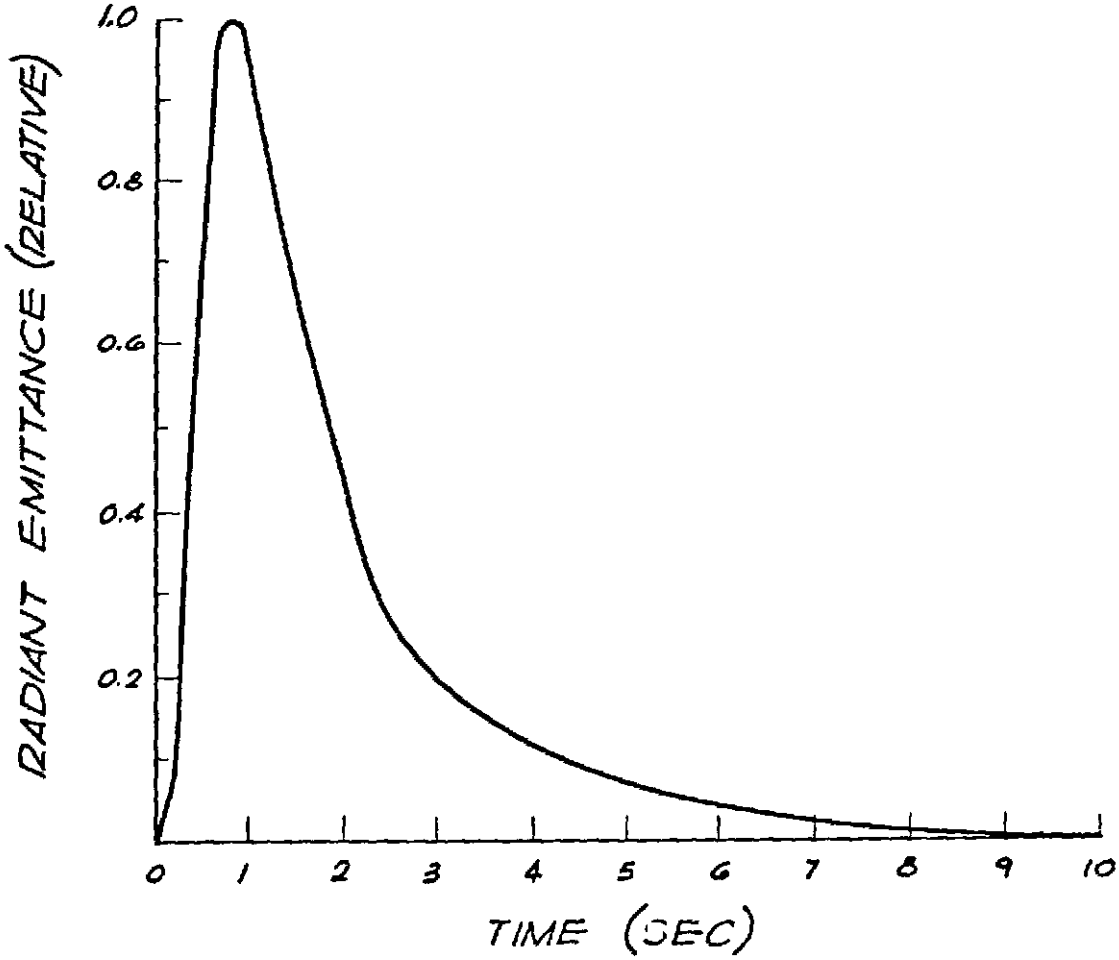

Figure 19. Normalized radiant emittance for a 1 MT nuclear detonation.

Lt Col Dan Brown
USAF
SAM Records
Suitland

3. APPARATUS

A modified Zeiss photocoagulator provides the first, rapid pulse of the double pulse simulation, and a Schoeffel 2500 watt xenon arc system is used for the slow second pulse. (A block diagram of the system is shown in Figure 20). The modified Zeiss source is a Meyer Schwickerath photocoagulator that has been extensively altered under previous contracts. The instrument is described in detail in previous reports.[1-3] The modifications permit reliable pulsed operation of the source by means of power supplied either by aircraft batteries or by a bank of capacitors.

3.1 Optical System

A schematic diagram of the optical system is shown in Figure 21. Light from the Zeiss photocoagulator arc 2 is reflected from the concave mirror 1 back in the plane of the arc. The condenser lens 5 images the arc onto the image field diaphragm 9. The iris diaphragm 7 is used to control the attenuation of light in the image at 9.

Three mm thick KG-3 filters are inserted at 6 and 13 to remove the infrared portion of the beams above approximately 800 millimicrons. The arc image in the field diaphragm is at the focal point of the objective lens 10, and the parallel rays emerging from 10 are brought to a focus on the retina by the animal's eye. Lens 10 also produces a reduced image of the condenser lens 5 at the plane of the animal's entrance pupil.

Lt Col Dan Brown
USAF
SAM Records
Suitland

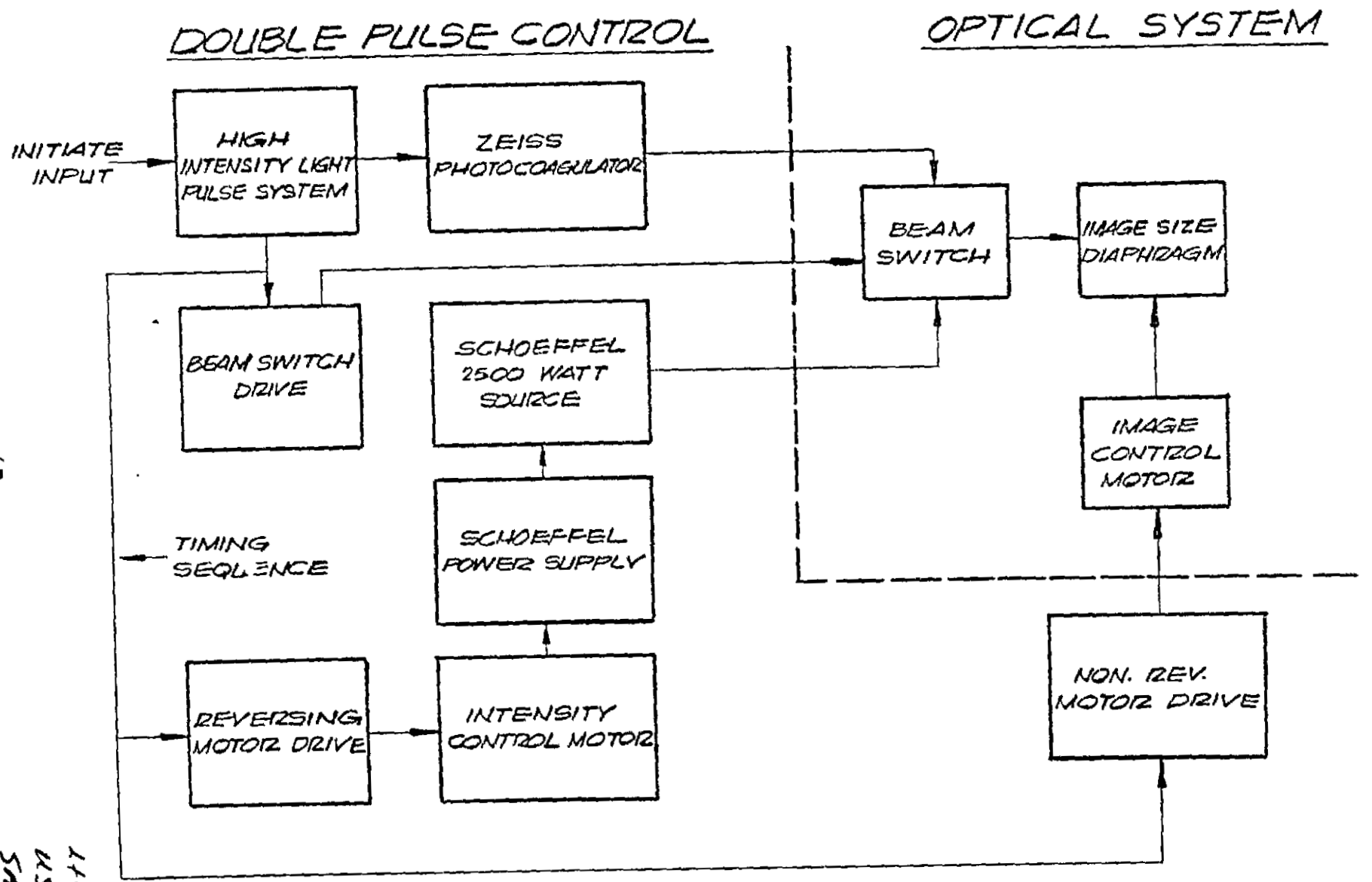

Figure 20. Block diagram of simulator system.

1Lt Col Don Brown
USAF
SAM Records
Switzland

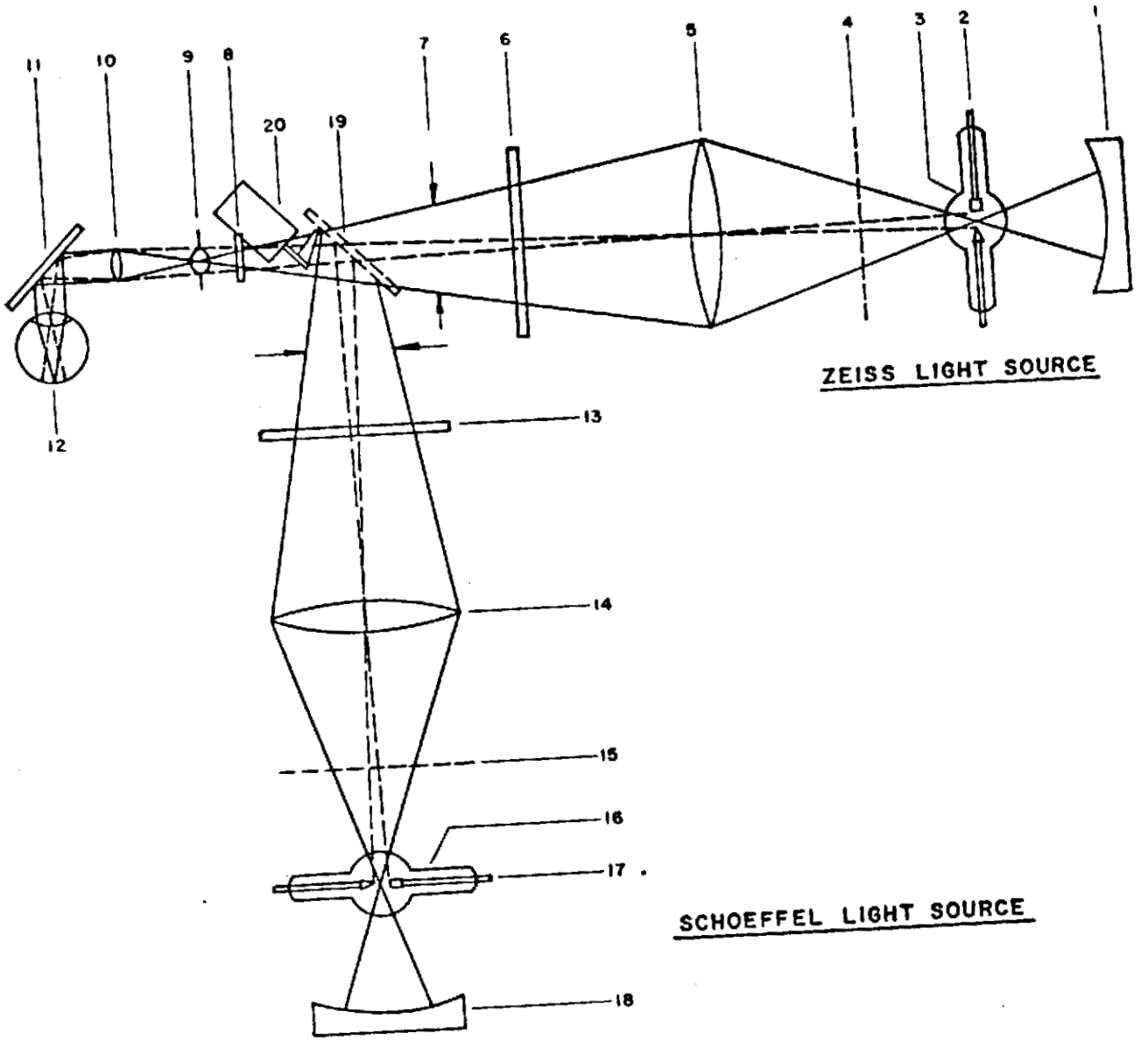

Figure 21. Optical diagram of simulator system.

Lt Col Don Brown
USAF
Sam Records
Suitland

The Schoeffel arc source 17 is imaged by a similar condenser lens system 14 onto the image field disphragm after reflection from the mirror 19, which is swung into place at the end of the first pulse.

3.2 The First Pulse Irradiance Profile

The time to the minimum between the two pulses for the 10 KT detonation is about 7.5 msec and about 75 msec for the 1 MT detonation. For simulation of the 10 KT first pulse, the Zeiss photocoagulator is operated on the capacitor bank. The SCR solid state switches[2] are used to initiate the discharge, and the time constants of the system results in an $f(e^{-t})$ decay of the gas discharge. The rise to peak radiance requires approximately 300 μ sec. The discharge time constant (to 1/e of peak) is 6 msec. This provides accurate simulation of the first pulse irradiance profile. The mirror, 19, is swung into the beam to reflect the light for the second pulse at about 6 msec.

The first pulse of the 1 MT simulation is accomplished by operating the Zeiss photocoagulator on batteries. The photocoagulator is operated in the normal manner for a 100 msec pulsewidth. A light activated SCR is mounted behind a beam splitter in the barrel of the photocoagulator. The signal from the SCR passes through a delay line and activates a stepping motor which swings the mirror 19, into position for the second pulse. As the mirror swings into position, it blocks the light from the

Lt Col Dan Brown
USAF
SAM Records
Suitland

se source, controlling the duration of the first pulse.

.3 The Second Pulse Irradiance Profile

The xenon lamp in the second source is operated by a Schoeffel ower supply which is variable up to 200 amps at 40 volts. The average rightness of the arc over an area 3 x 6 mm at maximum power is 250 andles/mm^2. The second pulse is shaped by a novel electromechanical levice (see Figure 20). One shaft of a high speed motor is coupled to .he knob of an integrated circuit speed controller. In operating the pulse shaper, the motor speed is set to a predetermined level by the speed controller before starting the motor. As the motor turns, the shaft drives the knob of the speed controller, increasing the speed of the motor. The same rotational speed wave form is produced in the opposite or falling direction by reversing the direction of rotation of the knob through a limit switch. The result is a rise and fall in motor speed which is proportional to $f(e^{-t})$.

The second shaft of the variable speed motor is coupled to the current control knob of the Schoeffel power supply through a gear box providing 1:1 and 1:4 gear ratios. Before starting the motor, the power supply current is set to a minimum. During the second pulse shaping cycle, the supply current rises to 200 amps before hitting the limit switch-microswitch reverse circuit. The 1:4 gear ratio is used for

Lt Col Dan Brown
USAF
SAM Records
Suitland

simulating the one megaton detonation and the 1:1 provides good simulation of the ten kiloton detonation. Due to the rapidly increasing rate of change of the motor speed, the current control knob is driven at a continuously increasing rate during the rising portion of the waveform. The resulting irradiance profile is similar in shape to the actual detonation profile. After the limit switch reverses the circuit, the control knob is turned at a continuously decreasing rate providing a $f(e^{-t})$ fall off in irradiance.

3.4 The Variation in Retinal Image Size

The image size is varied by a system rather similar to the pulse shaping system. A miniature iris diaphragm 9 (Figure 21), controls the retinal image diameter. The iris diaphragm can be varied from 1 to 9 mm in diameter. In operation, one shaft of a motor is coupled to the knob of its integrated circuit speed controller and the other shaft to the iris diaphragm control ring (see Figure 20). As the rate of change of the motor speed is increased, the iris diaphragm opens at an increasingly rapid rate. The result is a variation in image size that simulates the rate of growth of the fireball from a nuclear detonation.

At the end of the travel of the iris control ring, a limit switch closes a circuit which resets the diaphragm to minimum size. For the one megaton simulation, the motor is started at a fairly low speed, and as a result, the time to fully open the iris diaphragm is about 10 seconds.

Lt Col Dan Brown
USAF
SAM Records
Suitland

This can be reduced to the order of one second for the 10 kiloton simulation by starting the motor at a higher speed.

4. SUMMARY

The retinal irradiance profile and the image diameter profile produced by the simulator are shown in Figure 22. The pictures are tracings of Polaroid photographs of a CRT record of the exposures. The two traces in the upper picture represent the time history of the retinal irradiance as recorded by a photodiode placed at the exit pupil of the apparatus. During the exposure, the field diaphragm was kept constant in size. The upper trace was recorded at a sweep rate of 1.0 sec/division and corresponds closely to the actual radiant emittance profile for a 1 MT detonation as shown in Figure 19. The lower trace shows the same exposure conditions but recorded at a sweep rate of 0.2 sec/division in order to examine the leading edge of the second pulse in greater detail. The first pulse shows only as a small pip at the beginning of the two traces.

The lower picture of Figure 22 shows the form of the image diameter profile for the 1 MT detonation. The CRT trace was produced by a photodiode placed to receive a strip of light across the maximum diameter of the beam as the field diaphragm was driven by the system

Lt Col Dan Brown
USAF
SAM Records
Suitland

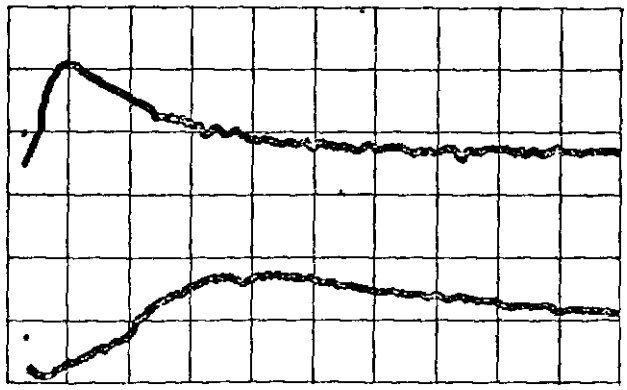

Upper trace - 1.0 sec/division, lower trace - 0.2 sec/division.

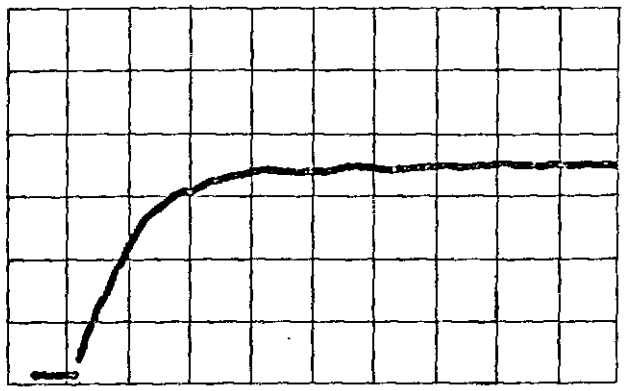

Horizontal sweep - 0.5 sec/division

Figure 22. Oscilloscope traces showing the retinal irradiance profile (upper picture) and image diameter profile (lower picture) produced by the 1 MT simulation.

Lt Col Dan Brown
USAF
SAM Records
Suitland

described in Section 3.4. The beam was maintained at constant intensity during the exposure. The horizontal sweep rate was 0.5 sec/division. In the actual 1 MT nuclear detonation that was adopted for simulation the fire ball diameter reached 85% of its maximum size in approximately 1 sec. The recorded image diameter profile is an excellent simulation of the actual detonation conditions.

5. REFERENCES

1. Alexander, T.A., R.G. Allen, et al., "Research on Ocular Effects Produced by Thermal Radiation," Final Report on Contract AF 41 (609)-2906 for USAF School of Aerospace Medicine, July 1966.

2. Alexander, T.A., E.R. Lawler, et al., "High D.C. Power, Solid-State Switch for Pulsing an Arc Lamp," Review of Sci. Inst., 36, 1707-1709, 1965.

3. Allen, R.G., Jr., et al., "Research on Ocular Effects Produced by Thermal Radiation," Final Report on Contract AF 41(609)-3099 for USAF School of Aerospace Medicine, July 1967.

Lt Col Dan Brown
USAF
SAM Records
Suitland

IV. FLASHBLINDNESS RECOVERY TIMES FOR HUMAN SUBJECTS

by

Norma D. Miller and William H. Bowie

I. INTRODUCTION

A considerable amount of work has been accomplished in the past few years in measuring flashblindness recovery times for human subjects.[1-6] In general, however, the recovery targets have been acuity letters or gratings, and the results are not directly applicable to the operational situation. In order to predict flashblindness recovery times for pilots who may be subjected to nuclear detonations, it is necessary to know the effect of the size of the flash field on recovery. Research was performed under this contract to determine the effect of the flash field size on the recovery for various target configurations, and to determine the course of recovery for target configurations that more nearly match the primary flight instruments.

The subjects participating in the experiments were college students and all were screened with simple acuity tests to insure that they fell within the normal range of visual performance. The flashblindness apparatus was built by the Life Sciences Division under a previous contract with the Air Force, and is fully described elsewhere.[7] The primary

Lt Col Dan Brown
USAF
SAM Records
Suitland

aim of the investigation was to determine flashblindness recovery times for conditions similar to operational situations.

2. APPARATUS

A schematic diagram of the optical system for the flashblindness apparatus is shown in Figure 23. The xenon flashlamp is focused in the plane of the subject's pupil to provide a Maxwellian view system for the flash field. The recovery target is presented at the center of the flash field stop by means of its optical system, shown at the left of the schematic. The flashlamp provides a rise time to peak radiance of about 600 microseconds, with a relatively flat radiance profile for the next 500 microseconds, and then an exponential decay of several milliseconds to the 10 percent power point. A shutter was interposed in the flashlamp optical system in order to chop a controlled trapezoidal waveform out of the flash discharge. The shutter is a radially slotted disc driven at a high speed of rotation in the flash beam. An additional slot is provided at a different radial position for triggering the flash tube in synchronization with the rotating shutter. A small focused light spot is transmitted by the second slot and strikes a photo SCR. A reset switch starts the motor drive for the disc and turns on the light exposing the SCR. A switch closes the SCR power supply circuit providing trigger voltage for

Lt Col Dan Brown
USAF
SAM Records
Suitland

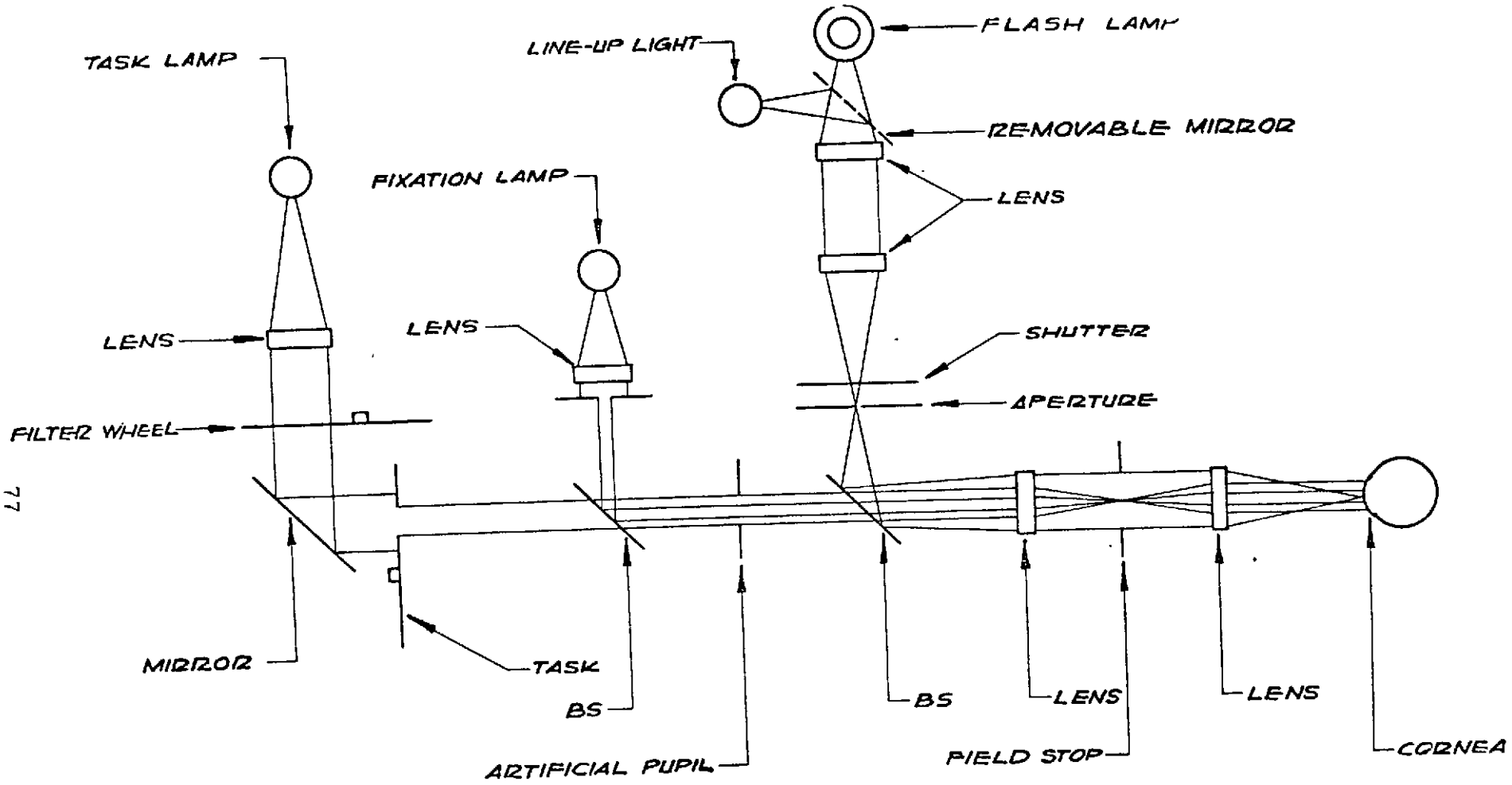

Figure 23. Schematic diagram of the optical system of the flashblindness apparatus.

Lt Col Dan Brown
USAF
SAM Records
Suitland

the flash source. The flash passes through the shutter slot when the flash discharge has reached its maximum radiance. When the SCR triggers the flash, a relay opens, stopping the motor drive, and extinguishing the light source. The resulting pulse has a duration of 0.6 msec at the 50% power points. The apparatus was modified, as shown in Figure 24, to provide a means of measuring the equivalent background luminance for each of the targets used in the recovery time measurements. A tungsten field lamp was focused by means of a Maxwellian view system on the subject's pupil in order to provide a continuously illuminated field of variable angular subtense. The visual task was presented in the center of the field stop by means of a beam splitter. A pair of crossed circular neutral density wedges were placed in the field lamp optical system to provide continuously controlled attenuation of the veiling field.

The subject sees a bright field of 8° subtense with a still brighter recovery ratget in the center of the field. Rotation of the circular neutral density filters is controlled by a rocker switch, which the subject operates with his right hand. He is therefore able to decrease or increase the luminance of the 8° field to such a level that the target is at detection threshold. When the background is at just threshold level for the task, the subject presses a button, and a new visual task is brought into the center of the field at a lower luminance. The subject again adjusts the

Appendix B

Lt Col Dan Brown
USAF
SAM Records
Suitland

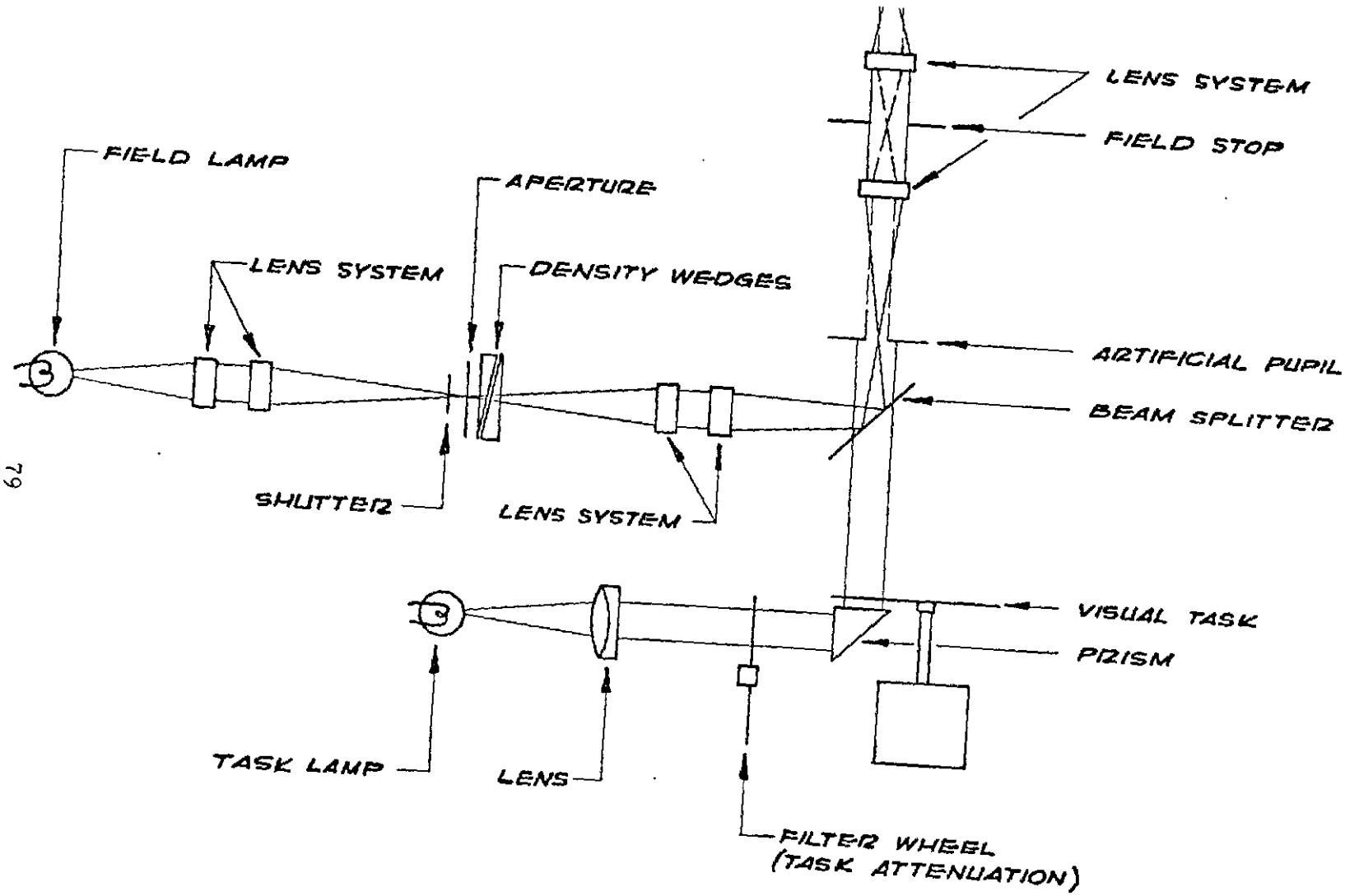

Figure 24. Modified flashblindness apparatus designed to accommodate a variable luminance field.

Office Dan Brown
USAF
Sam Records
Switzland

neutral wedges for threshold of the new target configuration. The wedges are calibrated against a voltage readout controlled by a potentiometer mounted on one of the gearbox shafts.

3. CALIBRATION.

One of the most difficult absolute calibration problems is the radiometry of a flash source. As a result, it has been relatively difficult to compare data issuing from different laboratories. The flash source used in the flashblindness apparatus was calibrated by two completely independent procedures. In one experiment, the radiance of the flash tube for narrow wavelength intervals was compared against a standardized tungsten ribbon filament lamp for the same wavelength intervals. In the second procedure, the light at the plane of the subject's entrance pupil was measured directly with a calibrated photodiode during a single flash. The calibrated photodiode is the same as is used in calibrating the Zeiss photocoagulator for the animal burn studies.

3.1 Measurement of the Steradiancy of the Flash Tube

Ribbon filament lamps were standardized against 250 watt coiled filament lamps traceable to the National Bureau of Standards. The 250 watt lamps were purchased from the Electrical Testing Laboratories, and had been previously calibrated for candle power and color temperature

Lt Col Dan Brown
USAF
SAM Records
Suitland

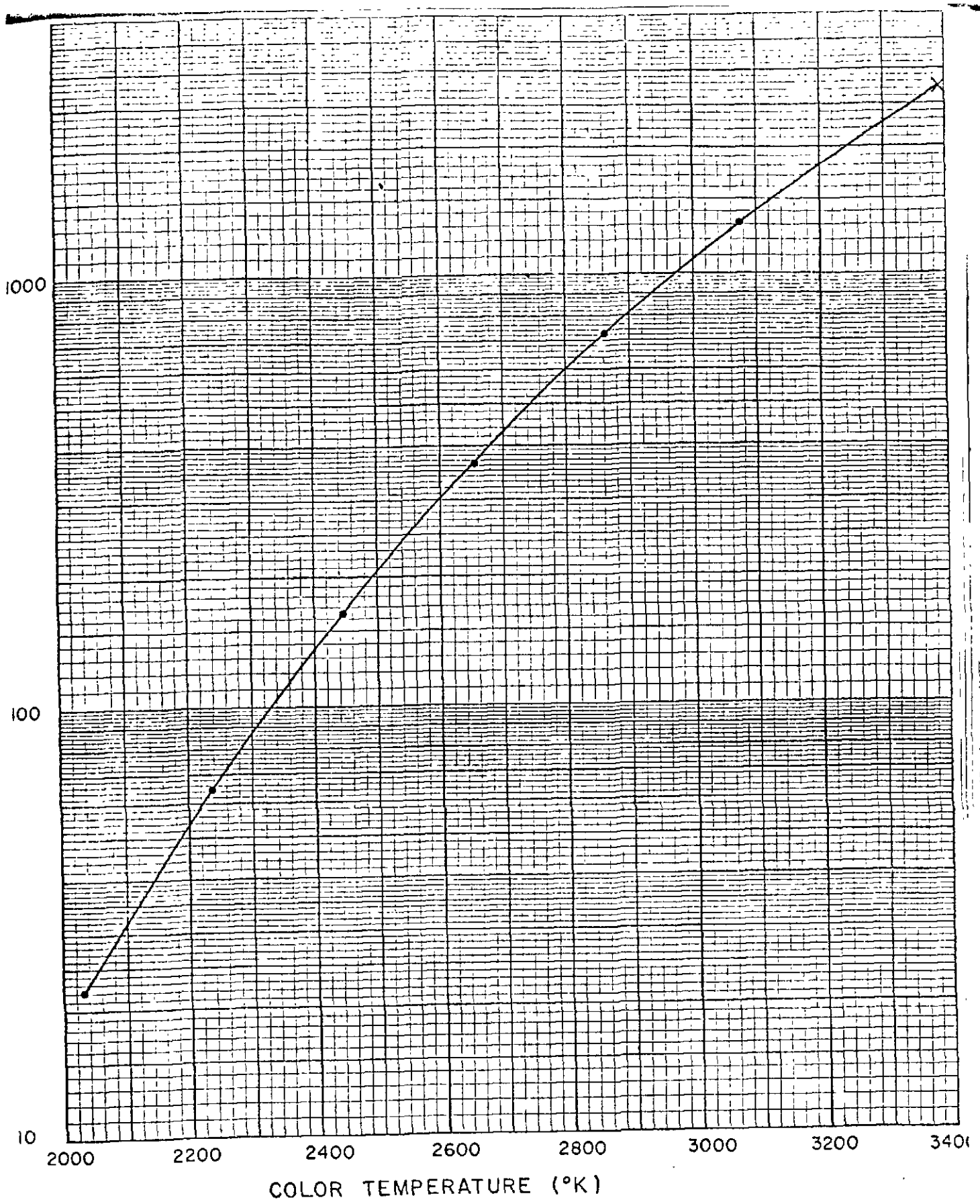

Figure 27. Tungsten ribbon filament luminance as a function of color temperature

Lt Col Dan Brown
USAF
SAM Records
Suitland

as a function of applied voltage. The ribbon filament lamps were compared with the standard lamps on a Leeds and Northrup 3 meter photometer bench.

The characteristics of tungsten ribbon filament has been carefully established in a long series of studies. One of the best series of measurement on filament steradiancy as a function of color temperature was made by Barnes and Forsythe.[8] In the published work on their measurements, they neglected to state the wavelength interval used. In order to determine this important quantity, their measurements were compared with calculated values of steradiancy. Planck's law was used to calculate the values of spectral radiant emittance of black body radiators, and the spectral emissivity values of tungsten from deVos were used to obtain the spectral steradiance of tungsten for 2000°, 2200°, 2400°, 2800°, and 3000°K. Comparison with Barnes' and Forsythe's measurements clearly show that their values refer to a 15 nm wavelength interval.

The graphs in Figure 25 show the spectral emittance in watts/cm^2 radiated in a unit solid angle for a 10 nm wavelength interval for tungsten temperatures between 2000°K and 3300°K with wavelength as a parameter. The dots are the calculated values and the crosses are the adjusted values from Barnes and Forsythe. The reduced

Lt Col Dan Brown
USAF
SAM Records
Suitland

emittance in the longer wavelengths in the measured values is probably due to absorption by the glass envelope of the ribbon filament lamp. Figure 26 shows the relationship between the absolute temperature of the filament and the color temperature. The luminance of the tungsten filament in candles/cm^2 as a function of the color temperature is shown in Figure 27. The luminance values in Figure 27 were calculated from the spectral steradiancy using the luminosity factors for the 1931 CIE Standard Observer. The equation:

$$\log (c/cm^2) = 6.63 - \frac{10,870}{\text{color temp}}$$

yields values within 5% of Barnes' and Forsythe's measurements for their full range of color temperatures from 2200°K to 3300°K.

The graphs in Figure 25 permit rapid determination of the absolute spectral steradiance of ribbon filaments when the color temperature is known. Thus, the flash tube was spectrally calibrated against a standard ribbon filament lamp operated at 18.0 amps. The lamp was compared with the laboratory color temperature standard lamp and was found to have a color temperature of 2950°K when operated at 18 amps. The light from the standard lamp was passed through a B and L grating monochromator and a photodiode was placed at the exit slit of the monochromator. The voltage across the load resistor in the photodiode circuit was fed into a Tektronix 531 A oscilloscope. The CRT trace

Lt Col Dan Brown
USAF
SAM Records
Suitland

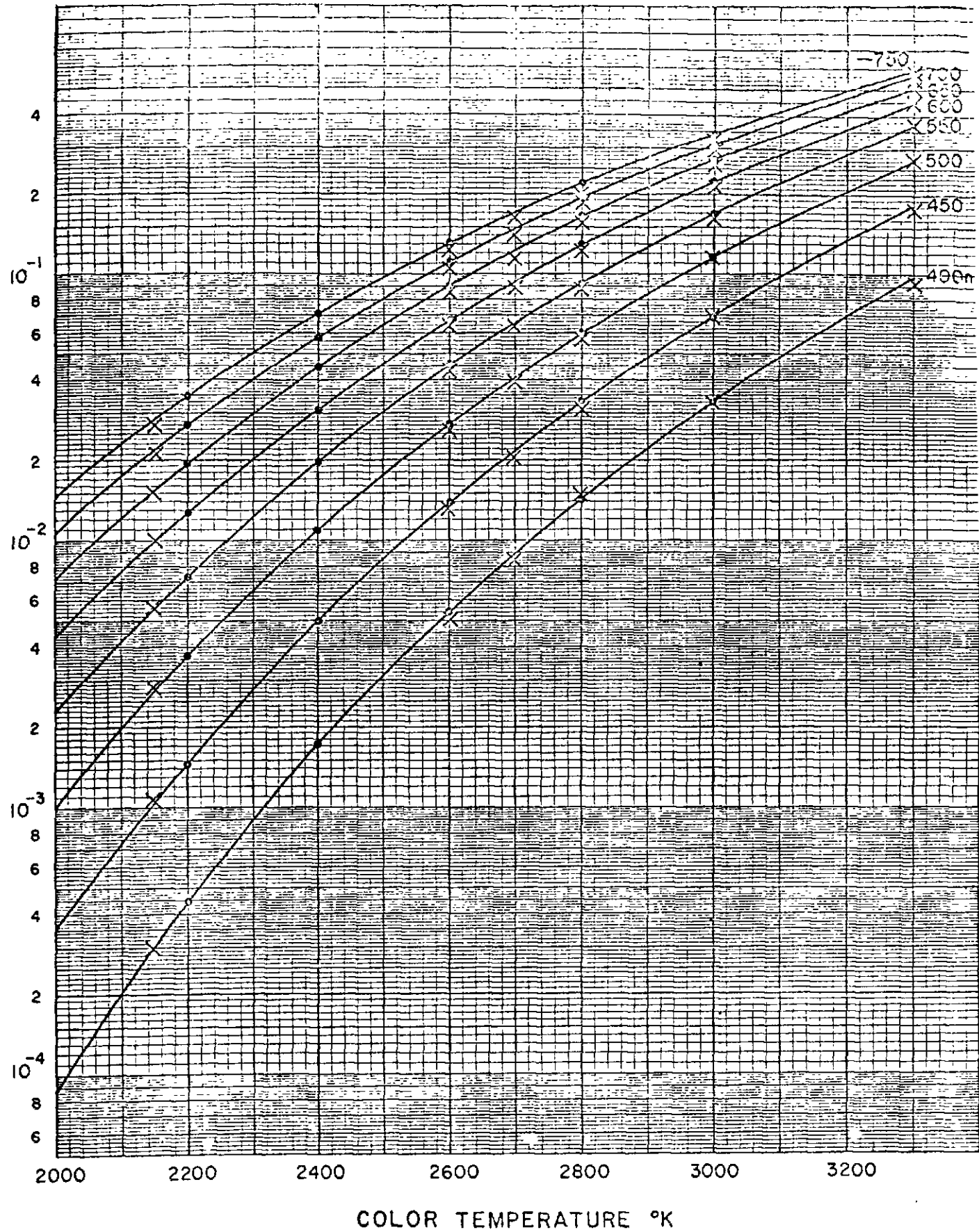

Figure 25. Calculated and measured values of tungsten steradiancy at various filament temperatures

Lt Col Dan Brown
USAF
SAM Records
Suitland

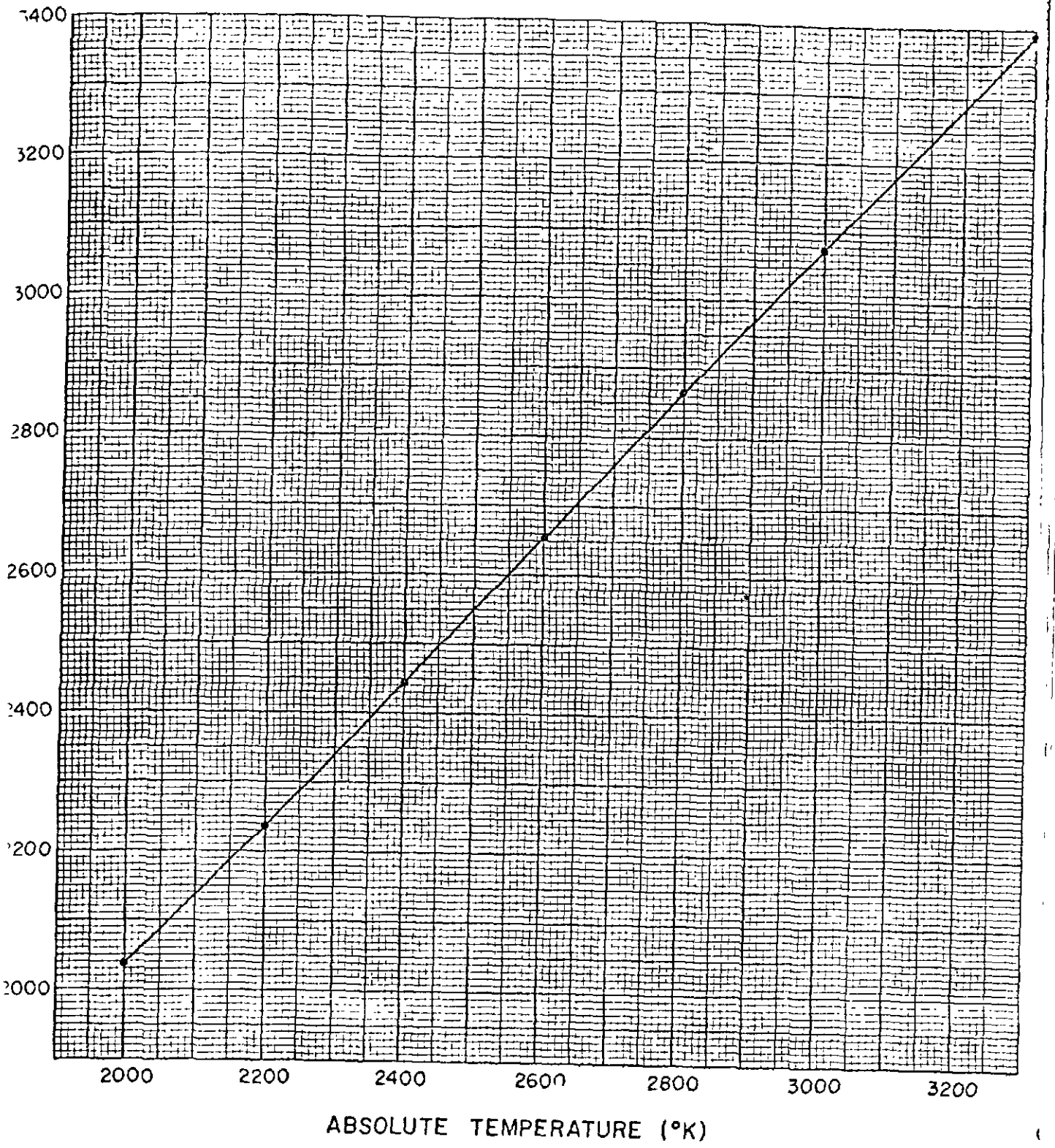

Figure 26. Relationship between correlated color temperature and filament temperature

Lt Col Dan Brown
USAF
SAM Records
Suitland

was photographed for each 10 nm wavelength interval from 420-720 nm. The bandpass of the monochromator was 5.6 nm (at the 50% points). The flash tube was imaged at the same position that the standard filament had occupied and the same wavelength intervals were used for measurement of the photodiode signal. The ratio of the photodiode signal from xenon to that from tungsten were used with the values from Figure 25 to calculate the xenon spectral steradiance.

The comparison with the standard lamp provides a very precise determination of the relative spectral distribution of the xenon flash lamp. However, considerable difficulty was experienced in aligning the flash tube in precisely the same position as the standard lamp relative to the entrance slit of the monochromator. An additional procedure was used to insure that the two lamps were compared in such a way as to provide an absolute calibration. The flash lamp was returned to the flashblindness apparatus and positioned so that the brightest portion of one turn of the helix was focused on the aperture adjacent to the shutter (Figure 23). The photodiode was placed against the aperture, blocking all ambient light from its surface and the flash tube was fired through a 600 nm interference and a 3.0 neutral density filter. The standard lamp was mounted to one side and a first surface mirror was positioned so that the image of the filament was formed at the aperture in precisely

Lt Col Dan Brown
USAF
SAM Records
Suitland

the plane of the image of the flash tube helix. The photodiode signal was again recorded for the tungsten through the 600nm filter. From this comparison, the xenon was found to be 1410 times brighter than tungsten at 2950°K color temperature for 600 nm.

During the experimental sessions, the flash lamp is always used with a 3-mm thick KG-3 and a Wratten 2B filter to block the infrared and ultraviolet spectral regions. The spectral radiance values found from the comparison with tungsten were multiplied by the filter factors and the results are shown in the graph of Figure 28. The calculated luminance (for the 1931 Standard Observer) of the flash lamp is 1.33×10^6 c/cm^2 through the blocking filters.

The luminance of the field in a Maxwellian view system is given by the source luminance times the transmittance of the optical system. The transmittance of the optical system was measured by placing a tungsten lamp at the plane of the entrance pupil of the subject's eye (Figure 23) and measuring the irradiance at the aperture near the shutter with a photodiode. The photodiode was then moved to the flash lamp surface and the irradiance at that point recorded. The ratio of the second measurement to the first is the transmittance of the system from the flash lamp to the aperture. The flash lamp was replaced by a tungsten lamp and the transmittance of the system between the aperture and the eye

Lt Col Dan Brown
USAF
SAM Records
Suitland

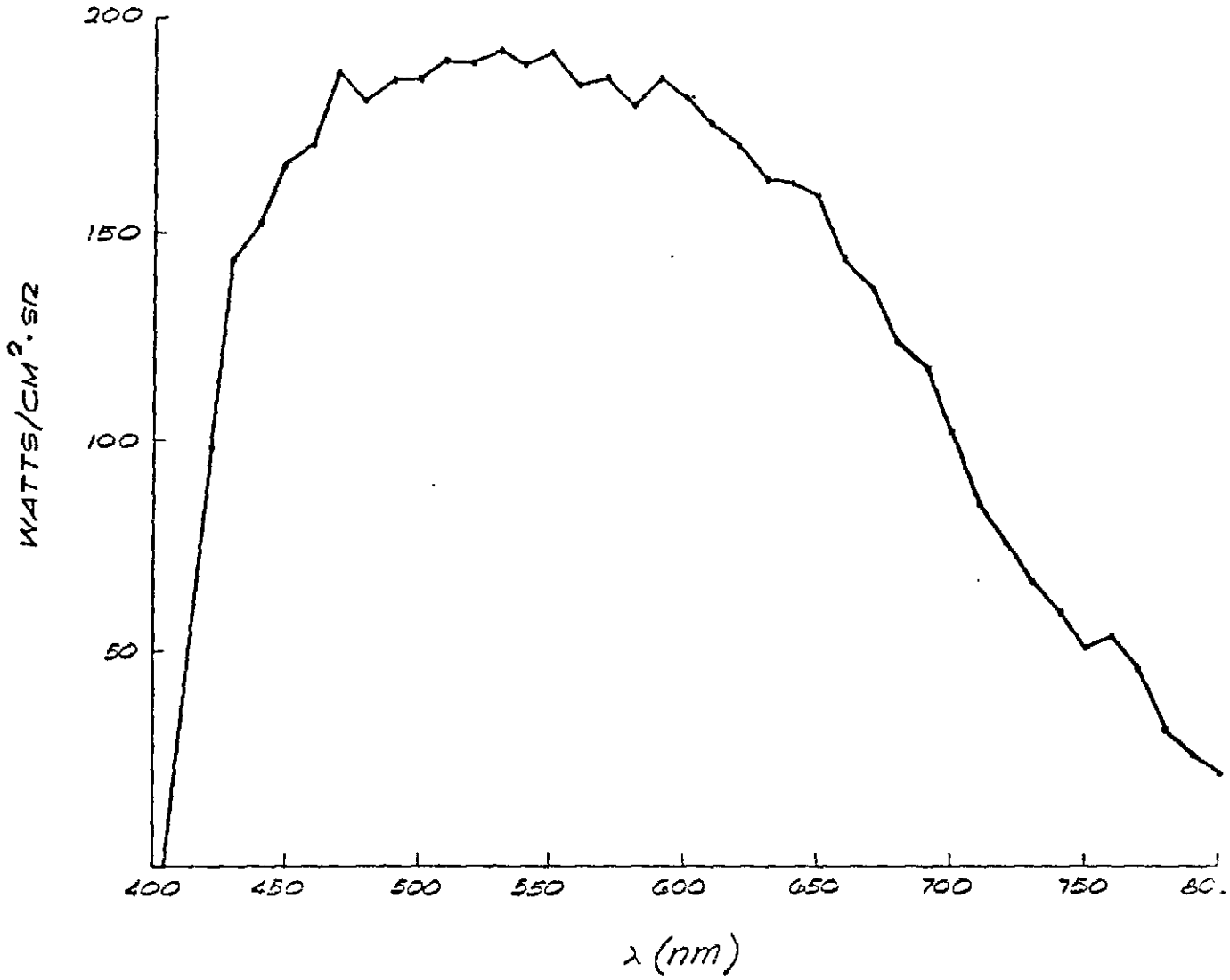

Figure 28. Spectral steradiance of the xenon flash lamp filtered through KG-3 and 2B filters.

Lt Col Dan Brown
USAF
SAM Records
Suitland

was determined in the same manner. The transmittance of the complete system is the product of the two measured ratios. The total transmittance was 18.5%, giving a flash field luminance of 2.46×10^5 c/cm^2.

The total integrated energy under the curve of Figure 22 gives a steradiance at peak discharge of 5350 watts/cm$^2 \cdot$ sr for the flash tube filtered through the KG-3 and 2B filters. The irradiance at the cornea is given by the product of the transmittance of the system and the steradiance and the solid angle subtended by the exit pupil of the system at the image. For a Maxwellian view system, the solid angle subtended by the exit pupil is given by $\pi \sin^2 \alpha$, where α is the half angle of the field. For an 8° field, the irradiance at the cornea is 15.1 watts/cm^2 or 3.61 cal/cm$^2 \cdot$ sec.

3.2 Direct Measurement of Irradiance at Cornea

An EG&G SGD-100 photodiode was calibrated against a Barnes thermopile with light from a xenon arc. The calibration of the thermopile was traceable to the National Bureau of Standards. The arc source was filtered through a 3-mm KG-3 filter so the spectral distribution closely approximated that of the flash tube in the flashblindness apparatus. The calibrated photodiode was placed in the center of the flash tube image formed by the optical system, at the plane of the subject's entrance pupil. The measured irradiance at the peak of the flash tube discharge

Appendix D

Lt Col Dan Brown
USAF
SAM Records
Suitland

was 3.25 cal/cm^2 · sec for an 8° flash field diameter.

The Maxwellian beam of the flash blindness apparatus is 4 x 4 mm at the plane of the subject's pupil. From the irradiance at the photodiode, the power entering the eye at the peak of the tube discharge is 0.52 cal/sec for an 8° field. A visual angle of 3.4° corresponds to 1 mm on the retina so an 8° circular field covers a retinal area of 0.043 cm^2. Assuming a transmittance of 0.59 for the ocular media of the eye, the retinal irradiance at the peak of the flash is 7.1 cal/cm^2 · sec.

3.3 Calibration of Flash Duration

The speed of the rotating shutter disc was measured with a General Radio strobotac and found to be 1742 rpm. The disc diameter was 23.0 cm at the center of the radial exposure slot. The slot was 1.2 cm long at the center. The source aperture, in close proximity to the disc, is 4 mm wide. The linear velocity of the center of the slot, given by the speed of rotation of the disc and the diameter, is 2.1 x 10^4 mm/sec. The rise time of the flash is therefore 190 μsec and the shutter is completely open for 380 μsec. This provides an equivalent square pulse of 570 μsec.

The calculations of pulsewidth were checked by direct measurement from a CRT trace for a photodiode placed at the source aperture. The CRT trace is reproduced in Figure 29.

Appendix B

Lt Col Dan Brown
USAF
SAM Records
Suitland

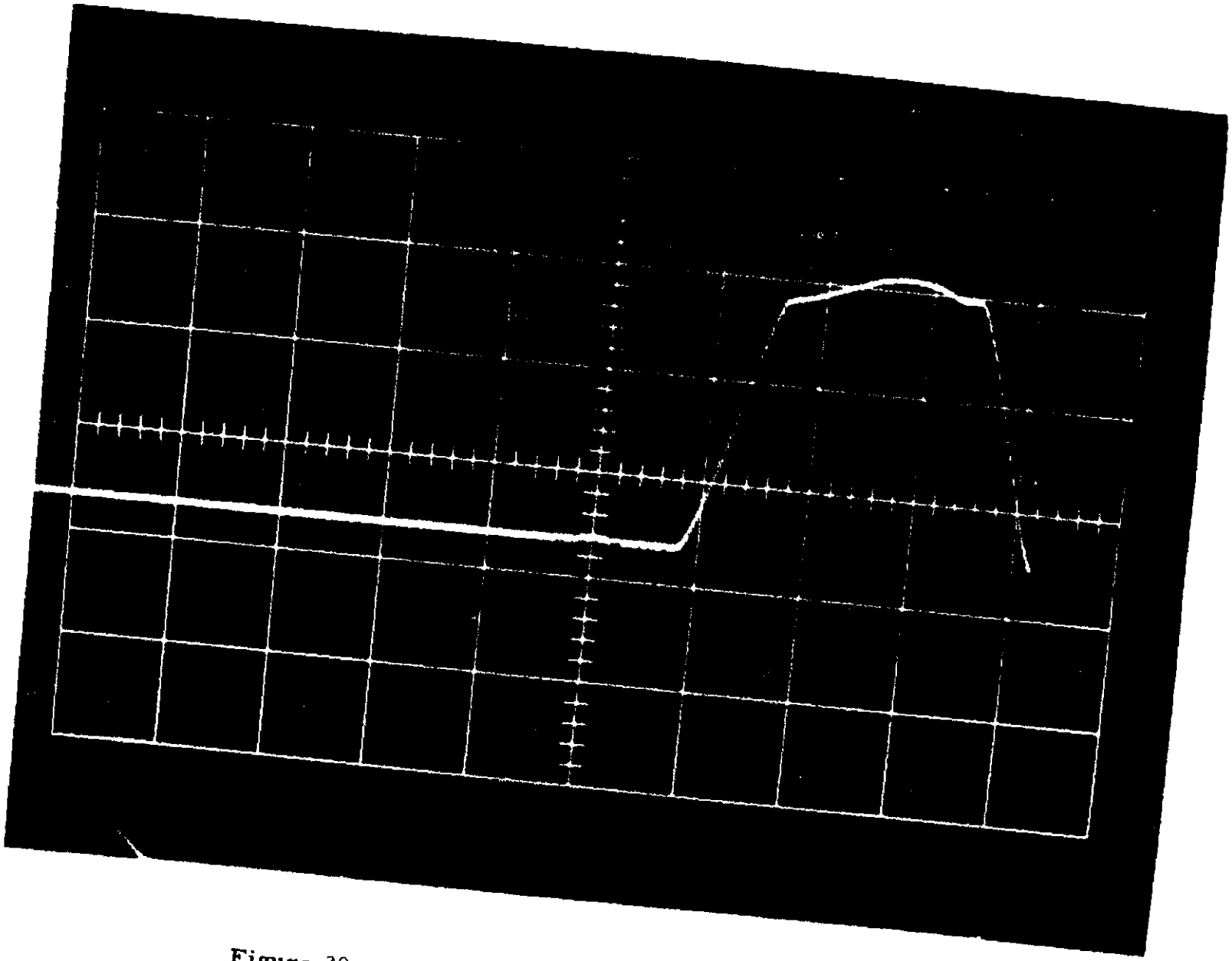

Figure 29. The waveform of the flash exposure. (Horizontal sweep 0.2 msec/division.)

Lt Col Dan Brown
USAF
Stan Records
Suitland

3.4 Calibration of Recovery Target Luminances

A Pritchard Spectra photometer was used for measuring the recovery target luminances. The Pritchard has a telescope optical system and the emerging beam from the flashblindness apparatus has a smaller diameter than the telescope objective. A calibration curve was constructed for the Pritchard for different aperture sizes by recording the readout for a known field luminance when different sizes of annular stops were placed over the objective. The true luminance value could then be found when the diameter of the beam entering the Pritchard was known.

In measuring the target luminances, the photometer objective lens was placed at the plane of the subject's entrance pupil. The beam diameter was measured and a field stop mirror was selected for the photometer to insure that the measurement was made at the desired position in the target. The grating target lines subtended such a small angle that the average luminance over a 15' area was measured rather than the bright line. For the photograph of the artificial horizon, the luminance measurement reflects the luminance of the bright wing configuration, which was large enough to cover the 6' field stop of the photometer.

Appendix B

Lt Col Dan Brown
USAF
SAM Records
Suitland

4. EXPERIMENTAL RESULTS

Sloan-Snellen letters and gratings were used for recovery targets ·der to compare the results of the current research with previously .shed work from other laboratories. Photographs of an actual ·ument panel artificial horizon were used in the latter portion of ·tudy for the recovery target. The use of the photograph allowed .vestigation of the critical size of the flash field in terms of a realistic ational situation.

Effect of Flash Field Size on Recovery Times using Sloan-Snellen Letters.

Five subjects participated in an experiment to determine recovery s for Sloan-Snellen letters subtending 19 min of arc visual angle for ·us sizes of centrally fixated flash fields. The range of angular sub- of the circular fields was 0.5° to 10°. The retinal luminous energy flashes was 2.3×10^{7} td· sec (7.5 cal/cm^{2} sec at the retina) for flash. The mean recovery times for all subjects for each flash field ·ter is shown in Table VII. The mean recovery times for each sub- or a number of replications are listed in Tables B-I - B-VII in ·dix B.

The mean recovery times for all subjects are shown in Figure 30

88 75-105 Appendix B

LtCol Dan Brown
USAF
SAM Records
Suitland

Table VII. Mean recovery times in seconds of 5 subjects using 19' Sloan-Snellen letters following 2.3×10^7 td·sec flashes of varying angular subtense.

lash ield grees)	Letter Luminance (mL)							
	38.0	9.5	3.8	0.76	0.38	0.12	0.076	0.06
).5°	2.52	4.42	6.20	8.18	10.88	14.22	18.38	21.50
.0°	3.22	5.18	7.23	9.18	11.18	14.13	17.9	20.9
°	5.24	8.52	11.70	16.76	24.10	40.26	58.56	69.24
°	5.78	8.54	10.28	15.82	25.40	40.24	60.82	73.46
°	5.70	7.96	10.20	15.98	29.20	55.44	68.08	78.32
°	6.66	8.50	11.38	16.36	25.06	47.86	65.32	79.78
°	6.88	8.70	10.54	19.58	27.14	42.10	63.10	77.28

Appendix B
LtCol Dan Brown
USAF
SAM Records
Suitland

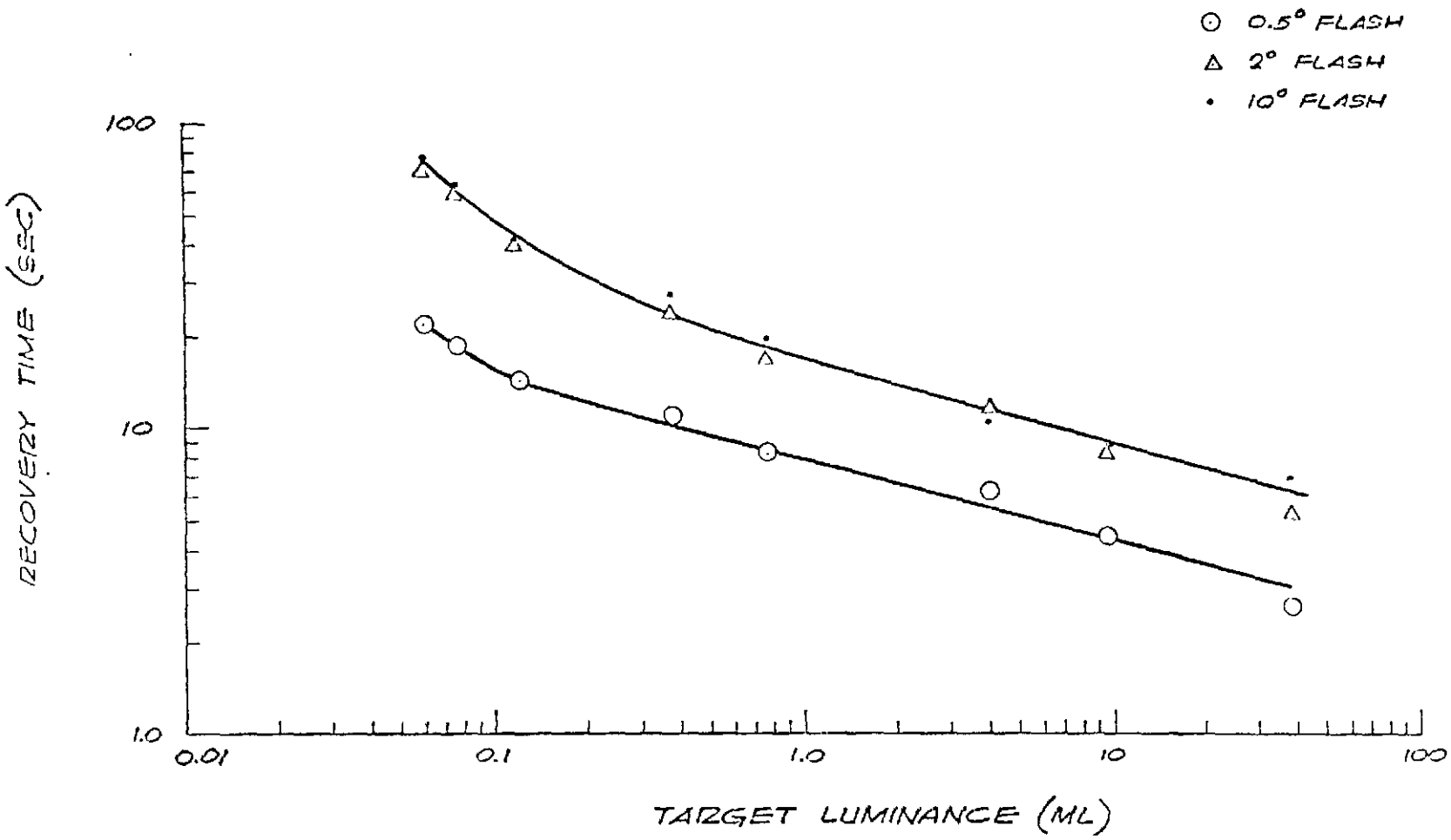

Figure 30. Mean recovery times for five subjects using Sloan-Snellen letters following flashes of 2.3×10^7 td·sec for three flash field sizes.

Lt Col Dan Brown
USAF
Stan Records
Suitland

for the 0.5°, 2.0° and 10.0° flash fields. The curve for the 0.5° flash field indicates the significant decrease in recovery time for the smaller afterimage, but the data for the 2° to 10° fields show no practical difference in recovery.

4.2 Recovery Times using a Grating Test Object and Various Flash Field Sizes

The effect of flash field size on the recovery times for a grating target with a period of 1'30" visual angle was tested on five subjects The visual acuity required for the fine test grating was a more demanding task than that for the Sloan-Snellen letters. This fact resulted in longer recovery times for the same luminance of the bright lines compared with the letters. The mean recovery times for the five subjects are listed in Table VIII, for a 2° and 4° field. There is no significant difference in recovery times for the two flash fields. This clearly indicates that once the foveal area is flashed, the gratings can not be seen by the para-foveal retina because it does not possess this degree of visual acuity.

A second experiment was performed by four of the same group of subjects to determine recovery times for flash fields from 0.5° to 10°. Their mean recovery times for several replications are listed in Table IX for several field sizes. There is a marked change in recovery between the 1° and the 2° field size. The results of the grating and

Appendix B

Lt Col Dan Brown
USAF
SAM Records
Suitland

Table VIII. Mean recovery times in seconds of 5 subjects for a grating test object† for a 2° and 4° flash field size. All flashes were 2.7×10^7 td · sec.

Average grating luminance (mL)	2° Field	4° Field
778	4.12	5.00
75.5	8.16	7.79
13.8	15.02	12.09
8.64	16.92	15.38
6.48	19.82	19.08
2.16	25.41	25.96
1.38	32.51	32.17
1.06	34.64	37.15
0.54	42.51	45.59
0.35	52.75	52.50

† The spacing between the lines of the grating subtended 1'30'' of visual angle.

Lt Col Dan Brown
USAF
SAM Records
Suitland

Table IX. Mean recovery in seconds for a grating test object † for various flash field sizes. The average grating luminance was 4.1 mL and all flashes were 2.7×10^7 td · sec.

Subject	Flash Field Diameter 0.5°	1.0°	2°	4°	6°	8°	10°
GG	11.20	10.10	21.81	19.21	17.44	18.80	25.58
DE	12.85	13.30	14.88	16.75	15.12	18.16	19.54
HG	20.00	17.70	21.87	24.53	20.53	22.97	22.43
JH	10.92	11.18	16.52	19.90	16.59	17.55	19.68
Mean	13.74	13.07	18.77	20.10	17.42	19.37	21.81

† The spacing between the lines of the grating subtended 1'30'' of visual angle.

Appendix B

Lt Col Dan Brown
USAF
SAM Records
Suitland

letter recovery targets are summarized in Figure 31. The letter targets show a clearly marked decrement between 0.5° and 2° with no change past 2° for the 9.5 mL target and a smaller slope for the 38 mL target past 2°. However, the grating data could be reasonably fitted with a line indicating a continual increase in recovery time as the field size increases.

4.3 Recovery Times using a Photograph of a Primary Flight Instrument

The recovery time data for acuity targets such as letters and gratings are useful in determining some parameters of flashblindness, but they are not directly applicable to predictions for operational conditions. A photograph was made of an instrument panel artificial horizon and it was presented as a recovery target in the flashblindness apparatus. The photograph was scaled so the visual angle subtended was equivalent to that subtended by the instrument in actual use. The photograph was transilluminated and its luminance was varied by inserting the usual filter series in the illuminating beam.

Three subjects participated in an experiment to determine the effect of flash energy on recovery times for various target luminances for the artificial horizon. The flash field diameter was 8°. The mean recovery times for the three subjects for several replications each are listed in Table X for seven flash energies. The duration of all flashes

Appendix B
LtCol Dan Brown
USAF
SAM Records
Suitland

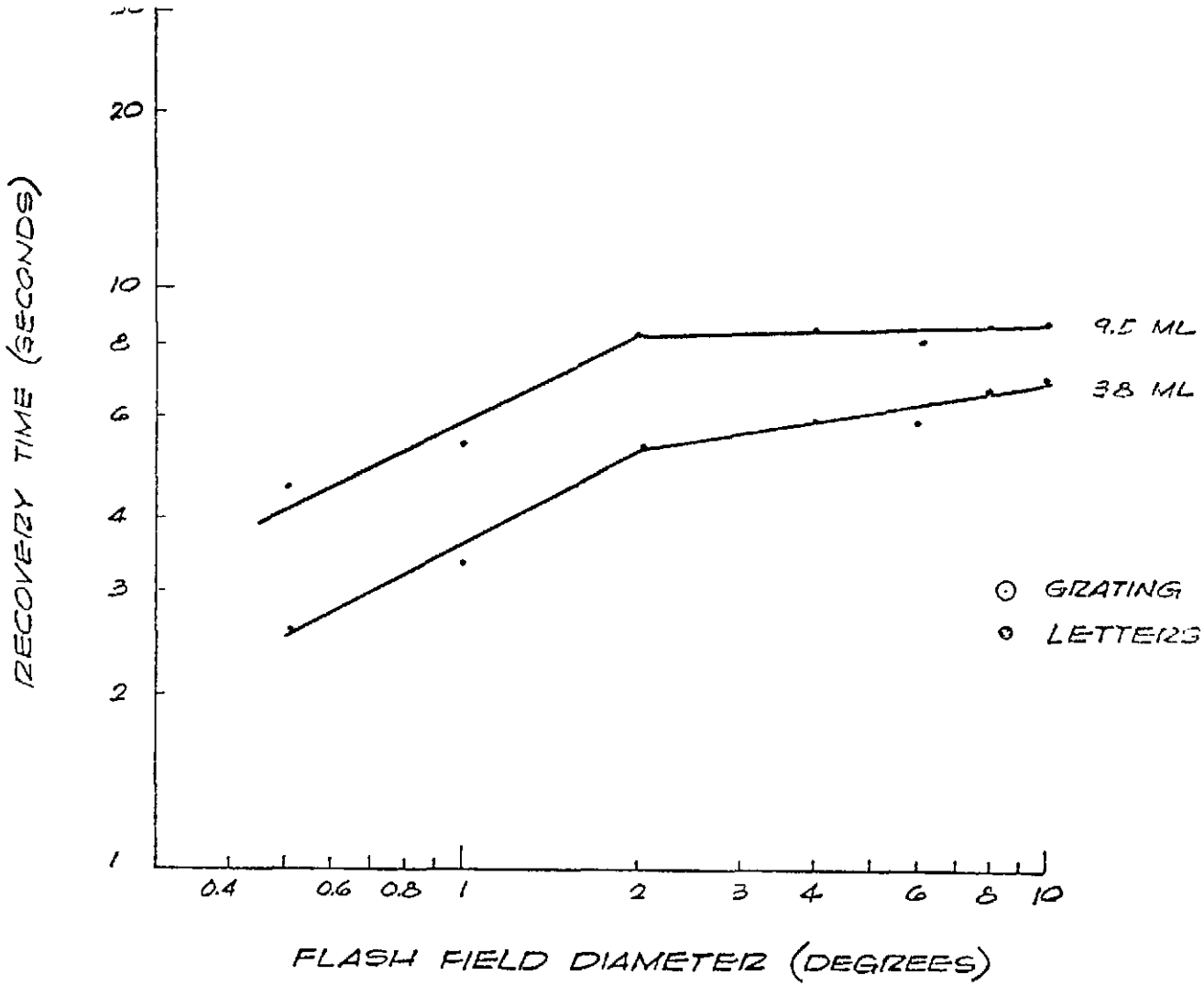

Figure 31. The effect of varying the flash field diameter on recovery times for three targets.

Lt Col Dan Benner
USAF
SAM Records
Suitland

Appendix B
pp 145 — 105

Table X. Mean recovery times of 3 subjects for a photograph of an artificial horizon following 8° flashes of various energy levels.

ash	Task Luminance (mL)						
·sec	1.62	0.081	0.041	0.026	0.016	0.010	0.002
30×10^7	1.7	2.8	4.3	5.6	7.8	12.9	23.7
45×10^7	1.5	2.4	3.4	4.6	5.9	10.4	16.5
20×10^6	1.5	2.3	3.3	4.8	6.1	10.5	13.2
80×10^6	1.6	2.2	3.3	4.4	5.4	8.3	11.5
60×10^6	1.3	2.1	2.9	3.8	4.8	6.4	9.4
30×10^6	1.05	1.9	2.7	3.6	4.6	5.9	7.4
45×10^6	1.2	1.8	2.6	3.5	4.4	5.4	7.1

Appendix B
LtCol Dan Brown
USAF
SAM Records
Suitland

was 0.57 msec, and the flash luminance was decreased by neutral filters for the various exposure levels. The target luminance values refer to the luminance of the center "wing" configuration and represent approximately 85% of the cockpit illumination values in foot candles.

The mean recovery times for the three subjects are shown as a function of flash exposure in Figure 32 for six levels of target luminance. The data points can be fitted with a straight line on the graphs, indicating a power relationship between the recovery time and the flash exposure. There is a different exponent for the very dim targets. The detail of the artificial horizon is very gross compared with the acuity targets that have been previously used in recovery measurements and the resulting lower visual performance required is reflected in the short recovery periods.

5. CONCLUSIONS

The recovery times measurements for operationally significant visual targets resulted in much shorter recovery than was predicted on the basis of acuity targets. For letters and gratings, the flash field diameters must be less than 2° to effect any decrease in recovery by looking around the afterimage. This is undoubtedly due to the fact that the acuity required for detection can only be [illegible] by the foveal area.

Appendix B
Lt Col Dan Brown
USAF
SAM Records
Suitland

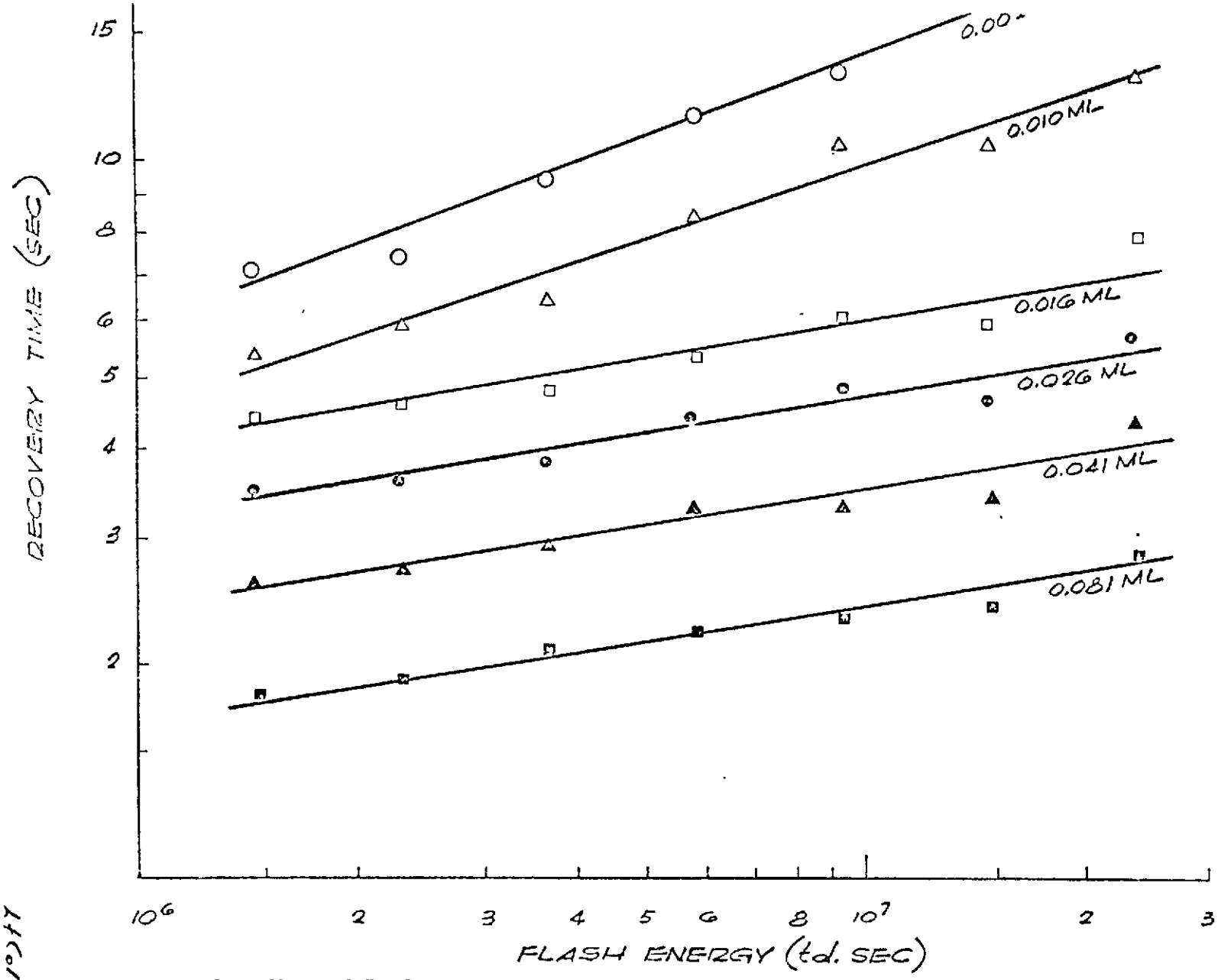

Figure 32. The effect of flash energy on recovery times for a primary flight instrument target.

Lt Col Dan Brown
USAF
SAM Records
Suitland

Appendix B
pp 75 – 105

For a primary flight instrument, however, the critical task detail can be observed even in the presence of a very bright afterimage.

The research performed under this contract has clearly shown the complexities in the problem of predicting flashblindness recovery times for operational situations. It is unlike the retinal burn problem where the critical physical effect is that of temperature rise due to varying amounts of energy and the rate of delivery of the energy. In addition to these variables, the flashblindness problem is complicated by the position of the flash on the retina relative to the fovea and by the size of the critical detail in the visual display.

6. REFERENCES

1. Miller, N. D., "Visual recovery from brief exposures to high luminance," J. Opt. Soc. Am., 55, 1661-1669, 1965.

2. Miller, N. D., "Positive afterimage as a background luminance," J. Opt. Soc. Am., 56, 1616-1620, 1966.

3. Miller, N. D., "Positive afterimage following brief high intensity flashes," J. Opt. Soc. Am., 56, 802-806, 1966.

4. Hill, J. H. and G. T. Chisum, "Flashblindness; A problem of adaptation," U. S. Naval Air Development Center, Johnsville, Pa., for Bureau of Naval Weapons, 1963.

Appendix B
Lt Col Dan Brown
USAF
SAM Records
Suitland

5. Chisum, G. T., "Intraocular effects on flashblindness," Aerospace Medicine, 39, 850-868, 1968.

6. Chisum, G. T., and J. H. Hill, "Flashblindness: The effects of pre-flash adaptation and pupil size," Aerospace Medicine, 38, 395-399, 1967.

7. Allen, R. G., Jr., et al., "Research on Ocular Effects Produced by Thermal Radiation" Final report on Contract AF 41(609)-3099 for USAF School of Aerospace Medicine, July 1967.

8. Barnes, B. T. and W. E. Forsyihe, "Spectral Radiant Intensities of Some Tungsten Filament Incandescent Lamps," J. Opt. Soc. Am. 26, 313-315, 1936.

OSR 75-105
Appendix B

LtCol Dan Brown
USAF
SAM Records
Suitland

V. MODEL FOR PREDICTION OF RETINAL TEMPERATURES

by

Thomas J. White, Martin A. Mainster,
James H. Tips, and Patrick W. Wilson, Jr.

Of the two approaches suggested in the work statement for development of an improved mathematical model for retinal burn prediction, it was decided that a digital computer solution of the equation of heat conduction was the only practical approach to a flexible, comprehensive and accurate description of the thermal injury process. Nevertheless, a detailed study was made of several possible analog simulations with the conclusion that this approach was not economically feasible. The results of this study were given in an interim report and are also included as Appendix C to this report.

The digital temperature rise model effort must be regarded as completely successful. Details of its development and examples of specific applications have been given in a series of papers submitted for publication in the open literature. Copies of these papers have been furnished to the Contract Monitor and to the Contracting Officer. Abstracts of these papers, journals to which submitted and current publication status

Appendix B 75-105

Lt Col Dan Brown
USAF
SAM Records
Suitland

re given in Appendix D.

Several versions of the digital program have been assembled for ıe various computations reported in the papers mentioned above. These ifferences relate to the size and configuration of the grid, the type of ource term used, the specification of thermal parameters and the hysical dimensions of the model. This approach results in a saving of nachine time by closely matching model complexity with minimum ·equired output.

The alternating direction implicit difference equations are solved ›y an algorithm which requires no more than 4 to 6 milliseconds per time ;tep per grid point. Thus, calculation of retinal temperature rise history 'or a nuclear weapon detonation can be made in less than 10 minutes when ;ource terms and atmospheric transmissions are precalculated. On he other hand, versions with reduced grids have been assembled which will calculate source terms and temperature rise in less than 2 minutes. The addition of air and water mass subroutines will add only a few seconds to the running time. Experience with use of the program indicates that it will be best to write as many versions of the source preparation subroutines as there are different kinds of input data: scaled Dominic test results, AFWL theoretical descriptions, black body, etc.

Appendix B
LtCol Dan Brown
USAF
SAM Records
Suitland

The basic grid which has been used is shown in Figure 1. Δz and Δr denote axial and radial mesh lengths respectively in the uniform mesh region. R_1 and R_2 are constant axial and radial stretching ratios respectively. Distances between adjacent grid points are given by the expressions:

$$z_{i+1} - z_i = \begin{cases} \Delta z (R_1)^{(M/2)-M_1-i} & 0 \le i \le (M/2)-M_1-1 \\ \Delta z & (M/2)-M_1 \le i \le (M/2)+M_1-1 \\ \Delta z (R_1)^{i-(M/2)-M_1+1} & (M/2)+M_1 \le i \le M-1, \end{cases}$$

and

$$r_{j+1} - r_j = \begin{cases} \Delta r & 0 \le j \le N_1-1 \\ \Delta r (R_2)^{j+1-N_1} & N_1 \le j \le N-1. \end{cases}$$

$M+1$ is the number of grid points on the z axis $2M_1+1$ is the number of grid points with uniform spacing on the axis, $N+1$ is the number of grid points on the r axis, and N_1+1 is the number of grid points with uniform spacing on the r axis.

For problems having cylindrical symmetry, the heat conduction equation has the form:

$$\rho c \frac{\partial v}{\partial t} = A + \frac{K}{r}\frac{\partial v}{\partial r} + \frac{\partial}{\partial r}\left(K \frac{\partial v}{\partial r}\right) + \frac{\partial}{\partial z}\left(K \frac{\partial v}{\partial z}\right), \qquad (1)$$

where $v(z, r, t)$ is temperature, $A(z, r, t)$ is source strength, $\rho(z)$ is density, $c(z)$ is specific heat, and $K(z)$ is thermal conductivity.[1] The following approximations are employed to obtain the finite difference representation of equation (1). For $i = 1, 2, \ldots, M-1$ and $k = 0, 1, 2, \ldots$:

Lt Col Dan Brown
USAF
SAM Records
Suitland

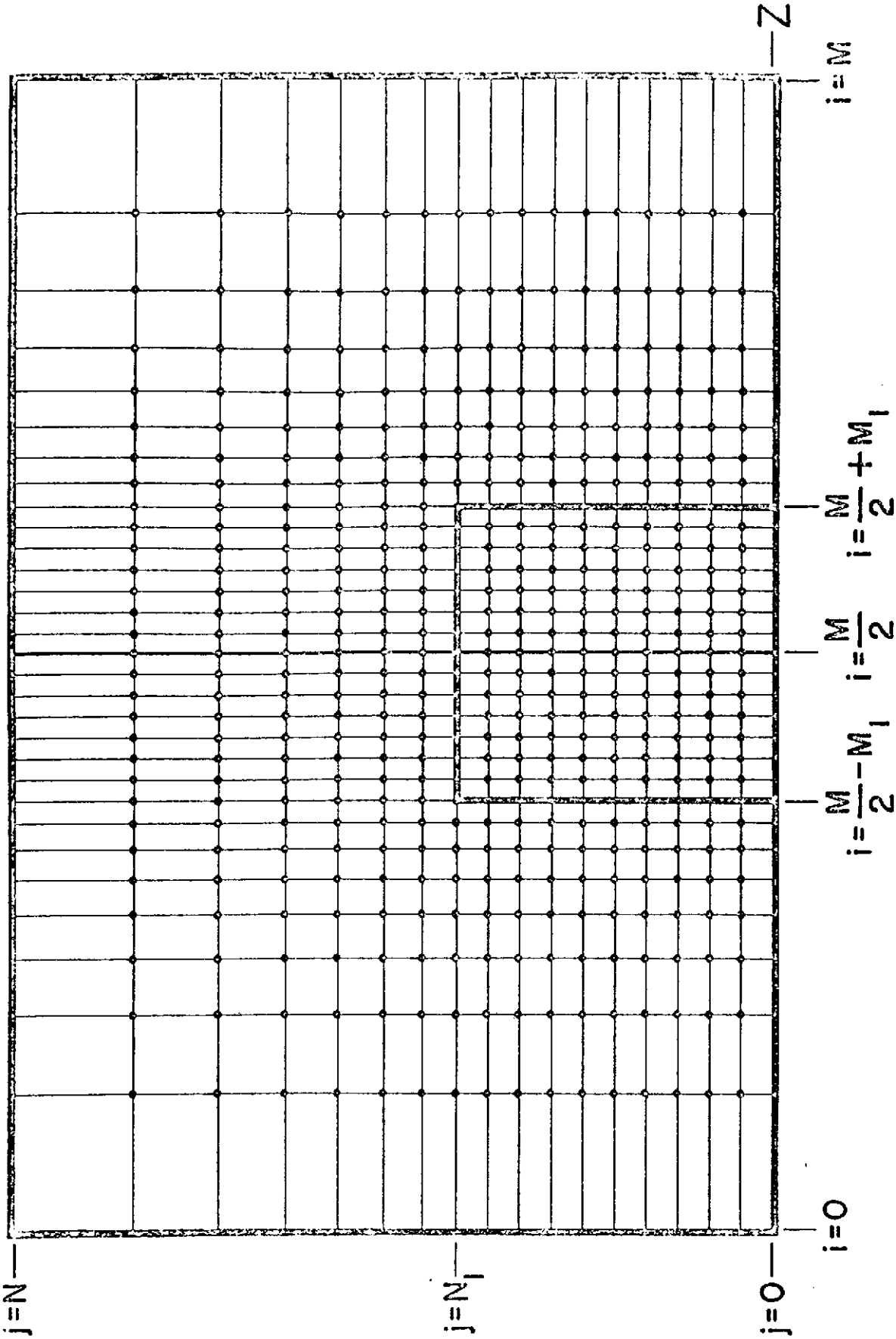

Figure 1. Finite difference grid.

Appendix B
LtCol Dan Brown
USAF
SAM Records
Suitland

$$\frac{K}{r}\left(\frac{\partial v}{\partial r}\right)\Bigg|_{i,j,k} \approx \frac{K_j}{r_j}\left[\frac{v_{i,j+1,k} - v_{i,j-1,k}}{r_{j+1} - r_{j-1}}\right] \qquad (j = 1, 2, \ldots, N-1)$$

$$\approx \frac{\partial}{\partial r}\left(K\frac{\partial v}{\partial r}\right)\Bigg|_{i,0,k} \qquad (j = 0), \qquad (2)$$

$$\frac{\partial}{\partial r}\left(K\frac{\partial v}{\partial r}\right)\Bigg|_{i,j,k} \approx \frac{2K_i}{r_{j+1} - r_{j-1}}\left[\frac{v_{i,j+1,k} - v_{i,j,k}}{r_{j+1} - r_j} - \frac{v_{i,j,k} - v_{i,j-1,k}}{r_j - r_{j-1}}\right]$$

$$(j = 1, 2, \ldots, N-1)$$

$$\approx \frac{2K_i}{r_1^2}\left[v_{i,1,k} - v_{i,0,k}\right] \qquad (j = 0), \qquad (3)$$

$$\frac{\partial}{\partial z}\left(K\frac{\partial v}{\partial z}\right)\Bigg|_{i,j,k} \approx \frac{2K_i}{z_{i+1} - z_{i-1}}\left[\frac{v_{i+1,j,k} - v_{i,j,k}}{z_{i+1} - z_i} - \frac{v_{i,j,k} - v_{i-1,j,k}}{z_i - z_{i-1}}\right]$$

$$+ \frac{K_{i+1} - K_{i-1}}{z_{i+1} - z_{i-1}}\left[\frac{v_{i+1,j,k} - v_{i-1,j,k}}{z_{i+1} - z_{i-1}}\right] \qquad (j = 0, 1, 2, \ldots, N),$$

nd

$$\rho c \frac{\partial v}{\partial t}\Bigg|_{i,j,k+\frac{1}{2}} = \frac{2\rho_i c_i}{\Delta t_k}\left[v_{i,j,k+\frac{1}{2}} - v_{i,j,k}\right] \qquad (j = 0, 1, 2, \ldots, N), \qquad (5)$$

here

$$\Delta t_k = t_{k+1} - t_k.$$

In equations (2)-(5), the indices i, j and k are integers which denote espectively the axial position of a grid point, the radial position of a rid point, and the time step. No attempt has been made to select weighting ıctors for equations (2)-(5) in order to account for higher order differences r the stretched grid. The accuracy of solutions obtained with these quations is already quite adequate for physiological problems, and the

List of Tables
BR 75-105
Appendix B

LtCol Dan Brown
USAF
SAM Records
Suitland

mall possible increase in accuracy does not justify the additional omplexity.

Row half step and column half step difference approximations o the heat conduction equation are computed by substituting equations (2)-5) into equation (1).[2] For the row half step:

$$E_{i,1}v_{i-1,j,k+\frac{1}{2}}-[E_{i,2}+2\rho_i c_i(\Delta t_k)^{-1}]v_{i,j,k+\frac{1}{2}}+E_{i,3}v_{i+1,j,k+\frac{1}{2}} \tag{6}$$
$$= -[K_iB_{j,1}v_{i,j-1,k}-K_iB_{j,2}v_{i,j,k}+K_iB_{j,3}v_{i,j+1,k}+2\rho_i c_i v_{i,j,k}(\Delta t_k)^{-1}+A_{i,j,k+\frac{1}{2}}].$$

For the column half step:

$$K_iB_{j,1}v_{i,j-1,k+1}-[K_iB_{j,2}+2\rho_i c_i(\Delta t_k)^{-1}]v_{i,j,k+1}+K_iB_{j,3}v_{i,j+1,k+1} \tag{7}$$
$$= -[E_{i,1}v_{i-1,j,k+\frac{1}{2}}-E_{i,2}v_{i,j,k+\frac{1}{2}}+E_{i,3}v_{i+1,j,k+\frac{1}{2}}+2\rho_i c_i v_{i,j,k+\frac{1}{2}}(\Delta t_k)^{-1}+A_{i,j,k+\frac{1}{2}}].$$

'he values of B and E are listed in Table XI.

Equations (6) and (7) must be used with a reasonable set of initial onditions and boundary conditions. It is convenient to select $0^{\circ}C$ for nitial and boundary conditions so that computed temperatures directly epresent the temperature increase above ambient temperature. The hange in temperature relative to this choice of initial and boundary onditions is calculated by solving equations (6) and (7) with the matrix eduction algorithm given in Table XII.

In computing chorioretinal temperature rises, it is assumed that

Lt Col Dan Brown
USAF
SAM Records
Suitland

$1 \le i \le (M/2)-M_1$	$\dfrac{R_1K_{i-1}+2(R_1+1)K_i-R_1K_{i+1}}{(\Delta z)^2(R_1+1)^2(R_1)^{M-2i-2M_1+1}}$	$\dfrac{2K_i}{(\Delta z)^2(R_1)^{M-2i-2M_1+1}}$	$\dfrac{K_{i+1}+2(R_1+1)K_i-K_{i-1}}{(\Delta z)^2(R_1+1)^2(R_1)^{M-2i-2M_1}}$
$M/2-M_1<i<(M/2)+M_1$	$\dfrac{K_{i-1}+4K_i-K_{i+1}}{4(\Delta z)^2}$	$\dfrac{2K_i}{(\Delta z)^2}$	$\dfrac{K_{i+1}+4K_i-K_{i-1}}{4(\Delta z)^2}$
$(M/2)+M_1 \le i \le M-1$	$\dfrac{K_{i-1}+2(R_1+1)K_i-K_{i+1}}{(\Delta z)^2(R_1+1)^2R_1^{2i-M-2M_1}}$	$\dfrac{2K_i}{(\Delta z)^2R_1^{2i-M-2M_1+1}}$	$\dfrac{R_1K_{i+1}+2(R_1+1)K_i-R_1K_{i-1}}{(\Delta z)^2(R_1+1)^2R_1^{2i-M-2M_1+1}}$
Range	$B_{j,1}$	$B_{j,2} = B_{j,1}+B_{j,3}$	$B_{j,3}$
$j = 0$	0	$\dfrac{4}{(\Delta r)^2}$	$\dfrac{4}{(\Delta r)^2}$
$1 \le j \le N_1-1$	$\dfrac{1}{(\Delta r)^2}\left(\dfrac{2j-1}{2j}\right)$	$\dfrac{2}{(\Delta r)^2}$	$\dfrac{1}{(\Delta r)^2}\left(\dfrac{2j+1}{2j}\right)$
$N_1 \le j \le N-1$	$\dfrac{\dfrac{2}{R_2^{j-N_1}}-\dfrac{1}{N_1+\sum_{n=1}^{j-N_1}(R_2)^n}}{(\Delta r)^2(R_2+1)R_2^{j-N_1}}$	$\dfrac{2}{(\Delta r)^2R_2^{2j-2N_1+1}}$	$\dfrac{\dfrac{2}{R_2^{j-N_1+1}}+\dfrac{1}{N_1+\sum_{n=1}^{j-N_1}(R_2)^n}}{(\Delta r)^2(R_2+1)R_2^{j-N_1}}$

Lt Col Don Brown
USAF
SAM Records
Suitland

	Row half step	Column half step
Tridiagonal to bidiagonal	$C_0 = 0,\ D_0 = 0.$ For $i = 1, 2, 3, \ldots, M-1;\ j=0, 1, \ldots, N-1$: $F_i = E_{i,2} + 2\rho_i c_i (\Delta t_k)^{-1} - E_{i,1} C_{i-1},$ $C_i = E_{i,3} F_i^{-1},$ and $D_i = [E_{i,1} D_{i-1} + K_i (B_{j,1} v_{i,j-1,k} - B_{j,2} v_{i,j,k}$ $+ B_{j,3} v_{i,j+1,k}) + 2\rho_i c_i (\Delta t_k)^{-1} v_{i,j,k}$ $+ A_{i,j,k}] F_i^{-1}.$	$C_{-1} = 0,\ D_{-1} = 0.$ For $j = 0, 1, 2, \ldots, N-1;\ i=1, 2, \ldots, M-1$: $F_j = K_i B_{j,2} + 2\rho_i c_i (\Delta t_k)^{-1} - K_i B_{j,1} C_{j-1},$ $C_j = K_i B_{j,3} F_j^{-1},$ and $D_j = [K_i B_{j,1} D_{j-1} + E_{i,1} v_{i-1,j,k+\frac{1}{2}} - E_{i,2} v_{i,j,k+\frac{1}{2}}$ $+ E_{i,3} v_{i+1,j,k+\frac{1}{2}} + 2\rho_i c_i (\Delta t_k)^{-1} v_{i,j,k+\frac{1}{2}}$ $+ A_{i,j,k+\frac{1}{2}}] F_j^{-1}.$
Bidiagonal to diagonal	$v_{M-1,j,k+\frac{1}{2}} = D_{M-1}.$ For $i = M-2, M-3, \ldots, 2, 1$: $v_{i,j,k+\frac{1}{2}} = D_i + C_i v_{i+1,j,k+\frac{1}{2}}.$	$v_{i,N-1,k+\frac{1}{2}} = D_{N-1}.$ For $j = N-2, N-3, \ldots, 2, 1, 0$: $v_{i,j,k+1} = D_j + C_j v_{i,j+1,k+1}.$

Lt Col Don Brown
USAF
Sam Records
Suitland

Appendix B
pp 75 — 105

: irradiance is exponentially attenuated by tissues which are thermally mogeneous. Since the only significant light absorption per unit length oducing chorioretinal heating occurs in the retinal pigment epithelium . E.) and the choroid, these regions contribute the most significant at sources. The source regions and the geometry of the problem are own in Figure 34. Source strengths for the P. E. and choroid are spectively

$$A_1 = h H_0 \, a_1 \exp[-a_1 z] \qquad \text{(P. E.)} \qquad (8)$$

l

$$A_2 = h H_0 \, a_2 \exp[d_1(a_2 - a_1) - a_2 z] \, . \qquad \text{(Choroid)}, \qquad (9)$$

ere d_1 is the depth of the P. E., a_1 and a_2 are the absorption coefficients the P. E. and the choroid respectively, H_0 is the retinal irradiance $(r, z) = (0, 0)$ and $h(r)$ is the radial distribution of retinal irradiance.

Absorption coefficients in equations (8) and (9) may be expressed 'he form

$$a_1 = -d_1^{-1} \ln \, [1 - mf] \qquad (10)$$

$$a_2 = d_2^{-1} \ln \, [(1 - mf)(1 - f)^{-1}], \qquad (11)$$

·re f is the fraction of light entering the P. E. that is absorbed in h the P. E. and the choroid, mf is the fraction of light incident on P. E. that is absorbed in the P. E., and d_2 is the depth of the choroid.

List of Tables
pg 75 - 105
Appendix B

LtCol Dan Brown
USAF
SAM Records
Suitland

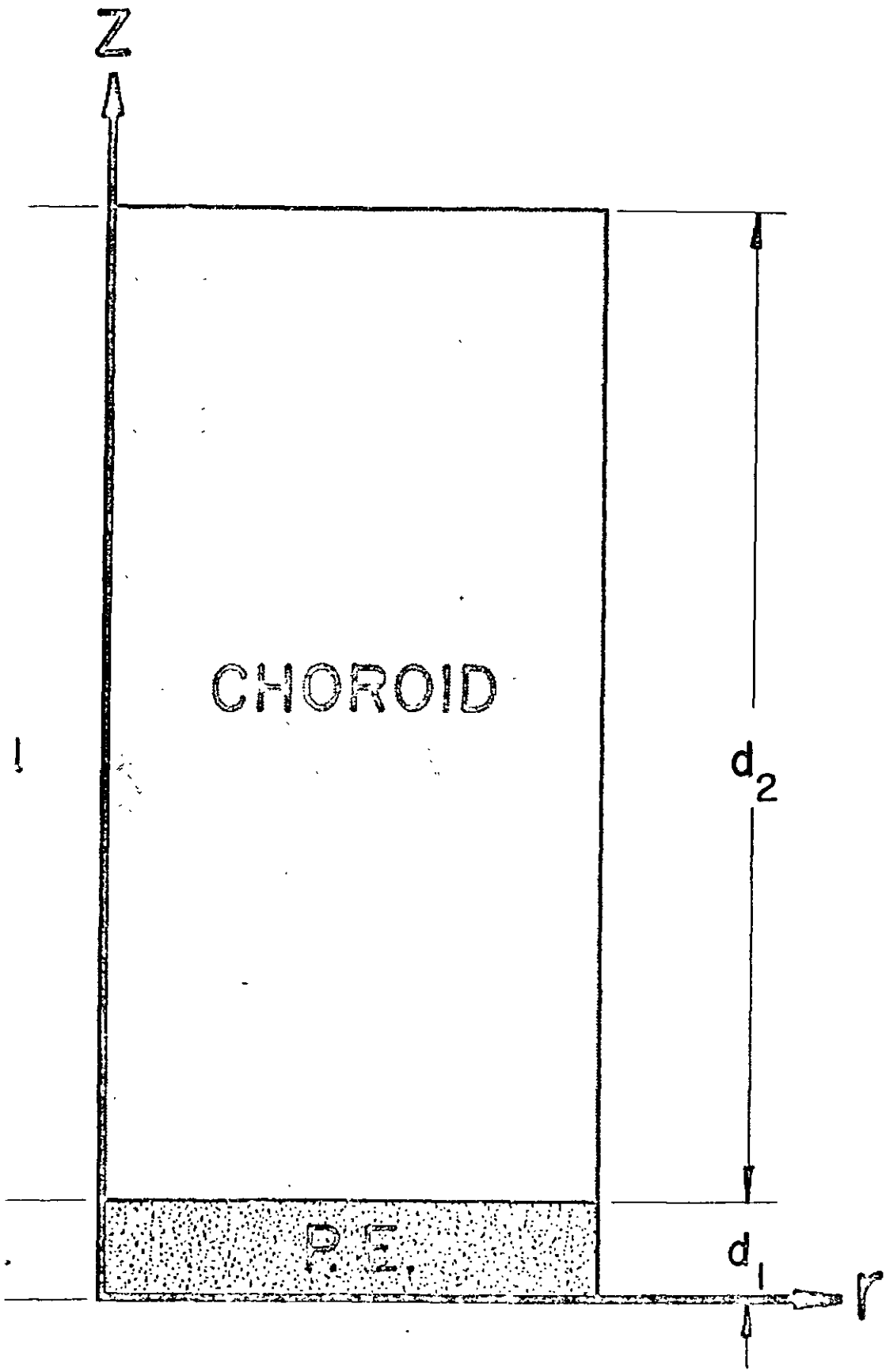

Figure 34. Chorioretinal heat source.

List of Tables
SR 75-105
Appendix B

LtCol Dan Brown
USAF
SAM Records
Suitland

Experimental data were used to solve equations (10) and (11), and the absorption coefficients then used in equations (8) and (9) to compute source strengths for the P.E. and choroid.[3,4]

Calculations have been executed assuming that the thermal properties of ocular media are approximated by the thermal properties of water: $K = 1.5 \times 10^{-3}$ cal $^{\circ}C^{-1}$ sec^{-1} cm^{-1}, $c = 1$ cal $^{\circ}C^{-1}$ gm^{-1} and $\rho = 1$ gm cm^{-3}. The chorioretinal thermal response to the following radial distributions of retinal irradiance has been examined:

$$\left.\begin{array}{ll} h(r) = 1 & (r \le a) \\ h(r) = 0 & (r > a) \end{array}\right\} \quad \text{(Uniform)}, \qquad (12)$$

and

$$h(r) = \exp\left[-r^2/2\sigma^2\right] \qquad \text{(Gaussian)}, \qquad (13)$$

where a and σ characterize the uniform and Gaussian distributions respectively. A broad range of image sizes, exposure times and absorption coefficients has been studied.

No detailed calculation of safe observer distances have as yet been made with this model using Dominic scaled weapon data. However, several calculations using averaged values for transmissions and absorptions and using total power have been made. An example of this type is shown in Figure 35.

Appendix B
LtCol Dan Brown
USAF
SAM Records
Suitland

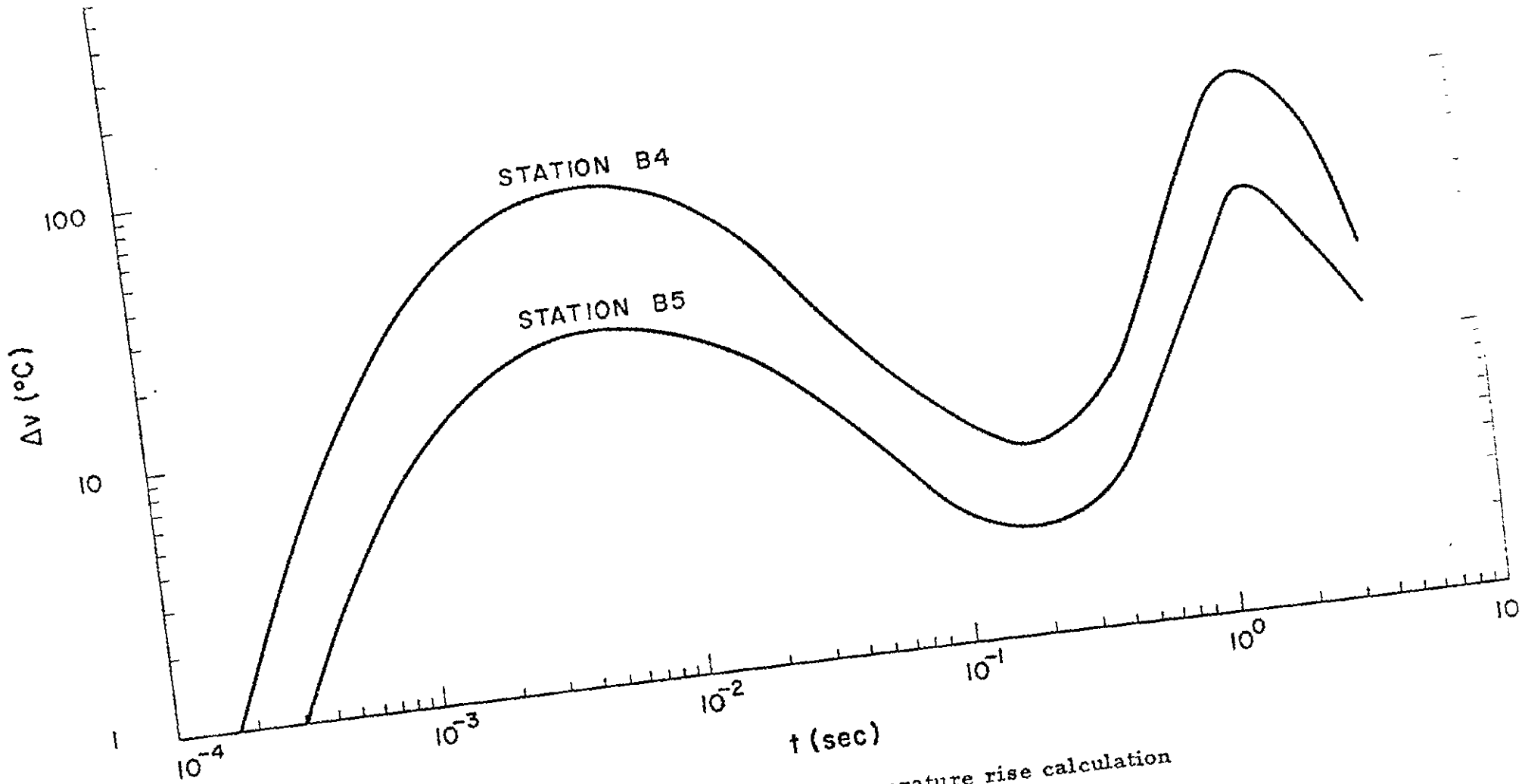

Figure 35. Example of temperature rise calculation for Dominic field test data.

All aspects of use of the model are well understood with two possible exceptions: the form of the energy distribution in the eye for small image sizes from nuclear sources and the thermal criterion for damage. The first question will require considerable effort and should be made a part of future development of the model particularly for application to high altitude bursts. The evidence regarding the second question seems to indicate that a simple temperature rise is adequate, but this is by no means certain, and until we have adequate understanding of the chemical processes which occur in the formation of observable burns, the proper thermal criterion for time varying sources remains in doubt.

1. REFERENCES

1. Carslaw, H. S. and J. C. Jaeger, Conduction of Heat in Solids. London: Oxford, 1959.

2. Peaceman, D. W. and H. H. Rachford, Jr. "The numerical solution of parabolic and elliptic differential equations," J. Soc Indust. Appl. Math., 3, 28-41, 1955.

3. Geeraets, W. J. and E. R. Berry. "Ocular spectral characteristics as related to hazards from lasers and other light sources," Am. J. Ophthal., 66, 15-20, 1968.

4. Beottner, E. A. and J. R. Wolter. "Transmission of the ocular media," Invest. Ophthal., 1, 776-783, 1962.

Lt Col Dan Brown
USAF
SAM Records
Suitland

Copy Cover, TOC
List of Figures
List of Tables
pp 75 - 105
Appendix B
Appendix D

APPENDIX A

Lt Col Dan Brown
USAF
SAM Records
Suitland

Table A-I. Rabbit threshold data for 6.1° beam divergence. (Calculated 1.07 mm image diameter.)

Animal #	Burn/ No Burn	Retinal Exposure Energy (mj)	Retinal Threshold Energy - U_R(mj)
9F7L	(+)	13	12
	(-)	11	
9F3L	(+)	12	11
	(-)	9.8	
9F3R	(+)	13	12
	(-)	11	
0H8L	(+)	12	11
	(-)	10	
0H8R	(+)	12	11
	(-)	10	
9F7R	(+)	13	12
	(-)	12	
6U6L	(+)	9.3	8.9
	(-)	8.5	
TI5L	(+)	8.1	7.9
	(-)	7.8	
3T0L	(+)	8.2	7.7
	(-)	7.2	
3T0R	(+)	9.2	8.7
	(-)	8.2	
		Average Threshold 10 ± 1.7	

(+) Burn
(-) No Burn

† This threshold energy corresponds to an average retinal exposure, Q_R, of 0.27 cal/cm^2 with σ = 0.046.

LtCol Dan Brown
USAF
SAM Records
Suitland

Table A-II. Rabbit threshold data for 3.0° beam divergence. (Calculated 0.52 mm image diameter.)

Animal #	Burn/ No Burn	Retinal Exposure Energy (mj)	Retinal Threshold Energy - U_R (mj)
9T8R	(+)	4.0	4.0
	(-)	3.9	
2E1L	(+)	5.4	5.2
	(-)	5.0	
2E1R	(+)	4.6	4.3
	(-)	4.0	
9T4R	(+)	4.7	4.7
	(-)	4.6	
9T4L	(+)	3.6	3.5
	(-)	3.4	
6U6R	(+)	3.9	3.8
	(-)	3.6	
6U6L	(+)	3.3	3.2
	(-)	3.0	
None	(+)	2.9	2.9
	(-)	2.8	
None	(+)	3.0	2.9
	(-)	2.8	
T16R	(+)	1.8	1.7
	(-)	1.6	
		Average Threshold 3.6 ± 1.1	

+) Burn
-) No Burn

This threshold energy corresponds to an average retinal exposure, Q_R, of 0.41 cal/cm^2 with σ = 0.11.

LtCol Dan Brown
USAF
SAM Records
Suitland

Table A-III. Primate long pulse threshold data for 5.08° beam divergence. (Calculated 1.20 mm image diameter.)

Animal #	Burn/ No Burn	Retinal Exposure Energy (mj)	Retinal Threshold Energy - U_R(mj)
CR2R	(+) (-)	3.8 3.3	3.6
CR2L.	(+) (-)	3.5 3.2	3.4
CR6R	(+) (-)	3.4 3.1	3.1
CR6L	(+) (-)	3.5 2.9	3.2
11NR	(+) (-)	3.2 2.4	2.8
11NL	(+) (-)	2.7 2.3	2.5
		Average Threshold 3.1 ± 0.	

(+) Burn
(-) No Burn

† This threshold energy corresponds to an average retinal exposure, Q_R, of 0.066 cal/cm^2 with c = 0.0087.

Lt Col Dan Brown
USAF
SAM Records
Suitland

Table A-IV. Primate threshold data for 2.5° beam divergence. (Calculated 0.59 mm image diameter.)

Animal #	Burn/ No Burn	Retinal Exposure Energy (mj)	Retinal Threshold Energy - U_R(mj)
O1NL	(+)	0.69	0.68
	(-)	0.66	
O1NR	(+)	0.69	0.68
	(-)	0.66	
CR0L	(+)	0.72	0.69
	(-)	0.66	
O3NR	(+)	0.75	0.71
	(-)	0.66	
O3NL	(+)	0.69	0.66
	(-)	0.63	
		Average Threshold 0.68, σ = 0.01	

(+) Burn
(-) No Burn

† This threshold energy corresponds to an average retinal exposure, Q_R, of 0.060 cal/cm^2 with σ = 0.0016.

LtCol Dan Brown
USAF
SAM Records
Suitland

Table A-V. Primate threshold data for 1.23° beam divergence. (Calculated 0.29 mm image diameter.)

Animal #	Burn/ No Burn	Retinal Exposure Energy (mj)	Retinal Threshold Energy - U_R(mj)
21NR	(+)	0.52	0.48
	(-)	0.44	
21NL	(+)	0.41	0.41
	(-)	0.38	
23NR	(+)	0.38	0.36
	(-)	0.34	
23NL	(+)	0.36	0.35
	(-)	0.34	
CL4R	(+)	0.55	0.52
	(-)	0.48	
CL4L	(+)	0.50	0.48
	(-)	0.46	
		Average Threshold	0.43 . $\sigma = 0.070$

(+) Burn
(-) No Burn

† This threshold energy corresponds to an average retinal exposure, Q_R, of 0.16 cal/cm^2 with σ = 0.025.

Lt Col Dan Brown
USAF
SAM Records
Suitland

Table A-VI. Primate Q-switched (1 pulse) threshold data for 1.2 mm image diameter.

Animal #	Burn/ No Burn	Retinal Exposure Energy (mj)	Retinal Threshold Energy - U_R (mj)
OX1L	(+)	1.4	1.4
	(-)	1.4	
OX2R	(+)	1.2	0.85
	(-)	0.51	
OX2L	(+)	0.75	0.80
	(-)	0.85	
		Average Threshold	1.0

(+) Burn
(-) No Burn

Table A-VII. Primate Q-switched (4 pulses) threshold data for 1.2 mm image diameter.

nimal #	Burn/ No Burn	#	Retinal Exposure Energy (mj)	Retinal Threshold Energy - U_R (mj)
OX1R	(+)	4	4.4	4.0
	(-)	4	3.5	
OX1L	(+)	4	3.7	3.4
	(-)	4	3.1	
OX2R	(+)	5	3.1	3.0
	(-)	5	2.9	
X2L	(+)	6	3.3	3.1
	(-)	6	2.9	
			Average Threshold	3.4

Burn
No Burn

LtCol Dan Brown
USAF
SAM Records
Suitland

Table A-VIII. Primate Q-switched (5-8 pulses) threshold data for 0.59 mm image diameter.

Animal #	Burn/ No Burn	#	Retinal Exposure Energy (mj)	Retinal Threshold Energy - U_R (mj)
OX1L	(+)	6	1.2	1.1
	(-)	7	0.95	
OX1R	(+)	8	1.7	1.7
	(-)	7	1.6	
OX2L	(+)	5	1.3	1.3
	(-)	5	1.3	
			Average Threshold	1.4

(+) Burn
(-) No Burn

Lt Col Dan Brown
USAF
SAM Records
Suitland

APPENDIX B

LtCol Dan Brown
USAF
SAM Records
Suitland

Table B-I. Mean recovery times in seconds for each subject for 19' Sloan-Snellen letters following 2.3×10^7 td·sec flashes subtending 0.5° visual angle.

	Task Luminance (mL)							
Subject	38.0	9.5	3.8	0.76	0.38	0.122	0.076	0.0605
GG	2.2	3.5	5.1	6.7	8.3	10.2	11.7	13.7
TD	1.8	3.8	5.5	7.5	9.6	11.5	14.5	16.8
TG	2.9	4.8	6.5	8.6	13.0	18.3	28.6	33.1
LS	3.4	5.7	7.9	10.2	13.7	17.6	21.4	25.7
KM	2.3	4.3	6.0	7.9	9.8	13.5	15.7	18.2
$\bar{X}$	2.52	4.42	6.20	8.18	10.88	14.22	18.38	21.50

Table B-II. Mean recovery times in seconds for each subject for 19' Sloan-Snellen letters following 2.3×10^7 td·sec flashes subtending 1.0° visual angle.

	Task Luminance (mL)							
Subject	38.0	9.5	3.8	0.76	0.38	0.122	0.076	0.0605
GG	2.4	4.0	5.5	7.3	9.3	11.4	13.6	15.4
TD	3.6	5.2	7.0	8.6	10.3	12.9	15.4	17.5
LS	4.2	6.2	8.6	10.6	12.9	15.7	18.9	22.2
KM	2.7	5.3	7.8	10.2	12.2	16.5	23.7	28.4
$\bar{X}$	3.22	5.18	7.23	9.18	11.18	14.13	17.9	20.9

LtCol Dan Brown
USAF
SAM Records
Suitland

Table B-II. Mean recovery times in seconds for each subject for 19' Sloan-Snellen letters following 2.7×10^7 td·sec flashes subtending 2° visual angle.

	Task Luminance (mL)							
ıbject	38.0	9.5	3.8	0.76	0.38	0.122	0.076	0.0605
TD (5)	2.8	4.3	6.3	10.7	13.7	21.9	29.6	35.6
GG (11)	3.6	7.7	12.7	19.4	33.4	57.6	85.2	99.3
TG (8)	8.3	11.1	15.3	20.6	26.5	52.6	80.8	94.1
CV (4)	6.2	11.4	14.1	18.5	25.4	30.4	45.0	52.7
KM (5)	5.2	8.1	10.1	14.6	21.5	38.8	52.2	64.5
$\bar{X}$	5.24	8.52	11.70	16.76	24.10	40.26	58.52	69.24

Table B-III. Mean recovery times in seconds for each subject for 19' Sloan-Snellen letters following 2.7×10^7 td·sec flashes subtending 4° visual angle.

	Task Luminance (mL)							
ject	38.0	9.5	3.8	0.76	0.38	0.122	0.076	0.0605
D (5)	3.5	6.1	7.6	11.2	16.0	29.2	38.6	41.4
G (12)	4.8	9.1	11.5	18.2	33.1	51.5	85.5	111.1
G (7)	6.8	9.3	9.8	13.5	20.6	32.4	48.6	63.1
V (5)	7.0	9.3	11.6	18.8	24.9	41.6	59.0	63.6
M (6)	6.8	8.9	10.9	17.4	32.4	46.5	72.4	88.1
	5.78	8.54	10.28	15.82	25.40	40.24	60.82	73.

† Numbers in parentheses refer to the number of flashes for each subject

Lt Col Dan Benwal
USAF
SAM Records
Suitland

Table B - IV. Mean recovery times in seconds for each subject for 19' Sloan-Snellen letters following 2.7×10^7 td·sec flashes subtending 6° visual angle.

	Task Luminance (mL)							
›ject	38.0	9.5	3.8	0.76	0.38	0.122	0.076	0.0605
D (11)	3.4	5.3	7.0	10.5	16.0	23.8	31.7	40.1
G (6)	5.6	9.9	10.8	21.4	24.2	91.1	98.8	109.1
G (1)	4.7	6.2	10.8	13.8	53.1	65.2	88.0	104.8
V (4)	6.3	8.7	11.3	17.8	22.6	43.0	64.6	64.9
M (1)	8.5	9.7	11.1	16.4	30.1	54.1	57.3	72.7
	5.70	7.96	10.20	15.98	29.20	55.44	68.08	78.32

Table B - V. Mean recovery times in seconds for each subject for 19' Sloan-Snellen letters following 2.7×10^7 td·sec flashes subtending 8° visual angle.

	Task Luminance (mL)							
ects	38.0	9.5	3.8	0.76	0.38	0.122	0.076	0.0605
) (3)	5.7	7.1	10.4	17.5	24.7	41.2	58.4	70.1
; (6)	6.8	9.6	12.8	19.0	32.6	59.3	74.0	110.0
; (7)	7.1	8.6	12.0	14.1	22.2	50.8	63.6	83.0
' (3)	7.6	10.0	11.9	20.0	24.1	46.3	55.9	57.7
I (1)	6.1	7.2	9.8	11.2	21.7	41.7	74.7	78.1
	6.66	8.50	11.38	16.36	25.06	47.86	65.32	79.78

† Numbers in parentheses refer to the number of flashes for each subject.

Lt Col Dan Brown
USAF
SAM Records
Suitland

Table B-VI. Mean recovery times in seconds for each subject for 19' Sloan-Snellen letters following 2.7×10^7 td·sec flashes subtending 10° visual angle.

	Task Luminance (mL)							
ıbject	38.0	9.5	3.8	0.76	0.38	0.122	0.076	0.0605
TD (7)	5.9	8.6	9.7	14.7	18.7	31.0	38.8	47.6
GG (11)	6.9	9.5	11.2	23.8	33.8	55.6	94.0	109.6
TG (8)	8.4	9.8	12.2	21.8	32.9	51.3	67.6	85.8
EV (5)	6.7	7.8	9.8	19.2	23.6	36.8	51.6	63.2
KM(6)	6.5	7.8	9.8	18.4	26.7	35.8	63.5	80.2
$\bar{X}$	6.88	8.70	10.54	19.58	27.14	42.10	63.10	77.28

† Numbers in parentheses refer to the number of flashes for each subject.

LtCol Dan Brown
USAF
SAM Records
Suitland

APPENDIX C

THE FEASIBILITY OF ANALOG OCULOTHERMAL SIMULATION

Lt Col Dan Brown
USAF
SAM Records
Suitland

INTRODUCTION

This report is written to satisfy the requirements of Paragraph 4.2(f), contract F41609-68-C-0023, which concerns the "feasibility of constructing a two-dimensional analog computer circuit to predict temperature levels within the exposed retina".

Two previous communications on this subject have been issued. Progress Report Number 2 for the period of 20 February 1968 to 20 May 1968 contained a summary of our initial assessment of the practicability of an analog device. A later oral communication on 14 August 1968 with Mr. E. O. Richey, the contract monitor, contained the results of a more detailed analysis of this matter by T. J. White, P. W. Wilson, D. E. Jungbauer, D. Hegedus, and D. Golden of the Life Sciences Division. This later study indicated that although the construction of an analog computer was conceptually feasible, the results would not warrant the effort required because of certain practical considerations.

In the following discussion, we shall use the term "simple eye model" to denote a physical description of the ocular system which possesses:

1. laminar structure,
2. laminar boundaries constant in the coordinate system, and
3. thermal conductivity and diffusivity which are independent of time, temperature, and laminar region.

Lt Col Dan Brown
USAF
SAM Records
Suitland

2. RESISTANCE-CAPACITANCE ANALOG

2.1 The Thermal Problem

Theoretical difficulties are not encountered in the construction of a tw dimensional resistor-capacitor network to simulate the thermal behav of a simple eye model.[1-3] Indeed, techniques for simulating much mor general situations are well known.[4] It is the practical considerations i the development of an analog device which present the principal difficul The range of values available for passive electrical components and the requirements of recording node voltages limit the range of thermal variables which can be adequately described. Time scaling and the accurate simulation of a source which is varying in both space and time must be performed if the electrical analog is to be capable of simulating nuclear weapon thermal pulses.

Techniques for the simulation of heat conduction in solids are based upon a difference equation approximation to the partial differential equa tion which describes heat flow. The heat sources which will be conside have azimuthal symmetry. Therefore, the differential equation which must be solved has the form:

$$\frac{\partial^2 \theta}{\partial r^2} + \frac{1}{r}\frac{\partial \theta}{\partial r} + \frac{\partial^2 \theta}{\partial z^2} = \frac{1}{k}\frac{\partial \theta}{\partial T} - \frac{A}{K}$$

where

r and z are radial and longitudinal distances in cm,

Lt Col Dan Brown
USAF
SAM Records
Suitland

k is thermal diffusivity in cm^2/sec,

K is thermal conductivity in $cal/^oC\ cm\ sec$,

$A(r, z, t)$ is source strength in $cal/cm^3 sec$,

$\theta(r, z, t)$ is temperature in ^oC, and

T is time in seconds.

Since we are interested only in the changes of initial temperature values, we will employ the initial condition

$$\lim_{T \to 0} \theta(r, z, T) = 0.$$

Since regions of the eye which absorb the most energy and therefore have the largest source strengths constitute only a small part of the total ocular structure, we will use the boundary conditions,

$$\lim_{r \to \infty} \theta(r, z, T) = 0$$

and

$$\lim_{z \to \infty} \theta(r, z, T) = 0.$$

2 Thermal-Electrical Correspondence

Replacing the terms in the left hand member of Equation (1) by differences centered at (r_o, z_o), we obtain

$$\frac{1}{\Delta r}\left[\frac{\theta_1 - \theta_0}{\Delta r} - \frac{\theta_0 - \theta_2}{\Delta r}\right] + \frac{1}{2r_o}\left[\frac{\theta_1 - \theta_0}{\Delta r} + \frac{\theta_0 - \theta_2}{\Delta r}\right] + \frac{1}{\Delta z}\left[\frac{\theta_3 - \theta_0}{\Delta z} - \frac{\theta_0 - \theta_4}{\Delta z}\right].$$

Subscripts 1 and 2 refer to points on either side of r_o which are displaced in the r direction, while subscripts 3 and 4 refer to points displaced in

Lt Col Dan Brown
USAF
SAM Records
Suitland

the z direction. $\frac{\partial\theta}{\partial r}$ has been replaced by the average rate of chang θ between 1 and 2. Terms containing derivatives in the r direction then be combined in the following manner:

$$\frac{1}{(\Delta r)^2}\left[(\theta_1-\theta_0)-(\theta_0-\theta_2)\right]+\frac{\Delta r}{2r_o}\left[\frac{\theta_1-\theta_0}{(\Delta r)^2}+\frac{\theta_0-\theta_2}{(\Delta r)^2}\right]$$

$$=\frac{\theta_1-\theta_0}{(\Delta r)^2}(1+\Delta r/2r_o)+\frac{\theta_2-\theta_0}{(\Delta r)^2}(1-\Delta r/2r_o)$$

$$=\frac{1}{r_o}\left[\frac{\theta_1-\theta_0}{\frac{(\Delta r)^2}{r_o+\Delta r/2}}+\frac{\theta_2-\theta_0}{\frac{(\Delta r)^2}{r_o-\Delta r/2}}\right].$$

Equation (1) may therefore be put in the form:

$$\frac{1}{r_o}\left[\frac{\theta_1-\theta_0}{\frac{(\Delta r)^2}{r_o+\Delta r/2}}+\frac{\theta_2-\theta_0}{\frac{(\Delta r)^2}{r_o-\Delta r/2}}+\frac{\theta_3-\theta_0}{\frac{(\Delta z)^2}{r_o}}+\frac{\theta_4-\theta_0}{\frac{(\Delta z)^2}{r_o}}\right]=\frac{1}{k}\frac{\partial\theta}{\partial T}\bigg|_{r_o,z_o}-\frac{A}{K}\bigg|_{r_o,z}$$

Note that difference expressions are not used on the right hand side of Equation (2). These terms then represent continuous variation of temperature and continuous thermal input which will in turn be seen to correspond to continuous recording of data and continuous electrical input in the electrical analog.

In Table I, we have detailed the correspondence between electrical and thermal quantities which forms the basis for simulating heat conduction problems by an electrical analog.

Multiplying Equation (2) by $2\pi r_o\Delta r\Delta zK$, we obtain

Lt Col Dan Brown
USAF
SAM Records
Suitland

Table I. Correspondence between electrical and thermal parameters

Thermal Parameter	Thermal Units	Electrical Parameter	Electrical Units
$\Delta\theta$ Temperature Rise	^{o}C	V Voltage	volts
Q Quantity of Heat	cal	q Charge	coulomb
T Thermal Time	sec	t Electrical Time	seconds
P Thermal Power	cal/sec	i Current	amperes
R_θ Thermal Resistance	^{o}C sec/cal	ρ Resistance	ohm
C_θ Thermal Capacitance	cal/^{o}C	C Capacitance	farad

LtCol Dan Brown
USAF
SAM Records
Suitland

$$\frac{\theta_1-\theta_0}{\dfrac{\Delta r}{K2\pi(r_o+\Delta r/2)\Delta z}} + \frac{\theta_2-\theta_0}{\dfrac{\Delta r}{K2\pi(r_o-\Delta r/2)\Delta z}} + \frac{\theta_3-\theta_0}{\dfrac{\Delta z}{K2\pi r_o\Delta r}} + \frac{\theta_4-\theta_0}{\dfrac{\Delta z}{K2\pi r_o\Delta r}}$$

$$= \frac{\left.\dfrac{\partial\theta}{\partial T}\right|_{r_o,z_o}}{\dfrac{k}{K}\,\dfrac{1}{2\pi r_o\Delta r\Delta z}} - \frac{\left.A\right|_{r_o,z_o}}{\dfrac{1}{2\pi r_o\Delta r\Delta z}} .$$

Each term in Equation (3) has the units of thermal power, cal/sec. The terms on the right hand side have the respective forms (temperature)·(thermal capacitance/time) and (thermal power/unit volume)·(volume). This suggests an electrical analog in which each term is a current (see Table I). The terms on the left side will be voltage divided by resistance. The term involving the time derivative will be voltage times capacitance divided by time. The source term will be current per unit volume times volume.

Figure 1A shows how the denominator of each term in the left hand side of Equation (3) may be interpreted ($\frac{1}{K}$ is thermal resistivity). In the $0\rightarrow 1$ direction which corresponds to the first term of Equation (3), path length is Δr and average axial area is $(1/2)\,2\pi\,[\,r_o+(r_o+\Delta r)\,]\,\Delta z = 2\pi(r_o+\frac{\Delta r}{2}$ Thermal resistance in this direction is then (thermal resistivity) (length average area), or

$$R\theta_r = \frac{\Delta r}{K2\pi(r_o+\Delta r/2)\Delta z} .$$

Lt Col Dan Brown
USAF
SAM Records
Suitland

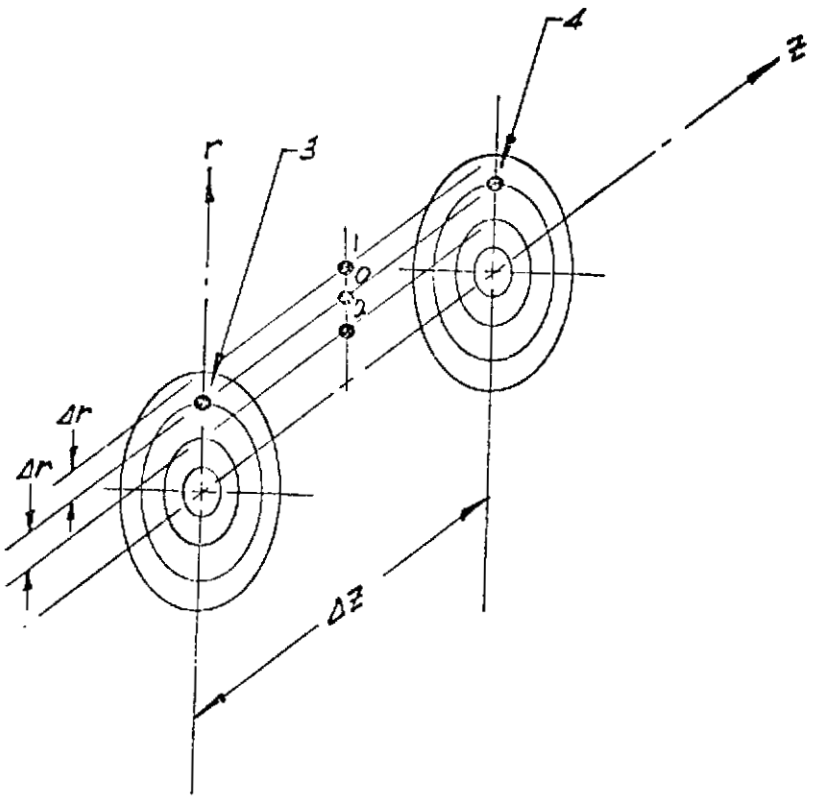

Figure 1A.

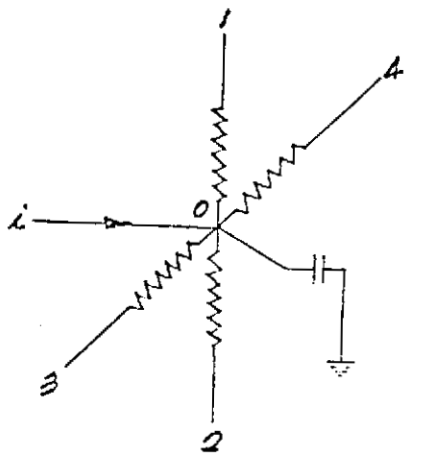

Figure 1B.

Figure 1. Correspondence of Thermal and Electrical Resistance.

Lt Col Dan Brown
USAF
SAM Records
Suitland
Md. 20746

Similarly in the 0→2 direction,

$$R_{\theta r} = \frac{\Delta r}{K2\pi(r_o - \Delta r/2)\,\Delta z}.$$

Note that Equation (4') reduces to Equation (4) when r_o is replaced by $r_o + \Delta r$. Therefore, we need only consider Equation (4) in order to determine appropriate resistances.

In the 0→3 and 0→4 directions, path length is Δz and area is

$$\pi(r_o + \Delta r/2)^2 - \pi(r_o - \Delta r/2)^2 = 2\pi r_o \Delta r.$$

Thus

$$R_{\theta z} = \frac{\Delta z}{K2\pi r_o \Delta r}.$$

The quantity

$$V_o = 2\pi r_o \Delta r \Delta z$$

in the right side of Equation (3) is the volume element associated with the point P_o. For those points along the z axis (r_o=0), these expression must be respectively modified to obtain

$$R_{\theta r} = \frac{1}{K\pi\Delta z},$$

$$R_{\theta z} = \frac{4\Delta z}{K\pi(\Delta r)^2},$$

and

$$V_o = \frac{\pi(\Delta r)^2 \Delta z}{4}.$$

We may therefore construct an electrical analog device to simulate the temperature at a fixed number of points in our ocular model. Such a

Lt Col Dan Brown
USAF
SAM Records
Suitland

device consists of an electrical circuit which has the form of a grid (net) in which each grid point (node) is the combination of electrical components illustrated in Figure 1B. Resistors have values proportional to the thermal resistances in Equations (4) and (5) or Equations (7) and (8). Thermal capacitance is simulated by an electrical capacitance which leads to ground at each node. Since thermal capacitance is equal to the product of $\frac{K}{k}$ and the nodal volume V_o,

$$C_\theta = \frac{K}{k} 2\pi r_o \Delta r \Delta z, \tag{10}$$

and on the z axis

$$C_\theta = \frac{K}{k} \frac{\pi}{4} (\Delta r)^2 \Delta z. \tag{11}$$

The current supplied to each node represents the source term, $A\Big|_{r_o, z_o} \times V_o$.

Assigning scale factors as suggested by Karplus[3] for voltage, time and capacitance, we have

$$V = j\theta,$$

$$t = nT,$$

and $$C = C_\theta / m.$$

Hence, $\rho = mn\, R_\theta$ and $i = \frac{j}{mn} P$,

where ρ is resistance, i is current and P is thermal power (see Table I).

Equation (3) may be transformed into electrical variables if each side of the equation is multiplied by j/mn. Thus,

LtCol Dan Brown
USAF
SAM Records
Suitland

$$\frac{j(\theta_1-\theta_0)}{mn\left\{\frac{\Delta r}{K2\pi(r_o+\Delta r/2)\Delta z}\right\}} + \frac{j(\theta_2-\theta_0)}{mn\left\{\frac{\Delta r}{K2\pi(r_o-\Delta r/2)\Delta z}\right\}} + \frac{j(\theta_3-\theta_0)}{mn\left\{\frac{\Delta z}{K2\pi r_o\Delta r}\right\}} + \frac{j(\theta_4-\theta_0)}{mn\left\{\frac{\Delta z}{K2\pi r_o\Delta r}\right\}}$$

$$= \frac{\frac{j}{n}\frac{\partial\theta}{\partial T}\Big|_{r_o,z_o}}{m\left\{\frac{k}{K}\frac{1}{2\pi r_o\Delta r\Delta z}\right\}} - \frac{j}{mn}\,2\pi r_o\Delta r\Delta z\;\; A\Big|_{r_o,z_o}. \qquad ($$

The electrical equivalent of Equation (3) is therefore

$$\frac{V_1-V_0}{R_{10}} + \frac{V_2-V_0}{R_{20}} + \frac{V_3-V_0}{R_{30}} + \frac{V_4-V_0}{R_{40}} = C\Big|_{r_o,z_o}\frac{\partial V}{\partial t}\Big|_{r_o,z_o} - i_s\Big|_{r_o,z_o}.$$

The current sum at node (r_o,z_o) is then

$$i_1 + i_2 + i_3 + i_4 = i_C\Big|_{r_o,z_o} - i_s\Big|_{r_o,z_o},$$

where $i_C\Big|_{r_o,z_o}$ is the current in the capacitor and $i_s\Big|_{r_o,z_o}$ is the source term at the node.

The above expressions assume uniform, symmetrical grid meshes. In order to simulate the boundary conditions and to minimize the number o electrical components, mesh size must become quite coarse near the edges of the grid. However, errors in the solutions result if two different mesh sizes are joined without a corrective network between them. This corrective network is best determined by adjustment to a known steady state solution of the heat conduction problem.[5] The electrical equivalent of the boundary condition ($\theta=0$) is the grounding of the edges of the network. The initial condition ($\theta=0$) is obtained by grounding all nodes before a simulation run.

Lt Col Dan Brown
USAF
SAM Records
Suitland

2.3 Practical Circuit Considerations

In order to determine the numerical range of thermal resistances and capacitances required, we must consider the eye model being simulated. Figure 2 illustrates the approximate dimensions assumed for each layer of the model and the percentage of energy incident on the cornea which each layer absorbs. For these ocular dimensions, an axial increment (Δz) of no more than 1μ must be employed if accurate temperature distributions within the pigmented epithelium are to be obtained. This increment would also be adequate for investigations of the thermal behavior of the retina and the forward part of the choroid. A radial increment (Δr) of 10μ near the z axis is fine enough to describe radial temperature distributions, since calculations of safe separation distances from nuclear weapons using animal exposure data have shown that image diameters at critical exposure levels are betweem 0.1 mm and 1 mm. For a maximum image radius of 0.5 mm, extension of the resistance-capacitance network to an equivalent model radius of 5 mm is assumed to be enough to simulate an infinite medium. Thus $r_o \leq 0.5$ cm.

The range of electrical capacitances used to simulate thermal capacitance must be restricted to avoid extensive circuit tuning for small capacitances and excessive leakage current for large capacitances. A suitable range of capacitors would be

$$100\text{pf} \leq C \leq 100\mu\text{f}.$$

Lt Col Dan Brown
USAF
SAM Records
Suitland

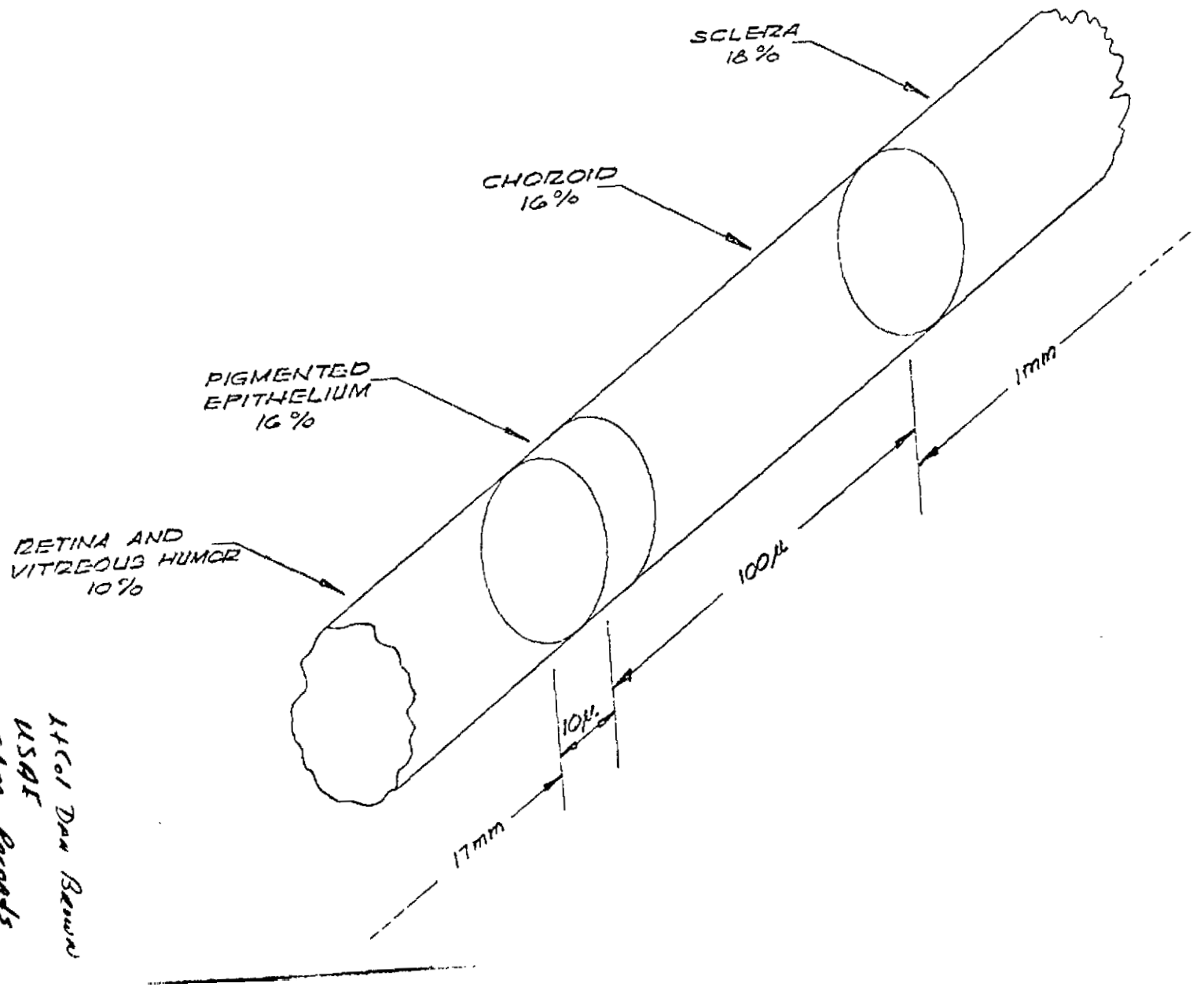

LtCol Don Brown
USAF
SAM Records
Suitland

$\underline{C_\theta}$, the minimum value of C_θ necessary to achieve the desired accuracy near the axis, may be calculated from Equation (11). For $\Delta r = 10\mu$ and $\Delta z = 1\mu$,

$$C_\theta = \frac{\pi}{4}\frac{K}{k}(10^{-3})^2\, 10^{-4} = \frac{\pi}{4}\frac{K}{k} \times 10^{-10}.$$

For a maximum thermal capacitance, $\overline{C_\theta}$, corresponding to the desired electrical capacitance range,

$$\overline{C_\theta} \leq 10^6 \times \underline{C_\theta}.$$

From Equation (10),

$$2\pi \frac{K}{k} \max\left\{r_o \Delta r \Delta z\right\} \leq 10^6 \frac{\pi}{4}\frac{K}{k} \times 10^{-10},$$

and

$$\max\left\{r_o \Delta r \Delta z\right\} \leq \frac{10^{-4}}{8}\ \text{cm}^3.$$

At the outer edges of the network where the mesh size will be the largest, $r_o = 0.5$ cm and

$$\max\left\{r_o \Delta r \Delta z\right\} \leq 0.5 \max\left\{\Delta r \Delta z\right\} \leq \frac{10^{-4}}{8}\ \text{cm}^3.$$

Therefore,

$$\max\left\{\Delta r \Delta z\right\} \leq \frac{10^{-4}}{4}\ \text{cm}^2 = \frac{10^4}{4}\ \mu^2. \tag{14}$$

Thus, with a minimum Δz of 1μ, the maximum Δr for the network will be 2500μ. The largest and smallest values of thermal resistance can be expected to occur in the radial and axial directions because of the physical dimensions of the regions of interest in the simple eye model. Using Equation (7), we find that

$$\overline{R_\theta} = \overline{R_{\theta r}} = \frac{1}{K\pi \min(\Delta z)} = \frac{1}{K\pi \times 10^{-4}} = \frac{10^4}{K\pi}.$$

Lt Col Dan Brown
USAF
SAM Records
Suitland

From Equation (5),

$$\underline{R_\theta} = \underline{R_{\theta z}} = \frac{1}{2\pi K} \min \frac{\Delta z}{r_o \Delta r} .$$

If extreme values of Δz, Δr, and r_o are now used in the expression for $\underline{R_\theta}$ ($\Delta z = 10^{-4}$ cm, $\Delta r = 0.25$ cm, $r_o = 0.5$ cm),

$$\underline{R_\theta} \geq \frac{1}{2\pi K} \frac{10^{-4}}{0.5 \times 0.25} = \frac{4 \times 10^{-4}}{\pi K} .$$

The range of thermal resistances would then be

$$\frac{\overline{R_\theta}}{\underline{R_\theta}} = \frac{10^4}{K\pi} \frac{K\pi}{4 \times 10^{-4}} = \frac{10^8}{4} .$$

This thermal resistance range could correspond to a range of electric resistances from 1 ohm to 25 megohms.

If we assume that $K = 1.4 \times 10^{-3}$ cal/°C cm sec and $k = 1.4 \times 10^{-3}$ ca for all layers (the values for water), then

$$\underline{C_\theta} \cong 10^{-10}.$$

If $\underline{C} = 100$ pf $= 10^{-10}$ farad, m is approximately 1. For a minimum resistance of 1 ohm and for $\underline{R_\theta} \cong 10^{-1}$,

$$mn \cong 10 \text{ and } n \cong 10.$$

Thus, time in the electrical analog is 10 times the equivalent therma time.

The maximum value of thermal power a. any node determines the ma mum current which must be supplied to the node and for a given circ configuration, this maximum current corres [illegible] maximum ir

Lt Col Dan Brown
USAF
SAM Records
Suitland

Experimental data obtained by Technology Incorporated using rabbits can be described by the relationship,

$$H_r = \frac{P_o(T)}{d_i^2} + H_o(T),$$

where H_r is the threshold retinal irradiance, d_i is the image diameter and the quantities $P_o(T)$ and $H_o(T)$ are adjusted to obtain the best description of the data for exposure time T. Assuming that the outer annular volume for any image size has a thickness $\Delta r = d_i/20$, the maximum nodal power at a particular (r_o, z_o) may be estimated in the following manner:

$$\begin{aligned} P\Big|_{r_o,z_o} &= H\Big|_{r_o,z_o} \times (\text{annular area})\Big|_{r_o,z_o} \\ &= H\Big|_{r_o,z_o} \times 2\pi r_o \Delta r \\ &\le 2\pi H_r \times \max\left\{r_o \Delta r\right\} \\ &< 2\pi \left[\frac{P_o(T)}{d_i^2} + H_o(T)\right] \frac{d_i}{2} \cdot \frac{d_i}{20} \\ &\le \frac{\pi}{20} \max\left\{\left[\frac{P_o(T)}{d_i^2} + H_o(T)\right] d_i^2\right\}. \end{aligned}$$

The maximum value of the last expression occurs at the maximum value of d_i (0.1 cm in our model). If we wish to simulate an exposure time of 10μ sec, since rabbit experimental data gives an H_r of 10^4 cal/cm^{2}sec at $d_i = 0.1$ cm and $T = 10\mu$ sec,

$$P\Big|_{r_o,z_o} < \frac{\pi}{20} \times 10^4 \times 10^{-2} = 5\pi.$$

Lt Col Dan Brown
USAF
SAM Records
Suitland

Hence,

$$\max P\Big|_{r_o, z_o} = \max \left\{ A 2\pi r_o \Delta r \Delta z \right\} \cong 16,$$

and

$$\max i = \frac{j}{mn} \times 16 = 1.6\, j.$$

The selection of j is therefore dependent upon the current sources available and the voltage range chosen to represent temperatures.

2.4 Practical Difficulties

As we have noted earlier, time scaling in the simulation of nuclear thermal pulses is a problem with resistance-capacitance networks. Thermal time intervals as short as 10μ sec or as long as 32 seconds (ten times the time to thermal maximum for a 10 MT weapon at sea level) are of interest. Thus with n = 10, an electrical analog device would require a time range

$$100\mu\,\text{sec} \le t \le 320\ \text{sec}.$$

It is therefore necessary to use an oscilloscope to display the short interval output of the device. For long runs an electromechanical plotter must be employed.

An additional problem is encountered in the simulation of nuclear thermal pulses. Each node of the network must be supplied with a time varying current given by the last term in Equation (12). The nodal current is zero until the fireball radius reaches the equivalent radius

Lt Col Dan Brown
USAF
SAM Records
Suitland

corresponding to the node. It then follows the time history of an annular ring in the fireball source which corresponds to the volume associated with the radial distance of the node from the center of the image. Furthermore, nodal currents must decrease exponentially in the z direction to account for absorption of radiation in ocular media whichare assumed to be homogeneous. A network satisfying the criteria presented above would require approximately 2000 nodes, and half of these nodes would represent ocular sites at which significant source strengths are produced by absorbed light (sites in the choroid and the pigmented epithelium). The provision of 1000 individual programmable current supplies for these nodes is extremely expensive. This high cost is one of the principal arguments against further development of electrical analog devices for this problem.

2.5 Solution for the Current Supply Problem

D. Hegedus of Technology Incorporated has suggested a possible solution to the multiple current supply problem. An array of photodiodes would be used as current generators and would be arranged in rows and columns corresponding to the z and r nodal coordinates. A light source representing the weapon fireball could then be directed upon the array to simulate fireball radius (image diameter) and weapon thermal pulse (retinal irradiance). Neutral filters placed between rows would provide an exponential decrease in source strength with increasing depth.

File Copy

LtCol Dan Brown
USAF
SAM Records
Suitland

Figure 3 illustrates a possible diode-filter arrangement. Unfortunately, photodiodes of good linearity are quite expensive (approximately $40 per diode). Furthermore, they are limited to steady currents of a few milliamperes. Thus for a maximum current of 10 ma, the circuit described above would require

$$i = 1.6j \leq 10^{-2} \text{ amperes}$$

or

$$j = 6 \times 10^{-3} \text{ volts}/^{\circ}\text{C}.$$

A 20° temperature rise would therefore be represented by a 120 millivolt change in nodal voltage.

Figure 4 is a comparison of the various choices available for resistance capacitance analog of the simple eye model.

We noted in an earlier progress report for this contract that a low resolution electrical analog device can be built with approximately 300 nodes. However, experimental data on monkeys now indicates that the retina may be more sensitive to increases in temperature than either the pigmented epithelium or the choroid. Therefore, it is desirable to have good resolution of isotherms in the first 100μ of the retinal structure nearest the pigmented epithelium as well as in the pigmented epithelium and forward part of the choroid. The accuracy required for useful investigation of the thermal damage process in the eye could be

Lt Col Dan Brown
USAF
SAM Records
Suitland

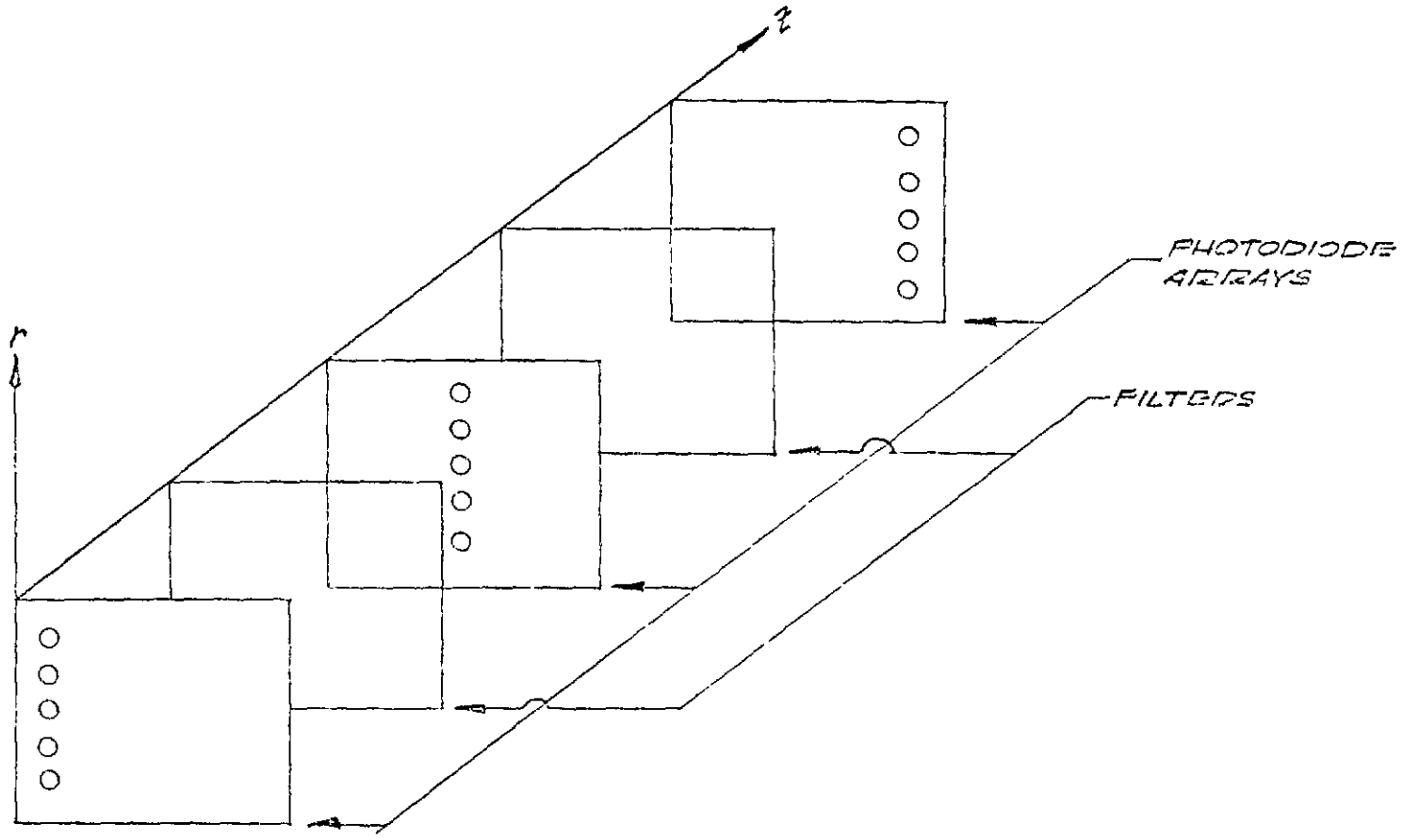

Figure 3. Photodiode Array for Simulation of Source Term.

Lt Col Dan Brown
USAF
SAM Records
Suitland

High Resolution Large range of weapon yield simulation	High construction cost High cost of source term simulation Variety of readout devices required
Low resolution Large range of weapon yield simulation	Reasonable construction cost High cost of source term simulation Variety of readout devices required
Very low resolution Restricted thermal time range	Reasonable construction cost High cost of source term simulation Single readout device

Figure 4. Resistance-capacitance analog characteristics for simple eye model.

Lt Col Dan Brown
USAF
SAM Records
Suitland

obtained only by a large electrical network whose cost would be quite high because of the large number of current sources needed for thermal source simulation. It should be noted that the problem of the simultaneous generation of large number of source currents is precisely the same problem which is encountered in the application of a commercial analog computer to the description of the simple eye model. Thus, an economical method of simulating the weapon source term does not seem to be presently available.

3. OTHER ANALOG DEVICES

One method of avoiding this high cost has been proposed by M. A. Mainster of Technology Incorporated. This, suggestion entails the use of layers of plastic or gelatinous material which have been suitably colored and provide a description of the different light absorption properties possessed by different ocular media. An intense light source which is spatially and temporally programmed would be used to describe a nuclear weapon thermal pulse. Temperatures at locations throughout the model could then be directly monitored by thermistors.

Unfortunately, the thermistors themselves would behave as local heat sources. Liquid crystal sensors or temperature sensitive paints might be used instead of thermistors. But temperature sensitive paints have a response time of a few milliseconds and would yield information about

Lt Col Dan Brown
USAF
SAM Records
Suitland

maximum temperatures only. Liquid crystal detectors which could provide a direct three-dimensional display of thermal behavior would require a continuous photographic recording because of the reversibility of the crystal reaction. Furthermore, problems would be encountered in achieving good thermal conductivity at the interface of two regions having different absorption characteristics.

4. CONCLUSIONS

Practical difficulties are associated with both the direct thermal analog and the resistance-capacitance electrical analog. These difficulties limit us to the construction of either inexpensive devices of unsatisfactory accuracy, or accurate devices of unsatisfactory cost. The great expense of the high resolution analog is not acceptable because flexible, comparatively inexpensive digital methods for solving Equation (2) are available. Indeed, comparison with a digital solution is the only reliable means of assuring that an analog simulator is operating correctly. Therefore, we conclude that it is unwise to expend further effort in the development of analog devices to simulate the thermal characteristics of the simple eye model.

5. REFERENCES

1. Berger, R. L. and Davids, N. Review of Scientific Instruments, Vol. 36, p. 88, 1965.

2. Felstead, E. B. and Cobbold, R. S. C. Medical Electronics and Biologi Engineering. Vol. 3, p. 145, 1965.

Lt Col Dan Brown
USAF
SAM Records
Suitland

3. Karplus, W. J. Analog Simulations, Mc Graw-Hill Book Co., 1958.

4. Liebmann, G. British Journal of Applied Physics, Vol. 1, p. 92, 1950.

5. Liebmann, G. British Journal of Applied Physics, Vol. 5, p. 362, 1954.

Lt Col Dan Brown
USAF
SAM Records
Suitland

APPENDIX D

LIST OF PUBLICATIONS

Lt Col Dan Brown
USAF
SAM Records
Suitland

LIST OF PUBLICATIONS

1. Transient Thermal Behavior in Biological Systems.

   Accepted for publication in the Bulletin of Mathematical Biophysics.

The Peaceman-Rachford finite difference method is applied to cylindrically symmetric, transient heat conduction problems in biological media. Inhomogeneous media, and internal sources which vary in both space and time are permitted. Boundary conditions are satisfied without sacrificing high local resolution by means of an exponentially stretched grid. Computation time on a Philco 2000/210 computer is approximately 5 msec per grid point per time step.

2. Chorioretinal Thermal Behavior.

   Accepted for publication in the Bulletin of Mathematical Biophysics.

Chorioretinal thermal response to intense light exposure is calculated for light sources with a wide variety of spatial and temporal characteristics. Effects of variable conductivity are examined. Transient temperature distributions are computed by means of an alternating directions implicit method for solving cylindrically symmetric heat conduction problems in biological media. Chorioretinal thermal distributions are discussed in terms of a maximum temperature damage criterion for ocular tissue.

Lt Col Dan Berw
USAF
SAM Records
Suitland

3. Retinal Temperature Increases Produced by Intense Light Sources. Submitted for publication to the Journal of the Optical Society of America.

The heat conduction equation is used to describe retinal temperature increases produced by the exponential absorption of intense light in the retina and the choroid. Temporal, radial and axial temperature distributions are presented for both continuous and pulsed light sources. A point spread distribution of retinal irradiance is considered in addition to a wide range of uniform and gaussian distributions. The application of computed temperatures to the prediction of retinal damage is discussed in terms of a maximum temperature damage criterion, and dependence of these predictions upon the depth of the retinal pigment epithelium is detailed.

4. Corneal Thermal Response to the CO_2 Laser. Submitted for publication to Applied Optics.

A three-dimensional model of corneal thermal response to CO_2 laser radiation is constructed and numerical solutions for temperature rise are computed. Power distribution in the laser beam and a conducting air-cornea interface are considered explicitly. It is found that the radial distribution of temperature increases produced by a gaussian beam is also

Lt Col Dan Brown
USAF
SAM Records
Suitland

gaussian, for brief exposures. The corneal damage threshold is examined in terms of this result.

5. Spectral Dependence of Retinal Damage Produced by Intense Light Sources.

   Submitted for publication to the Journal of the Optical Society of America.

The retinal temperature increases produced by circularly symmetric exposures to electromagnetic radiation between 400 and 1200 nm are calculated for a wide range of image sizes. Temporal, axial and radial temperature distributions are described. Constant and exponentially decreasing source strengths are considered. Solutions of the heat conduction equation are expressed in terms of both retinal irradiance and the total power entering the eye. Application of solutions to the prediction of thresholds for retinal damage is discussed, and excellent agreement is noted between theoretical predictions and experimental observations of the spectral dependence of chorioretinal damage thresholds.

Lt Col Dan Brown
USAF
SAM Records
Suitland

UNCLASSIFIED
Security Classification

DOCUMENT CONTROL DATA - R&D

(Security classification of title, body of abstract and indexing annotation must be entered when the overall report is classified)

1. ORIGINATING ACTIVITY (Corporate author)
Technology Incorporated, Life Sciences Division
8531 N. New Braunfels Avenue
San Antonio, Texas 78217

2a. REPORT SECURITY CLASSIFICATION
UNCLASSIFIED

2b. GROUP

3. REPORT TITLE
Evaluation of Eye Hazards from Nuclear Detonations

4. DESCRIPTIVE NOTES (Type of report and inclusive dates)
Final Report - December 1967 - June 1969

5. AUTHOR(S) (Last name, first name, initial)
Miller, Norma D.; White, Thomas I.; Bowie, William H.; Bruce, William R., Bryson, Charles E.; Kay, Kenneth R.; Mainster, Martin A.; Smith, Margaret G.; Tips, James H.; and Wilson, Patrick W.

6. REPORT DATE
July 1969

7a. TOTAL NO. OF PAGES
290

7b. NO. OF REFS

8a. CONTRACT OR GRANT NO.
F41609-68-C-0023

b. PROJECT NO.
6301, Task 630103

c.
Work Unit 6301 03 031

d.

9a. ORIGINATOR'S REPORT NUMBER(S)

9b. OTHER REPORT NO(S) (Any other numbers that may be assigned this report)

10. AVAILABILITY/LIMITATION NOTICES
Distribution of this document is unlimited

11. SUPPLEMENTARY NOTES

12. SPONSORING MILITARY ACTIVITY
USAF School of Aerospace Medicine,
Aerospace Medical Division (AFSC)
Brooks Air Force Base, Texas 78235

13. ABSTRACT

I. White light primate retinal burn thresholds are reported for both foveal and extramacular regions. Rabbit and primate retinal burn thresholds are reported for a ruby laser used in the normal, semi-Q-switched, and Q-switched modes. Human flashblindness recovery time data are given for various flash field sizes and various recovery targets. A new double light source system for producing simulated nuclear detonations is described. A mathematical model for the prediction of retinal temperatures is developed.

II. Safe separation distance estimates are given at selected times for both 10 second recovery flashblindness and retinal burns for yields of 10^{-2} to 10^{4} KT and burst heights to 50 KT high and low visibility atmospheres and pupil diameters of 3 and 7 mm are additional parameters. The retinal burn estimates are based on primate exposure data gathered during the previous eighteen months.

LtCol Dan Brown
USAF
SAM Records
Suitland

DD FORM 1 JAN 64 1473

UNCLASSIFIED
Security Classification

Security Classification

14 KEY WORDS	LINK A ROLE	LINK A WT	LINK B ROLE	LINK B WT
Vision; flashblindness; retinal burns for laser and white light; visual effects safe separation distances; nuclear weapons effects; thermal energy from nuclear weapons; retinal burn threshold data; mathematical models; heat conduction; differential equations; oculothermal parameters.				

INSTRUCTIONS

1. ORIGINATING ACTIVITY: Enter the name and address of the contractor, subcontractor, grantee, Department of Defense activity or other organization *(corporate author)* issuing the report.

2a. REPORT SECURITY CLASSIFICATION: Enter the overall security classification of the report. Indicate whether "Restricted Data" is included. Marking is to be in accordance with appropriate security regulations.

2b. GROUP: Automatic downgrading is specified in DoD Directive 5200.10 and Armed Forces Industrial Manual. Enter the group number. Also, when applicable, show that optional markings have been used for Group 3 and Group 4 as authorized.

3. REPORT TITLE: Enter the complete report title in all capital letters. Titles in all cases should be unclassified. If a meaningful title cannot be selected without classification, show title classification in all capitals in parenthesis immediately following the title.

4. DESCRIPTIVE NOTES: If appropriate, enter the type of report, e.g., interim, progress, summary, annual, or final. Give the inclusive dates when a specific reporting period is covered.

5. AUTHOR(S): Enter the name(s) of author(s) as shown on or in the report. Enter last name, first name, middle initial. If military, show rank and branch of service. The name of the principal author is an absolute minimum requirement.

6. REPORT DATE: Enter the date of the report as day, month, year; or month, year. If more than one date appears on the report, use date of publication.

7a. TOTAL NUMBER OF PAGES: The total page count should follow normal pagination procedures, i.e., enter the number of pages containing information.

7b. NUMBER OF REFERENCES: Enter the total number of references cited in the report.

8a. CONTRACT OR GRANT NUMBER: If appropriate, enter the applicable number of the contract or grant under which the report was written.

8b, 8c, & 8d. PROJECT NUMBER: Enter the appropriate military department identification, such as project number, subproject number, system numbers, task number, etc.

9a. ORIGINATOR'S REPORT NUMBER(S): Enter the official report number by which the document will be identified and controlled by the originating activity. This number must be unique to this report.

9b. OTHER REPORT NUMBER(S): If the report has been assigned any other report numbers *(either by the originator or by the sponsor)*, also enter this number(s).

10. AVAILABILITY/LIMITATION NOTICES: Enter any limitations on further dissemination of the report, other than those imposed by security classification, using standa
such as:

(1) "Qualified requesters may obtain copie
report from DDC."

(2) "Foreign announcement and disseminat
report by DDC is not authorized."

(3) "U. S. Government agencies may obtai
this report directly from DDC. Other q
users shall request through

(4) "U. S. military agencies may obtain co
report directly from DDC. Other qualifi
shall request through

(5) "All distribution of this report is contr
ified DDC users shall request through

If the report has been furnished to the Offic
Services, Department of Commerce, for sale to t
cate this fact and enter the price, if known.

11. SUPPLEMENTARY NOTES: Use for addit
tory notes.

12. SPONSORING MILITARY ACTIVITY: Ent
the departmental project office or laboratory sp
ing for) the research and development. Include

13. ABSTRACT: Enter an abstract giving a bri
summary of the document indicative of the repor
it may also appear elsewhere in the body of the
port. If additional space is required, a continua
be attached.

It is highly desirable that the abstract of cl
be unclassified. Each paragraph of the abstract
an indication of the military security classificat
formation in the paragraph, represented as *(TS)*,

There is no limitation on the length of the
ever, the suggested length is from 150 to 225 w

14. KEY WORDS: Key words are technically m
or short phrases that characterize a report and n
index entries for cataloging the report. Key wo
selected so that no security classification is re
fiers, such as equipment model designation, tra
project code name, geographic location, may be
words but will be followed by an indication of t
text. The assignment of links, rules and

LtCol Dan Be
USAF
SAM Record
Suitland

UN